NTNU
Norwegian University of
Science and Technology

Pion Condensation in the Linear Sigma Model

Øyvind Almelid

Physics
Submission date: May 2011
Supervisor: Jens Oluf Andersen, IFY

Norwegian University of Science and Technology
Department of Physics

Abstract

In this thesis we study the phase diagram of quantum chromodynamics in an effective low-energy theory at zero baryon chemical potential but finite temperature and isospin density. We investigate pion condensation at finite temperature and isospin chemical potential μ_I in two different approximation schemes of the linear sigma model; the Large-N and Hartree approximations. While being a simple model, the linear sigma model allows for phase transitions of both the first and second order, as well as crossover transitions at the physical point. The large-N approximation yields results typical for mean-field approaches, including a second order phase transition with critical exponent $\nu = \frac{1}{2}$. At the physical point we find that pion condensation occurs below a threshold temperature $T_c(\mu_I)$ only for $\mu_I \geq m_\pi$. Due to the symmetry of the $O(N)$ expansion, the large-N approximation also obeys Goldstone's theorem, yielding a massless Goldstone mode in the pion condensed phase.

By contrast, we find a large violation of Goldstone's theorem in the Hartree approximation, with the Goldstone mode achieving a mass of 200 MeV $\approx 1.4\ m_\pi$. It is possible that the Hartree approximation's violation of symmetry makes the Goldstone mode tachyonic at low temperatures. However, it appears that the Hartree approximation yields a phase structure much more similar to what has been found in lattice studies, with a first order phase transition at high isospin densities and crossover transitions at lower densities. We have only been able to study the Hartree approximation under the condition that either the chiral condensate or the pion condensate is zero, however, and accurate probing of the phase diagram at the physical point is therefore not possible.

Acknowledgements

The author would like to thank professor Jens O. Andersen for guidance and illuminating discussions, and Hannah Brunsdon for her endless patience. A warm thanks is also extended to family, friends, study companions and everyone at Programvareverkstedet. The cover art is copyrighted by CERN, record CERN-EX-11465, and shows pions decaying in a bubble chamber. The image has been modified for artistic purposes and is used with permission.

Contents

Nomenclature

2PI	Two-particle irreducible
2SC	Two-colour superconducting
CFL	Colour-flavour-locked
GWS	Glashow-Weinberg-Salam model
IR	Infrared
NQ	Normal quark matter phase
QCD	Quantum chromodynamics
UV	Ultraviolet

List of figures

Conventions

Throughout this thesis we will use a number of conventions which are simply a matter of convenience and choice. These are as follows.

- We use natural units where $\hbar = k_b = c = 1$.
- Our metric signature is $(+,-,-,-)$.
- We will be utilising sum-integrals and dimensional regularization. As a shorthand we write

$$\not{\int} = \left(\frac{\Lambda^2 e^{-\gamma}}{4\pi}\right)^{\epsilon} T \sum_{\omega = 2\pi i n T} \int \frac{d^d p}{(2\pi)^d}. \tag{1}$$

  In the above, $d = 3 - 2\epsilon$, Λ is the renormalisation scale in the $\overline{MS}$ subtraction scheme, T is the temperature and γ is the Euler-Mascheroni constant. As a shorthand $\omega = p^0$ and we write $\omega_n = -i\omega$ in Euclidean space.
- The Einstein summation convention is used throughout this thesis. Repeated indices are summed over unless stated otherwise. We use Greek indices for four-vectors in spacetime and roman indices for everything else.
- In Euclidean space, we sometimes use capital letters to describe four-vectors $P = (\omega_n, \vec{p})$.

Chapter 1

Introduction

The theory of strong interactions – Quantum chromodynamics, or QCD [1] – is at once a startlingly accurate and mystifyingly complex theory. It describes a wide range of experimental results and has predicted the existence and properties of a number of exotic particles, later verified in collider experiments. With regards to complexity, Quantum Chromodynamics describes nuclear matter as a composition of bound states of six different quarks. The binding force is the strong nuclear force, which is mediated by eight massless particles, the so-called gluons. This myriad of particles allow us to describe the behaviour of nuclear matter through a vast number of possible interactions and outcomes between the different constituents of the theory. The large number of degrees of freedom as well as the nonlinearity of QCD makes calculations complex both analytically and numerically. Indeed, computer simulations such as *lattice QCD* – a computational technique involving a discretised version of QCD suitable for computer simulation [2] – typically require large supercomputing facilities to make reasonable predictions of scattering cross-sections.

Suppose now that we could somehow simplify the picture. Indeed, all the chemicals in the periodic table of elements are composed of only one family of quarks and leptons. The other families are short-lived due to their tendency to decay to lower-mass particles and radiation. We might simply throw out four quarks and four leptons. This would be at the price of accuracy and generality, of course. We would be discarding a number of particles which have been observed to exist, and which have a small but nonzero effect on the world we inhabit. However, one might hope to simplify QCD sufficiently to come up with meaningful predictions without having to spend valuable computing time calculating the probabilities of increasingly unlikely interactions involving a host of exotic particles.

To this end, physicists have developed a number of approximation schemes to simplify calculations within various quantum field theories. In particular, the study effective field theories provides a systematic way of constructing simplified models which reproduce the dominant degrees of freedom and symmetries of a field theory. Some general reviews and an overview of the field can be found in [3–5]. Of course, the previous paragraph is only an example of how one might simplify QCD. Depending on the situation – the energies and densities of the system under study – different symmetries may be broken or unbroken, and the field theory might behave qualitatively very differently. To each situation, its own set of approximations. In this manner we hope to at least sketch a map of the terrain by stitching together a patchwork quilt of approximations, each valid in its own regime. We need fabric for the patchwork, however.

In this thesis, we will study processes relevant to the normal hadronic phase of quark matter, as well as a region referred to as the NQ phase, for normal quark matter . It is known that in the presence of a nonzero *isospin chemical potential* – a statistical preference for a certain electrical charge present in the system – these phases allow for a condensate of elementary particles known as pions [6, 7]. To this end we will study pion condensation in an idealised model with no baryon density, but a statistical preference for a certain electrical charge. First, however, we must lay out some preliminaries.

1.1 Symmetry and conserved quantities

By symmetry we refer to an operation – some continuous transformation of parameters – which leave the physics of a system unaltered. Specifically, if the action S of a system is unaltered by a transformation then the solution to the equations of motion of that system will also be unaltered by the transformation and

hence we have a symmetry of the system. There is a connection between symmetries of physical systems and conservation laws which will be of fundamental importance to our treatment of chemical potentials later in this thesis. This connection is described by Noether's theorem [8], which states that a continuous symmetry in the Lagrangian gives rise to a conserved current. Detailed derivations and discussion of Noether's theorem can be found in most textbooks on quantum field theory, for instance [9, 10].

As a simplified derivation, assume a transformation of the fields ϕ_i, $i = 1, \cdots, n$ such that $\phi_i \to \phi_i + \epsilon_i \delta\phi_i$ with no summation implied and where ϵ_i are some infinitesimal parameters. Furthermore, assume that the Lagrangian is invariant with respect to the transformation, in other words $\mathcal{L}(\phi_i) \to \mathcal{L}(\phi_i + \epsilon_i \delta\phi_i) = \mathcal{L}(\phi_i)$. If we vary the Lagrangian according to our transformation, then by our assumption of symmetry we have

$$\begin{aligned} 0 &= \delta\mathcal{L} \\ &= \frac{\partial\mathcal{L}}{\partial\phi_i}\delta\phi_i + \frac{\partial\mathcal{L}}{\partial(\partial_\mu\phi_i)}\delta(\partial_\mu\phi_i) = \partial_\mu\left[\frac{\partial\mathcal{L}}{\partial(\partial_\mu\phi_i)}\delta\phi_i\right] + \left[\frac{\partial\mathcal{L}}{\partial\phi_i} - \partial_\mu\frac{\partial\mathcal{L}}{\partial(\partial_\mu\phi_i)}\right]\delta\phi_i. \end{aligned} \tag{1.1}$$

We recognise the Euler-Lagrange equation in the rightmost square brackets above, and therefore define the Noether current j^μ by

$$j^\mu \equiv \frac{\partial\mathcal{L}}{\partial(\partial_\mu\phi_i)}\delta\phi_i. \tag{1.2}$$

By inserting this definition into Eq. (1.1), we obtain the current conservation equation

$$\partial_\mu j^\mu = 0. \tag{1.3}$$

To see that this is a conservation law, we integrate the above equation over $\vec{x}$

$$0 = \int d^3x \left[\frac{\partial}{\partial t} j^0(\vec{x}, t) - \nabla\vec{j}(\vec{x}, t)\right]. \tag{1.4}$$

We now apply Gauss' theorem to the last term to obtain

$$\frac{d}{dt}\int d^3x j^0(\vec{x}) = \int_{\partial S} dS\vec{j}\cdot\vec{n}. \tag{1.5}$$

The term on the right-hand-side is a surface term, assumed to approach zero as $|\vec{x}| \to \infty$. We define the charge Q as

$$Q \equiv \int d^3x j^0(\vec{x}, t). \tag{1.6}$$

And Eq. (1.4) thus becomes a conservation law.

$$\frac{d}{dt}Q = 0. \tag{1.7}$$

As mentioned earlier, Noether's theorem concerns symmetries under which the *action* is invariant. The action is invariant even under the addition of surface terms, or equivalently under the addition of a total divergence $\partial_\mu\mathcal{J}^\mu$ to the Lagrangian such that $\mathcal{L} \to \mathcal{L} + \partial_\mu\mathcal{J}^\mu$. This alters the above derivation slightly, adding an extra term to the current [10]

$$j^\mu \equiv \frac{\partial\mathcal{L}}{\partial(\partial_\mu\phi_i)}\delta\phi_i - \mathcal{J}^\mu. \tag{1.8}$$

1.1.1 $U(1)$ symmetry

As a familiar example of a symmetry giving rise to a conserved current, consider the Lagrangian of a single complex scalar field Φ

$$\mathcal{L} = (\partial_\mu\Phi)^\dagger(\partial^\mu\Phi) - m^2\Phi^\dagger\Phi - \lambda(\Phi^\dagger\Phi)^2. \tag{1.9}$$

The above Lagrangian is invariant under a global phase transformation $\Phi \to e^{i\alpha}\Phi$, as can be seen simply by inserting the transformation and moving $e^{i\alpha}$ past the partial derivatives. We may now attempt to

derive the Noether current and the corresponding charge. Let α be infinitesimal, then our transformation rule becomes $\Phi \to (1 + i\alpha)\Phi$, which shows that $\delta\Phi = i\Phi$. Taking the complex conjugate of $\delta\Phi$ also yields $\delta\Phi^\dagger = -i\Phi^\dagger$. Inserting this into Noether's theorem yields the conserved current

$$j^\mu = i\left[(\partial^\mu\Phi^\dagger)\Phi - \Phi^\dagger(\partial^\mu\Phi)\right]. \tag{1.10}$$

We now turn our attention to the conserved charge.

$$Q = i\int d^3x\ \left[(\partial^\mu\Phi^\dagger)\Phi - \Phi^\dagger(\partial^\mu\Phi)\right] \tag{1.11}$$

We can interpret this charge by considering Φ in the free field expansion, namely

$$\Phi = i\int \frac{d^3p}{(2\pi)^3}\ \frac{1}{\sqrt{2E_p}}\left[a_p e^{ipx} + b_p^\dagger e^{-ipx}\right] \tag{1.12}$$

$$\Phi^\dagger = \int \frac{d^3p}{(2\pi)^3}\ \frac{1}{\sqrt{2E_p}}\left[b_p e^{ipx} + a_p^\dagger e^{-ipx}\right] \tag{1.13}$$

$a_p^\dagger$ and $b_p^\dagger$ are here creation operators for particles and antiparticles, respectively, and $E_p = p_0 = \sqrt{p^2 + m^2}$ is a convenient normalisation. Writing out the charge, we obtain

$$\begin{aligned} Q = -\frac{1}{2}\int d^3x \int \frac{d^3p}{(2\pi)^3}\frac{d^3p'}{(2\pi)^3}\Bigg[&\sqrt{\frac{E_{p'}}{E_p}}\left(b_{p'}e^{ip'x} - a_{p'}^\dagger e^{-ip'x}\right)\left(a_p e^{ipx} + b_p^\dagger e^{-ipx}\right) \\ &-\sqrt{\frac{E_p}{E_{p'}}}\left(a_p e^{ipx} - b_p^\dagger e^{-ipx}\right)\left(b_{p'}e^{ip'x} + a_{p'}^\dagger e^{-ip'x}\right)\Bigg]. \end{aligned} \tag{1.14}$$

We recall that

$$\int d^3x\ e^{i(p-p')x} = (2\pi)^3\delta^3(p - p'). \tag{1.15}$$

Multiplying out the parentheses and carrying out the integration over x thus yields delta-functions containing p and p'. We use this to further calculate one of the momentum integrals, and commute everything to normal ordering by using the relation $[a_p, a_p^\dagger] = 1$, the result is

$$Q = \int \frac{d^3p}{(2\pi)^3}\left(a_p^\dagger a_p - b_p^\dagger b_p\right) = \hat{N}_a - \hat{N}_b. \tag{1.16}$$

The conserved charge is thus the number of particles minus the number of antiparticles. It is perhaps particularly apparent what this number represents in the case of charged particles, where Q is the total charge of the system.

1.1.2 $U(1)$ gauge symmetry

The example of a $U(1)$ symmetry can be extended to describe electromagnetism by making the symmetry local. This serves to outline a general procedure in quantum field theory by which one may introduce gauge fields to describe various forces. A more advanced example will be given in the section on quantum chromodynamics, Sec.1.2.1. We make the $U(1)$ symmetry local by allowing the phase α to be different for each point in spacetime, i.e.

$$\Phi \to e^{i\alpha(x)}\Phi, \tag{1.17}$$

$$\Phi^\dagger \to e^{-i\alpha(x)}\Phi^\dagger. \tag{1.18}$$

Clearly the Lagrangian density is not invariant under this transformation unless $\alpha(x)$ is constant, otherwise $\alpha(x)$ does not commute with the partial derivatives. However, we could modify the Lagrangian to include a gauge field A_μ; a field which for every point in space transforms so as to absorb the extra terms produced by commuting ∂_μ and $\alpha(x)$. This is done by introducing the covariant derivative D_μ defined by

$$\partial_\mu \to D_\mu \equiv \partial_\mu - igA_\mu. \tag{1.19}$$

Here, g is a coupling constant which we may choose. We now observe how the covariant derivative transforms, we have

$$\begin{aligned} D_\mu \Phi &= (\partial_\mu - igA_\mu)\,\Phi \\ &\to \left(\partial_\mu - igA'_\mu\right) e^{i\alpha(x)}\Phi, \end{aligned} \tag{1.20}$$

where A'_μ is the transformed gauge field. We use the chain rule to separate out a factor $e^{i\alpha(x)}$ from the right hand side above

$$D_\mu \Phi \to e^{i\alpha(x)}\left(\partial_\mu \Phi + i(\partial_\mu \alpha(x))\Phi - igA'_\mu\right) \tag{1.21}$$

We can absorb the extra partial derivative with respect to $\alpha(x)$ by letting A_μ transform as

$$A_\mu \to A'_\mu = A_\mu + \frac{1}{g}\partial_\mu \alpha(x). \tag{1.22}$$

This yields the transformation

$$D_\mu \Phi \to e^{i\alpha(x)} D_\mu \Phi, \tag{1.23}$$

and by taking the adjoint we also find

$$(D_\mu \Phi)^\dagger \to (D_\mu \Phi)^\dagger e^{-i\alpha(x)}. \tag{1.24}$$

Thus we obtain the gauge invariant Lagrangian

$$\mathcal{L} = (D_\mu \Phi)^\dagger (D^\mu \Phi) - m^2 \Phi^\dagger \Phi - \lambda(\Phi^\dagger \Phi)^2. \tag{1.25}$$

The gauge field is currently not propagating. Apart from its appearance in the covariant derivative, there are no kinetic terms for the field itself. However, we may introduce a kinetic term, provided it preserves gauge invariance [9]. The electromagnetic field strength tensor is gauge invariant, and defined by

$$F_{\mu\nu} \equiv \partial_\nu A_\mu - \partial_\mu A_\nu. \tag{1.26}$$

The Lagrangian is a Lorentz scalar, and hence we may only insert a contraction of $F_{\mu\nu}$. The simplest nonzero contraction of $F_{\mu\nu}$ is $F_{\mu\nu}F^{\mu\nu}$ We therefore modify the Lagrangian to include a kinetic term quadratic in the field-strength tensor. The final Lagrangian is

$$\mathcal{L} = (D_\mu \Phi)^\dagger (D^\mu \Phi) - m^2 \Phi^\dagger \Phi - \lambda(\Phi^\dagger \Phi)^2 - \frac{1}{4} F_{\mu\nu} F^{\mu\nu}. \tag{1.27}$$

1.1.3 Symmetry breaking and Goldstone's theorem

While a Lagrangian might exhibit a symmetry, it is not granted that the ground state is equally symmetric. This phenomenon – commonly referred to as spontaneous symmetry breaking – has some general implications, described by Goldstone's theorem [11]. A practical formulation for relativistic, Lorentz-invariant field theories – as formulated by Goldstone, Salam and Weinberg [12] – states that

> If there is a continuous symmetry transformation under which the Lagrangian is invariant, then either the vacuum state is also invariant under the transformation or there must exist spinless particles of zero mass.

The number of such massless fields are determined by the so-called Nielsen-Chadha counting rules, and is equal to the number of broken symmetry generators [13]. As an example, we follow the derivation in Ref. [10] and consider the linear sigma model with a negative mass term. We will discuss the linear sigma model in much greater detail later, for now it will suffice to simply state the Lagrangian. Let ϕ_i be N real scalar fields and consider the Lagrangian

$$\mathcal{L} = \frac{1}{2}(\partial_\mu \phi_i)(\partial^\mu \phi_i) - \frac{1}{2} m^2 \phi_i \phi_i - \frac{\lambda}{4N}(\phi_i \phi_i)^2. \tag{1.28}$$

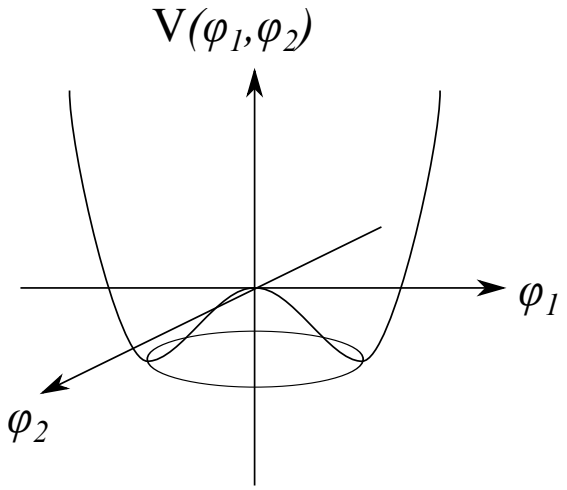

Figure 1.1: A Mexican hat-potential for the case $N = 2$. The degenerate global minima of $V(v)$ form a circular well, due to the $O(2)$-invariance.

This Lagrangian is manifestly $O(N)$ invariant, as can be seen by performing an orthogonal transformation $\phi_i \to R_{ij}\phi_j$ where $R_{ij}R_{ik} = \delta_{jk}$. The transformation is coordinate-independent, and hence we obtain

$$\begin{aligned}\mathcal{L} &\to R_{ij}R_{ik}\frac{1}{2}\left[(\partial_\mu\phi_j)(\partial^\mu\phi_k) - m^2\phi_j\phi_k\right] - \frac{\lambda}{4N}(R_{ij}R_{ik}\phi_j\phi_k)^2 \\ &= \frac{1}{2}(\partial_\mu\phi_i)(\partial^\mu\phi_i) - \frac{1}{2}m^2\phi_i\phi_i - \frac{\lambda}{4N}(\phi_i\phi_i)^2. \end{aligned} \tag{1.29}$$

Furthermore, if $m^2 < 0$, the ground state of the linear sigma model has a nonzero vacuum expectation value. To observe this, let $\phi_1 \to v + \phi_1$, where v is a classical field. Inserting this into the Lagrangian, we obtain

$$\mathcal{L} = \frac{1}{2}(\partial_\mu v)(\partial^\mu v) - \frac{1}{2}m^2v^2 - \frac{\lambda}{4N}v^4 - \frac{1}{2}(\partial_\mu\phi_i)(\partial^\mu\phi_i) \ - \frac{1}{2}m_i^2\phi_i\phi_i + \mathcal{L}_{int} \tag{1.30}$$

The term $\mathcal{L}_{int}$ is an interaction term containing cubic and quartic interactions between ϕ_i, in addition, the classical field v has altered the mass-term such that.

$$m_i^2 = m^2 + \begin{cases} \frac{3\lambda}{N}v^2 & \text{if } i = 1, \\ \frac{\lambda}{N}v^2 & \text{otherwise.} \end{cases} \tag{1.31}$$

The cubic interactions are proportional to v. We will later develop a more formal approach to the effective potential, for now suffice it to say that the above Lagrangian corresponds to that of a classical field governed by the potential

$$V(v) = \frac{1}{2}m^2v^2 + \frac{\lambda}{4N}v^4. \tag{1.32}$$

Our choice for the direction of v was arbitrary and was allowed due to the rotational symmetry. The potential is therefore really rotationally invariant, and in the case of $m^2 < 0$ it has a Mexican hat shape, as illustrated for the $O(2)$ case in Fig. 1.1. The potential has a minimum for $v = \sqrt{\frac{-Nm^2}{\lambda}}$, representing a nonzero expectation value of ϕ_1. We thus have spontaneous symmetry breaking, and should expect Goldstone bosons. The mass of the fields are defined by the terms in the potential quadratic in the fields, and can therefore be described by a mass-matrix $(m^2)_{ij} = \frac{\partial^2 V(\phi_i)}{(\partial\phi_i)(\partial\phi_j)}$. Having chosen the direction of ϕ_1 for our nonzero expectation value, we observe that the second derivative in the ϕ_1-direction is nonzero, moving perpendicular to the direction of the well in Fig. 1.1. Conversely, moving along the trough the second derivative is zero and so we expect that the corresponding fields should be massless. Inserting the solution for v into Eq.(1.31), we obtain

$$m_i^2 = \begin{cases} -2m^2 & \text{if } i = 1, \\ 0 & \text{otherwise.} \end{cases} \tag{1.33}$$

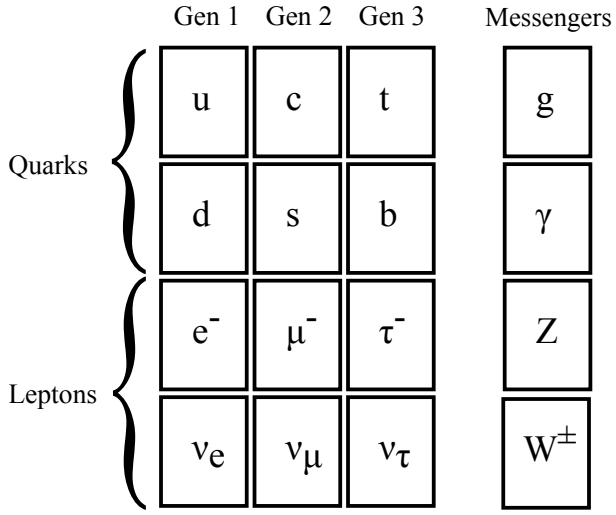

Figure 1.2: A table showing the constituents of the standard model divided into families and generations.

What has happened here is entirely according to Goldstone's theorem. The ground state of the system is $(v, 0, 0, \cdots)$, which is not rotationally symmetric. However, the fields $\phi_2, \phi_3, \cdots$ are still rotationally symmetric, so the $O(N)$ symmetry has been spontaneously broken and what remains is an $O(N-1)$ symmetry. The number of generators in the $O(N)$ group is $\frac{1}{2}N(N-1)$. We therefore expect $N-1$ massless modes, which is what we have obtained.

1.2 Quantum chromodynamics

Quantum chromodynamics is the theory of strong interactions, and forms part of the standard model of particle physics along with the Glashow-Weinberg-Salam (GWS) model of electroweak interactions. The standard model as a whole describes the world as composed of six quarks and six leptons, divided into three families by their respective masses. In addition there are three forces mediated by twelve different mediator particles: the strong force, mediated by eight gluons, the weak force, mediated by the Z^0 and $W^{\pm}$ bosons, and the electromagnetic force, mediated by the photon. Fig. 1.2 shows a short summary of these particles according to their "generations"; groupings of the particles according to their masses.

The fundamental particles of QCD are the quarks and gluons. There are six quarks, divided into three families according to their approximate mass. The up, charm and top quark have a positive charge of two thirds the electron charge, whereas the down, strange and bottom quark have a negative one-third electron charge. QCD describes the strong force as being mediated by the gauge field of a local $SU(3)$ symmetry group. Since $SU(3)$ has eight generators, there are eight such gluon fields. The gluons are mediators of colour charge and unlike the photon, the gluons carry charge themselves.

The discovery of the quarks and their $SU(3)$ colour charge came about when high-energy collider experiments started detecting large numbers of new hadronic particles in the 1960s. As physicists attempted to make sense of the newly discovered particles and their properties, several patterns and symmetries emerged. One well-known example of this is Gell-Mann and Neeman's eightfold way, in which particles were organised according to strangeness and electric charge. The baryon decuplet that Gell-Mann found was missing a particle which he called Ω^-, and predicted would have charge $-e$, strangeness 3 and a mass of around 1680 MeV [14]. Ω^- was discovered two years later at the Brookhaven National Laboratory accelerator facility [15]. Gell-Mann and Zweig went on to suggest independently that all baryons were composed of three smaller spin-1/2 constituents called quarks [16, 17].

However, the Ω^- would then be a pure triplet of strange quarks, in clear violation of Pauli's exclusion principle. It would therefore be necessary to introduce another quantum number. This quantum number was proposed to be generated by an $SU(3)$ gauge group, a fact which was discovered independently by Han working with Nambu, and Greenberg in 1965 [18, 19]. $SU(3)$ introduces a quantum number referred to as colour charge, hence the name chromodynamics. There are three colours, red, green and blue. Antiquarks similarly have anticolours: antired, antigreen and antiblue. In addition to resolving the

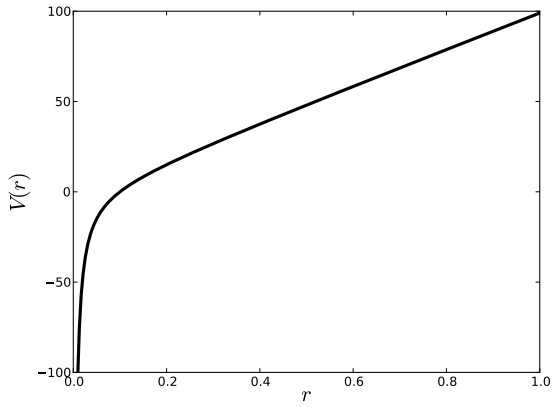

Figure 1.3: The Cornell potential $V(r)$ with $\kappa = 1$ and $\sigma = 100$. At large r, $V(r)$ grows linearly and is therefore unbounded, giving rise to confinement.

conundrum of the apparent violation of the exclusion principle, colour charge also conveniently explains the subdivision of nuclear particles – or hadrons – into baryons and mesons. Baryons are bound states of three quarks or antiquarks, whereas mesons are bound states of a quark and an antiquark. Any stable bound state must be colour neutral. Thus mesons must be composed of the same colour and anticolour, and baryons must be composed of all three colours or anticolours.

Due to its non-Abelian nature (the $SU(3)$ generators do not commute), QCD has some rather peculiar properties not found in quantum electrodynamics or the GWS-model[1]. Asymptotic freedom provides that whereas most coupling constants increase with increasing energy scales, the coupling constant of QCD decreases. This means that at high energies (and conversely at small distances) the strong force becomes negligibly small, allowing for the formation of a quark-gluon plasma which we will discuss in detail when dealing with the phase diagram of QCD. On the other hand, at low energies (and large distances) the coupling constant becomes arbitrarily strong, giving rise to what we know as quark confinement. It is well known from collider experiments that quarks are never observed outside of the hadrons they compose. When attempting to tear apart a bound state of quarks, the gluon field forms a flux tube tying the quarks together, with increasing strength as the distance increases [20]. An early effective potential to describe this behaviour is the so-called Cornell potential $V(r)$ where r is the distance between two quarks [21]:

$$V(r) = -\frac{\kappa}{r} + \sigma r. \tag{1.34}$$

In more recent versions of this potential, κ is often taken to be a slowly changing function of r, but to a first approximation we may take it to be constant. An illustration of the potential is provided in Fig. 1.3. One may interpret κ as the string tension of the flux tube, giving rise to a term linear in the distance between the quarks. Such potentials have been studied in lattice QCD for mesons [22, 23], and baryons [24, 25]. As $r \to \infty$ the linear term dominates and approaches infinity. Therefore, as one attempts to tear the quarks apart, one needs prohibitively large amounts of energy to do so, eventually enabling the creation of new quark-antiquark pairs. These new quark-antiquark pairs bind to the quarks already present to form new particles. Cascades of such behaviour occur in high-energy particle accelerators, and typically give rise to jets of new particles emerging from the collision centre [26].

1.2.1 The theory

The quarks are fermions, governed by the Dirac Lagrangian.

$$\mathcal{L} = \bar{\psi}\left(i\gamma^\mu \partial_\mu - m\right)\psi. \tag{1.35}$$

[1]This is not entirely true, as $SU(2)$ is also non-Abelian. The GWS-model does not exhibit these properties due to technicalities surrounding the "breaking" of a gauge symmetry. The gauge fields of the GWS model absorb the Goldstone modes arising from electroweak symmetry breaking and acquire a mass.

Furthermore to accommodate colour charge each quark field is a colour triplet, which introduces a global $SU(3)$ symmetry. $SU(3)$ has eight generators θ^a which satisfy the commutation relation

$$\left[\theta^a, \theta^b\right] = if^{abc}\theta^c. \tag{1.36}$$

f^{abc} is a tensor containing structure constants and is by an appropriate choice of basis completely antisymmetric. We wish to make the symmetry local by introducing gauge fields. To this end we introduce a covariant derivative $D_\mu = \partial_\mu - igA^a_\mu\theta^a$ and study the local transformation $\psi \to e^{i\alpha^a\theta^a}\psi$

$$\mathcal{L} \to \bar{\psi}e^{-i\alpha^a\theta^a}\left[i\gamma^\mu(\partial_\mu - igA^a_\mu\theta^a) - m\right]e^{i\alpha^a\theta^a}\psi. \tag{1.37}$$

The mass term commutes with the transformation and is of no importance to what follows. We will therefore neglect it in further calculations. Assuming α^a to be infinitesimal, we expand the transformation to first order in α^a

$$\bar{\psi}(1 - i\alpha^a\theta^a)i\gamma^\mu(\partial_\mu - igA^a_\mu\theta^a)(1 + i\alpha^a\theta^a)\psi. \tag{1.38}$$

Next we attempt to commute the transformation on ψ past the Dirac operator. Term by term, we have

$$\partial_\mu(1 + i\alpha^a\theta^a)\psi = (1 + i\alpha^a\theta^a)\partial_\mu\psi + i(\partial_\mu\alpha^a)\theta^a\psi, \tag{1.39}$$

$$igA^b_\mu\theta^b(1 + i\theta^a\alpha^a) = (1 + i\alpha^a\theta^a)igA^b_\mu\theta^b + ig\alpha^aA^b_\mu f^{abc}\theta^c. \tag{1.40}$$

Having done this, we multiply together the terms containing α, discarding terms of order α^2 we obtain the transformed Lagrangian

$$\mathcal{L} \to \bar{\psi}i\gamma^\mu(\partial_\mu - igA^a_\mu\theta^a + i(\partial_\mu\alpha^a)\theta^a - ig\alpha^aA^b_\mu f^{abc}\theta^c)\psi. \tag{1.41}$$

In order to have gauge invariance, the new terms must vanish in the transformation of the gauge field. We therefore demand that the gauge fields transform as

$$A^a_\mu \to A^a_\mu + \frac{1}{g}\partial_\mu\alpha^a + f^{abc}A^b_\mu\alpha^c. \tag{1.42}$$

In order to complete our derivation of the QCD Lagrangian, we need to add a kinetic term for the gauge fields. As was the case in our study of $U(1)$ gauge symmetry we would like a term quadratic in the energy-momentum tensor of the field, $\frac{1}{4}\mathrm{Tr}[G_{\mu\nu}G^{\mu\nu}]$. However, the energy-momentum tensor we used for $U(1)$ is not gauge invariant here due to the noncommuting generators. D_μ on the other hand is gauge invariant and so we may attempt the following definition

$$G_{\mu\nu} \equiv \frac{i}{g}[D_\mu, D_\nu], \tag{1.43}$$

which should then also be gauge invariant. Calculating this quantity yields

$$G_{\mu\nu} = (\partial_\mu A^a_\nu - \partial_\nu A^a_\mu + gf^{abc}A^b_\mu A^c_\nu)\theta^a \tag{1.44}$$

We now utilise the property $\mathrm{Tr}[\theta^a\theta^b] = \delta^{ab}$ and write $G_{\mu\nu} = G^a_{\mu\nu}\theta^a$ to write the QCD Lagrangian

$$\mathcal{L} = \bar{\psi}_i(i\gamma^\mu D_\mu - m_i)\psi_i + \frac{1}{4}G^a_{\mu\nu}G^{a\mu\nu}. \tag{1.45}$$

A few comments are in order. Firstly, note that we are now summing over $i = 1, \ldots, 6$ quark fields and their corresponding masses m_i. Secondly, we observe that in the case of Abelian gauge theories, $f^{abc} = 0$ and thus we recover the energy-momentum tensor from the section on $U(1)$ gauge symmetry. The non-Abelian term $gf^{abc}A^b_\mu A^c_\nu$ in $G_{\mu\nu}$ gives rise to pure gluon-gluon interactions. We obtain three-gluon and four-gluon interaction terms of the form

$$gf^{abc}A^b_\mu A^c_\nu\partial^\mu A^{a\nu}, \tag{1.46}$$

$$g^2f^{abc}f^{ade}A^b_\mu A^c_\nu A^{d\mu}A^{e\nu}. \tag{1.47}$$

These interactions are illustrated diagrammatically in Figure 1.4.

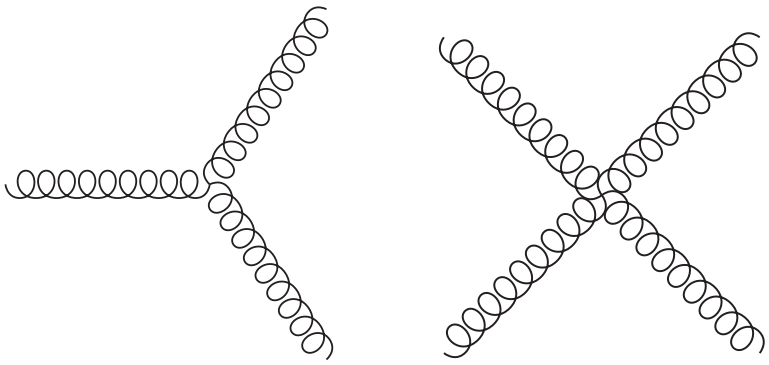

(a) Three-gluon interaction vertex (b) Four-gluon interaction vertex

Figure 1.4: Diagrammatic representation of the three- and four-gluon interaction vertices

1.2.2 Chiral symmetry breaking

Of particular interest to the study of pion condensation is chiral symmetry. If the masses of the up and down quark are exactly zero, QCD allows for a $U(2)\times U(2)$ symmetry. The construction of this symmetry is as follows: take the QCD Lagrangian for the up and down quark (the u and d fields, respectively)

$$\mathcal{L} = \bar{u}\left(i\gamma^\mu D_\mu - m_u\right)u + \bar{d}\left(i\gamma^\mu D_\mu - m_d\right)d + \frac{1}{4}\mathrm{Tr}[G^a_{\mu\nu}G^{a\mu\nu}]. \tag{1.48}$$

The kinetic term of the gluon field is of no importance to this derivation, so we will discard it. Suppose now that $m_u = m_d = 0$. These quark masses are certainly small compared to the other quark masses – the u and d mass both being smaller than 5 MeV when the next smallest mass is that of the strange quark at approximately 104 MeV – and at high energies their masses might become negligible, in this case the Lagrangian exhibits chiral symmetry. We now rewrite the fields in terms of their left- and right-handed components, $u = u_L + u_R$ where

$$u_L = \frac{1-\gamma^5}{2}u, \tag{1.49}$$

$$u_R = \frac{1+\gamma^5}{2}u. \tag{1.50}$$

And similarly for the d-field. Due to the fact that $(\gamma^5)^2 = 1$ as well as the anticommutation relation $\{\gamma^5, \gamma^\mu\} = 0$,

$$u_L\gamma^\mu D_\mu u_R = 0 \tag{1.51}$$

What remains in the Lagrangian are the diagonal elements

$$\mathcal{L} = i\bar{u}_L\gamma^\mu D_\mu u_L + i\bar{u}_R\gamma^\mu D_\mu u_R + i\bar{d}_L\gamma^\mu D_\mu d_L + i\bar{d}_R\gamma^\mu D_\mu d_R. \tag{1.52}$$

We arrange the left- and right-handed fields into doublets $L = \begin{pmatrix} u_L \\ d_L \end{pmatrix}$ to obtain

$$\mathcal{L} = iL^\dagger\gamma^\mu D_\mu L + iR^\dagger\gamma^\mu D_\mu R. \tag{1.53}$$

The remaining Lagrangian is invariant under unitary transformations of the doublets, thus yielding a $U(2)_L \times U(2)_R$ symmetry, where the subscripts refer to the L and R doublets. Exploiting that $U(2) \equiv SU(2)\times U(1)$, we may write the overall symmetry as $SU(2)_L \times SU(2)_R \times U(1)_A \times U(1)_V$. The A and V stand for axial and vector symmetry respectively, and stem from a decomposition of the $U(1)_L$ and $U(1)_R$ symmetry into simultaneous phase transformations in either the same or opposite directions for L and R. The $U(1)_V$ symmetry corresponds to conservation of quark number, as seen previously. If we choose to preserve the $U(1)_V$ symmetry, then the $U(1)_A$ symmetry is broken by what's known as the chiral anomaly.

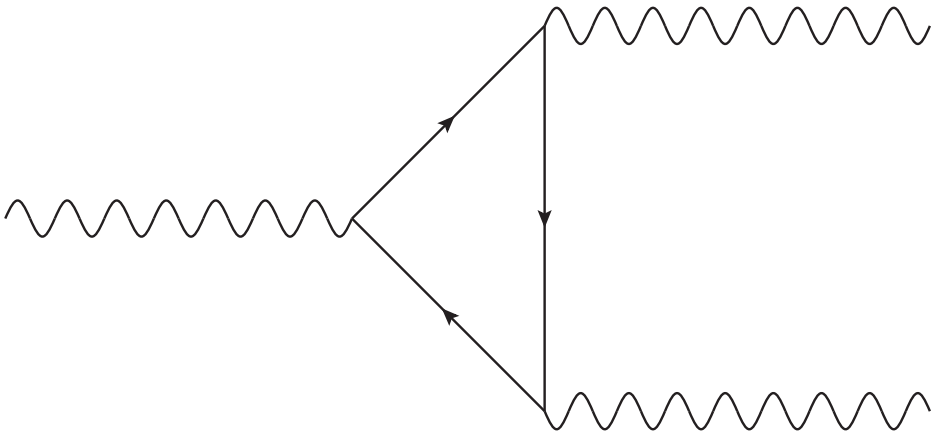

Figure 1.5: The triangle diagram, originally studied in connection with the process $\pi^0 \to \gamma\gamma$. This diagram gives rise to the chiral anomaly.

The chiral anomaly has been the subject of much study since its discovery in 1969 by Adler, Jackiw and Bell [27, 28]. Strictly speaking, the word anomaly is a bit of a misnomer since there is no symmetry in the first place. To be precise, if we choose to preserve the $U(1)_V$ symmetry, then the $U(1)_A$ symmetry is only a symmetry of the classical action, not of the quantum field theory. This is due to a change in the measure $\mathcal{D}\phi$ in the generating functional [9] of the path integral formalism (we derive the generating functional in Sec. 2.2). The chiral anomaly thus seems like a violation of the aforementioned $U(1)_A$ symmetry, corresponding to the phase transformation $\psi \to e^{i\alpha\gamma^5}\psi$, which has its root in the dynamics of QCD. The origin of the anomaly is the triangle diagram, illustrated in Fig. 1.5. This was originally studied in the context of the decay $\pi^0 \to \gamma\gamma$, prior to the formulation of QCD, as a consequence of which the original papers are formulated in a rather different manner to what modern formalism affords us. Today we view the chiral anomaly as being due to instantons breaking the conservation of the chiral charge, a view proposed in the late 1970s [29] and elaborated upon over the next decades [30], as well as tested against lattice QCD calculations [31].

The remaining $SU(2)_L \times SU(2)_R$ chiral symmetry is spontaneously broken by the appearance of what is referred to as a chiral condensate, retaining only an $SU(2)$ isospin symmetry among the up and down quarks [32]. Furthermore, since the up and down quark masses are not zero, the symmetry is explicitly broken. The up and down quark masses are – however – very light, both being below 5 MeV and so the symmetry is broken softly and we expect to retain some of the behaviour predicted by Goldstone's theorem. Specifically, we expect what is known as pseudo-Goldstone bosons, very light bosons which would be massless if the symmetry were exact. Since there are three generators of $SU(2)$, we expect three of these pseudo-Goldstone bosons, the pions [26, 33].

1.2.3 Pions

Pions are mesons, i.e. bound states of a quark and an antiquark. Specifically pions are the lowest-energy mesons formed by the up and down quarks. They are spinless, and very light, with the charged pion masses being approximately 139 MeV. This light mass is surprising when comparing the pions to other mesons, and is understood to be due to the role of the pions in chiral symmetry breaking.

The existence of pions was predicted prior to their discovery by Yukawa, in an attempt to describe the properties of the mediator particle of quantum chromodynamics. To account for the short range that the strong force had been found to have, Yukawa deduced that unlike the photon the messenger particle of the strong force must be massive. The potential energy of a force mediated by massive particles are subject to an exponential falloff, roughly behaving as

$$V(r) = \frac{e^{-mr}}{r}. \tag{1.54}$$

Yukawa predicted the mass of this messenger particle to be nearly 30 times that of the electron [34]. This was a mass range far larger than the known electron mass, and yet much smaller than the smallest known

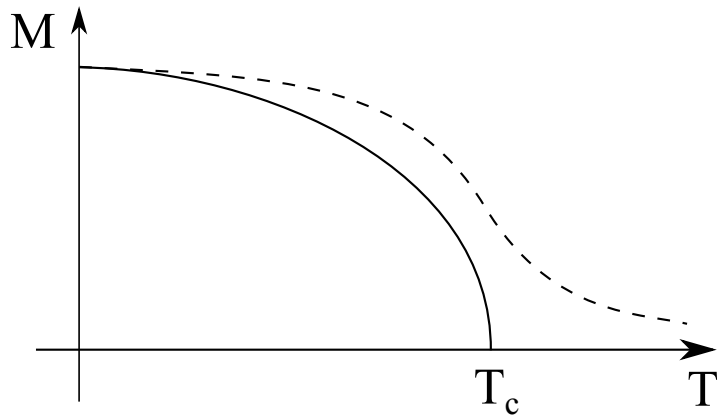

Figure 1.6: Sketch of the magnetization M of a ferromagnet as a function of the temperature T. The solid line is without the presence of an external magnetic field and reaches zero at a finite temperature T_c. The dashed line is with an external magnetic field.

baryon masses. Yukawa therefore named his particle a meson, for middle weight. After some confusion regarding the muon – which it later transpired was a lepton – the best candidate for Yukawa's meson was the pion.

Pions were discovered a few years after being predicted by Yukawa. This was prior to particle accelerator experiments, and so the pions were discovered in the study of cosmic rays by Powell, Lattes, Occalini *et al* [35]. Cosmic rays colliding with particles in the atmosphere causes a constant flux of pions heading towards earth's surface, and these were captured in experiments in which photographic plates were placed on high-altitude mountains. By this method, the pions were detected mainly due to their propensity to decay into muons, which would leave very discernible tracks on the plates [14].

Our interest in pions in this thesis is mainly due to their behaviour as pseudo-Goldstone bosons of chiral symmetry breaking. In the absence of a baryon chemical potential the up and down quarks will bind together in pions. Provided the energy scale is sufficiently low to exclude a large production of strange quarks (which have a mass of roughly 104 MeV), the dynamics of the pions along with another spinless meson called the sigma meson becomes a good effective theory of QCD. We will examine the reasoning behind this approximation in greater detail in the beginning of Chapter 3.

1.2.4 A short note on phases and phase transitions

Phase diagrams and phase transitions are well-known concepts from thermal physics. Substances may be in several distinct states such as solid, liquid, gas and plasma. One may transition between these by altering, say, the temperature or the pressure the substance is subjected to. In this manner, we may for instance boil water in order to have it transition from its liquid to its gaseous form.

Nuclear matter may also be in very distinct states, which we may describe in the language of phases and phase transitions. A phase is defined by certain symmetries being present or broken in the equilibrium state of nuclear matter, subject to appropriate parameters such as temperature and chemical potential. Consequently, a phase transition is the restoration or breaking of symmetries in the equilibrium state when continuously altering the parameters which the equilibrium state is subject to. We define an order parameter as some parameter which describes the restoration or breaking of a symmetry, for instance by being zero when the symmetry is present in the equilibrium state and nonzero when the symmetry is broken. An example of such an order parameter is the magnetisation of a ferromagnetic material. At zero temperature and external magnetic field, the material possesses a nonzero magnetisation, breaking $O(3)$ orthogonal[2] symmetry by giving the system a preferred direction. However, by increasing the temperature, the magnetisation of the material becomes zero at some critical temperature T_c and thus the $O(3)$ symmetry is restored.

If the order parameter at a phase transition is discontinuous, we refer to the transition as being first order. If – however – the order parameter at a phase transition is continuous, but its derivative

[2]We will sometimes refer to this as rotational symmetry. It is not entirely correct to do so. The rotation group in three dimensions is $SO(3)$, $O(3)$ includes reflections of the axes.

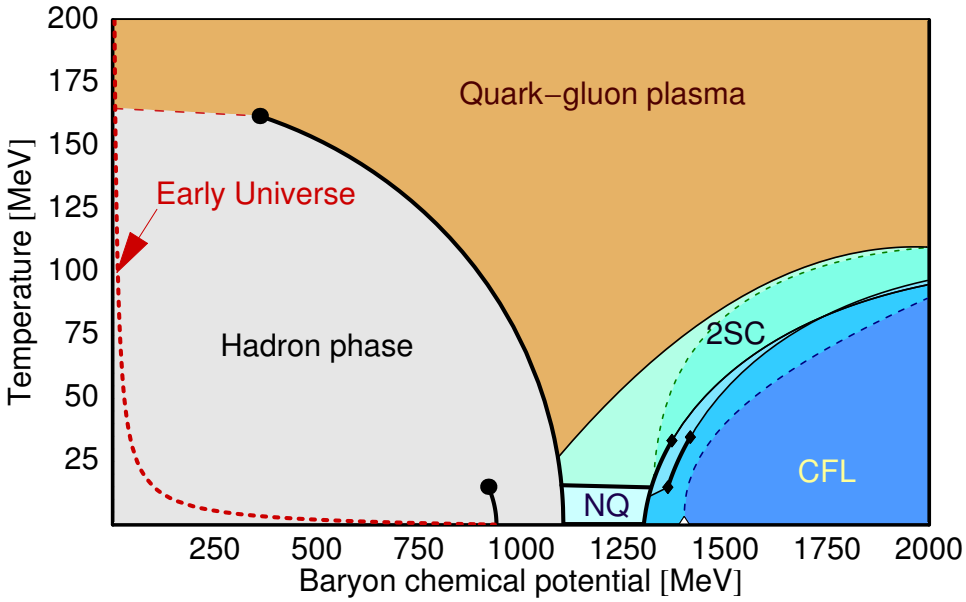

Figure 1.7: The phase diagram of QCD

is not, the phase transition is second order. Finally, if both the order parameter and its derivative is continuous the transition is referred to as a cross-over. In a cross-over phase transition there is no distinct critical temperature, but rather a range of temperatures in which the order parameter changes rapidly. We shall see examples of both first and second order transitions in our study of the linear sigma model, but an illustration is currently afforded us by the aforementioned magnetisation of a ferromagnetic material. Without an external magnetic field, the magnetisation goes to zero in a continuous manner, a second-order phase transition [36]. However, when applying an external magnetic field to the material, the magnetisation does not transition entirely to zero, but changes rapidly from its high original value to some small equilibrium value in a cross-over transition. A schematic of this behaviour is illustrated in Fig. 1.6.

1.2.5 The phase diagram of QCD

Because of the aforementioned asymptotic freedom, QCD scales very differently with energy than the other components of the standard model. Due to this there has been a large effort to map out the QCD phase diagram during the past decade [26, 32, 33, 37, 38]. In experiments at the Large Hadron Collider one hopes to be able to probe the so-called quark-gluon plasma phase, a phase in which the strong nuclear force is sufficiently weakened that the quarks and gluons behave like a "quark soup", characterised by the restoration of chiral symmetry. For a long time it was thought that this state was close to an ideal gas of quarks and gluons, however experiments at the Relativistic Heavy Ion Collider in Brookhaven seem to indicate that the physics of the quark-gluon plasma close to the critical temperature are better accommodated by models of a strongly interacting liquid [39]. Another area of high interest is the so called colour-flavour-locked (CFL) phase. This phase occurs at high densities and low temperatures, candidate systems for such conditions are the cores of very heavy neutron stars. However, it is as of yet not known whether the cores of neutron stars reach such high densities [38]. It is believed that under such extreme conditions, quarks may bind together to form Cooper pairs of colour charge, creating a colour superconducting superfluid [40]. Very recently, observations of the cooling rate of the neutron star Cassiopeia A has given the first tentative indications of superfluidity in neutron stars [41].

Fig. 1.7 shows an overview of our current understanding of the phase diagram of QCD. The phase diagram is here drawn as a function of baryon chemical potential – i.e. baryon density – and temperature. In the lower left corner – at low temperature and baryon chemical potential – we have hadronic matter. This phase is characterised by confinement and broken chiral symmetry, allowing the formation of nucleons. Quarks are bound in baryons and mesons forming droplets of nuclear matter surrounded by vacuum. At very low chemical potential and temperature we have what is essentially vacuum. Increasing the chemical

potential to $\mu \approx 924$ MeV we reach a transition from a gaseous to a liquid phase. Due to the interplay between repulsive and attractive nuclear forces, the ground state of nuclear matter at $T = 0$ is at these densities [32]. Transitioning further into the liquid state we reach the densities of neutron stars [38].

Moving along the temperature axis, the chiral condensate will eventually cross over and we will at some critical temperature $T_c \approx 170$ MeV reach the aforementioned quark-gluon plasma phase. In this phase, chiral symmetry is restored as asymptotic freedom becomes dominant, we refer to this transition as the *deconfinement transition*. At low nuclear chemical potential (and hence low density), this phase transition is – due to the explicit breaking of chiral symmetry by nonzero quark masses – not discontinuous but rather a crossover transition [33]. Upon increasing the chemical potential, this crossover period shortens until we recover a second-order phase transition at a critical point, marked by a dot in Fig. 1.7. Further increasing the density, T_c decreases, reaching zero at a chemical potential $\mu \approx 1100$ MeV.

In the lower right corner, at high baryon chemical potential and low temperature we reach the CFL phase. However, at slightly lower chemical potentials is a deconfined state which is non-superconducting. This state is referred to as normal quark matter (NQ), and is characterised by hadronic matter having such high densities that the nuclei overlap and the quarks are deconfined. Fig. 1.7 shows two colour superconducting states, the Two-colour superconducting (2SC) and CFL phase. The CFL phase is characterised by colour superconductivity, in which the up, down and strange quark participate in Cooper pairing of all three colours. By contrast, at slightly lower densities the strange quark's large mass prohibits it from participating in Cooper pairing, and thus the up and down quarks form Cooper pairs of two colours, say red and green [38]. In terms of symmetry, the CFL phase and the 2SC phase are invariant under simultaneous rotation of quark flavours and colours ($SU(3)$ and $SU(2)$, respectively), but not independent rotations. The flavours and colours are thus locked to one another in the pairing process, giving rise to the term colour-flavour locking. The Cooper pairs are spinless pairs of quarks with opposite momenta, thus the pairs share the same chirality. Due to the locking of colour and flavours, a colour rotation must be accompanied by a flavour rotation, which gives rise to chiral symmetry breaking [38].

In this thesis we will study something of relevance to the NQ phase, present at high baryon density but before entering the CFL phase. It is known that in this phase a pion condensate may arise in the presence of a preference for a certain charge, characterised by an isospin chemical potential. This charge preference introduces another axis to the phase diagram. With physical pion masses, pion condensation is known to arise only when the isospin chemical potential is larger than the pion mass [6, 7, 42, 43]. Such pion condensation at nonzero isospin chemical potential is thought to occur within neutron stars [44], prompting an interest in this part of the QCD phase diagram. We will study this phenomenon in an idealised model of zero baryon chemical potential and finite chemical potential. Whereas this is far from the baryon density of neutron stars, it allows us to compare our results with those of lattice QCD, which is intractable at nonzero baryon chemical potentials [6, 45]. Thus, the domain of zero baryon chemical potential and finite isospin chemical potential allows us the opportunity to compare a wide range of effective approximations with lattice computations, yielding insights into both the phase diagram of QCD and effective field theories.

Chapter 2

The basics of thermal field theory

Before proceeding to discuss pion condensation it is necessary to introduce the basic concepts which will be used throughout our treatment of the linear sigma model. We will start with the partition function of statistical mechanics, a probabilistic estimator of the most likely state of a system with a characteristic energy scale T. From there we will move on to quantum field theory and the path-integral formalism, before combining path-integrals and the partition function to obtain the generating functional of thermal field theory. We will briefly discuss chemical potentials, before proceeding to derive the effective potential – a generating functional for connected Green's functions – and finish by making a few notes on renormalisation and regularisation.

2.1 Partition function

Arguably the most fundamental quantity in statistical mechanics is the partition function Z. It is based on a maximum likelihood estimate of probabilities for an ensemble to be in a state j with energy E_j, when the system is at the temperature T. For the canonical ensemble it is defined as [36]

$$Z \equiv \mathrm{Tr}\left[e^{-\beta \hat{H}}\right]. \tag{2.1}$$

Tr denotes a trace over all available states and $\hat{H}$ is the Hamiltonan operator. An equivalent formulation of the partition function is thus that if $|\phi\rangle$ is a complete set of energy eigenstates with energies E_ϕ, then

$$Z = \int d\phi \, \langle\phi| e^{-\beta \hat{H}} |\phi\rangle = \int d\phi e^{-\beta E_\phi} \tag{2.2}$$

β is $1/T$, and so T generally describes a characteristic energy scale of the system. For example, the equipartition theorem states that for every quadratic term in the Hamiltonian of the system, there corresponds a term $\frac{1}{2}T$ in the average energy, yielding the average energy $\frac{3}{2}NT$ for a nonrelativistic ideal gas with N particles [36]. The probability of finding the system in the state ϕ is simply

$$P_j = \frac{e^{-\beta E_\phi}}{Z}. \tag{2.3}$$

The ensemble is fully described by the partition function, we can therefore derive any equilibrium quantity from it. For instance the average energy $\langle E \rangle$ and Helmholtz free energy F are given by [36]

$$\langle E \rangle = -\frac{\partial \ln Z}{\partial \beta}, \tag{2.4}$$

$$F = -\frac{\ln Z}{\beta}. \tag{2.5}$$

If the number of particles in the ensemble is not fixed, we must turn to the grand canonical partition function Θ. The grand canonical ensemble is characterised by both the temperature and the chemical potential μ. The latter affects the likelihood of there being a given number of particles N_i of type i in the

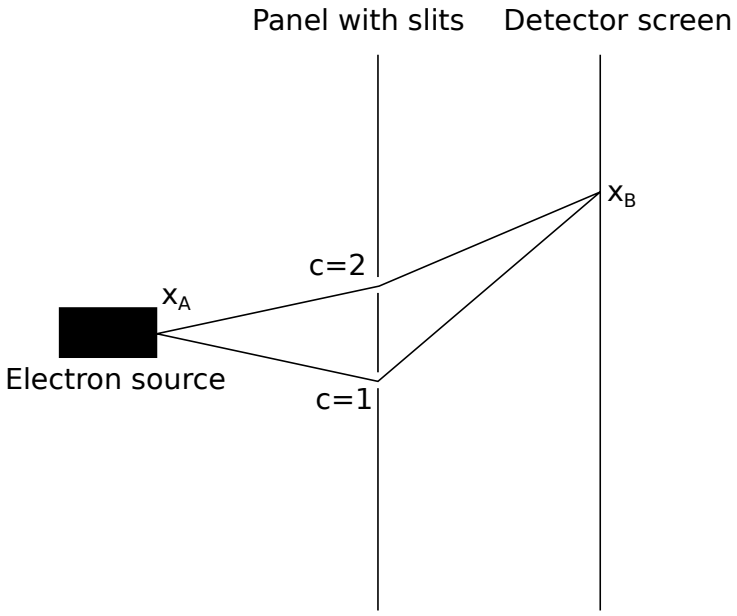

Figure 2.1: Schematic of the double slit experiment.

system. The grand canonical partition function is found by adding a chemical potential term $-\mu_i N_i$ to the Hamiltonian in the canonical partition function as follows

$$\Theta \equiv \mathrm{Tr}\left[e^{-\beta(\hat{H}-\mu_i N_i)}\right]. \tag{2.6}$$

The above trace is now over both particle types and energy states. In quantum field theory, we generally abstract the notion of the particle number N_i to be freely chosen charges, as will be shown in the section on the chemical potential (2.6).

2.2 Path integrals

Turning to quantum field theory, we will be utilising the path-integral formalism. The formalism is derived in a 1948 paper by Feynman [46], we will here use a more modern approach akin to what can be found in current textbooks on quantum field theory [9, 10]. Much like the partition function of statistical mechanics, a system in quantum field theory can be fully described by an integral over all space-time paths allowed by the system. This behaviour hinges upon the completeness relation of quantum mechanics, namely that if $|c\rangle$ is some complete set of states, then

$$\mathbb{1} = \int dc\, |c\rangle \langle c| . \tag{2.7}$$

The time evolution of a non-relativistic quantum mechanical state $|x\rangle$ is governed by the Schrödinger equation

$$\frac{\partial}{\partial t}|x\rangle = \hat{H}|x\rangle . \tag{2.8}$$

In the case of relativistic quantum mechanics it is more convenient to work with a quadratic equation such as the Klein-Gordon equation to avoid the operator $\hat{H} = \sqrt{-\nabla^2 + m^2}$. We shall restrict ourselves to the non-relativistic case for this derivation and later generalise our results to include relativistic fields.

If we observe a particle to be in the state $|x_A\rangle$ at some time t_0, then the wave function of the particle at some later time t_1 is $e^{-i\int_{t_0}^{t_1}\hat{H}\,dt}|x_A\rangle$. A further simplification is available if we assume the Hamiltonian to be time-independent, whereupon the time evolution of the state reduces to $e^{i\hat{H}(t_1-t_0)}|x_A\rangle$. The probability of observing the system in the state $|x_B\rangle$ at time t_1 is then

$$P_{AB}(t_0,t_1) = \left|\langle x_B| e^{i\hat{H}(t_1-t_0)}|x_A\rangle\right|^2 . \tag{2.9}$$

If we recall the famous double-slit experiment (Fig. 2.1) as an example, and let $|x_A\rangle$ be our initial state, $|x_B\rangle$ be the state of a particle present at the detector and $|c\rangle$ be a set of states inside the slits. Furthermore, assume that the particle passes through the slits at some time τ. Our time-dependent probability of observation at point x_B is then

$$P_{AB}(t_0, t_1, \tau) = \left| \sum_c \langle x_B | e^{i\hat{H}(t_1-\tau)} |c\rangle \langle c| e^{i\hat{H}(\tau-t_0)} |x_A\rangle \right|^2 . \tag{2.10}$$

The above formula is based on the assumption that the states $|c\rangle$ that are summed over form a complete set of available states for the particle at the time τ. One may of course integrate over τ to remove the dependence on the time when the particle passes through the slit.

There is a straightforward generalisation of the double-slit experiment, namely that the vacuum can be viewed as an infinitely dense grid of slits. This generalisation forms the basis of the path-integral formalism. For simplicity, we restrict ourselves to one particle in one dimension, subject to a time-independent potential $V(\hat{x})$. The generalisation to several particles and dimensions is straightforward and will be done when we proceed to quantum field theory. We start from the probability amplitude of Eq. (2.9), and divide it up into $N+1$ intermittent states at equal time intervals $\delta t = \frac{t_2-t_1}{N+1}$. For the purpose of illustration, we choose the basis of position eigenstates for the the initial, intermittent and final states. This yields the formula

$$P_{AB} = \left| \int dx_1\, dx_2 \cdots dx_N \langle x_B | e^{-i\hat{H}\delta t} |x_N\rangle \langle x_N| \cdots |x_1\rangle \langle x_1| e^{-i\hat{H}\delta t} |x_A\rangle \right|^2 . \tag{2.11}$$

The probability amplitude is now governed by the time-evolution from the initial state via all possible intermediate states at the time intervals δt. Our Hamiltonian is $\hat{H} = \frac{\hat{p}^2}{2m} + V(\hat{x})$, we wish to express this in terms of momentum and position eigenvalues. To this end we insert a complete set of momentum eigenstates into the intermittent amplitudes

$$\langle x_i | e^{-i\delta t\hat{H}} |x_{i-1}\rangle = \int dp \langle x_i | p\rangle \langle p| e^{-i\delta t\hat{H}} |x_{i-1}\rangle . \tag{2.12}$$

The inner product between the momentum and position eigenstate is the well known $\frac{e^{ipx_i}}{\sqrt{2\pi}}$. We Taylor expand the exponential in powers of δt to obtain

$$\langle x_i | e^{-i\delta t\hat{H}} |x_{i-1}\rangle = \int \frac{dp}{\sqrt{2\pi}} e^{ipx_i} \langle p| 1 - i\delta t\hat{H} + O(\delta t^2) |x_{i-1}\rangle . \tag{2.13}$$

It can be shown that $\hat{H}$ can always be made normal-ordered, i.e. all products of momentum and position operators are on the form $\hat{p}^n\hat{x}^m$. Given normal ordering, we are at liberty to let $\hat{H}$ act on the position and momentum eigenvectors and recover our exponential,

$$\langle x_i | e^{-i\delta t\hat{H}} |x_{i-1}\rangle = \int \frac{dp}{\sqrt{2\pi}} e^{ip(x_i-x_{i-1})} e^{-i\delta t(\frac{p^2}{2m}+V(x_{i+1}))} . \tag{2.14}$$

The integral is a simple Gaussian integral which we may now evaluate. Our final result is

$$\langle x_i | e^{-i\delta t\hat{H}} |x_{i-1}\rangle = \sqrt{\frac{im}{\delta t}} e^{i\left[\frac{m}{2}\frac{(x_i-x_{i-1})^2}{\delta t} - \delta t V(x_{i-1})\right]} . \tag{2.15}$$

The prefactor is divergent and inifinite in the continuum limit. This reflects a poor choice of normalisation, and so we discard it [10]. We may now take the continuum limit, this implies $x_i \to x(t)$, $\frac{x_i-x_{i-1}}{\delta t} \to \dot{x}$, $\delta t \to dt$ and so on. Our initial transition amplitude can now be written as

$$\langle x_B | e^{i\hat{H}(t_2-t_1)} |x_A\rangle = \int dx_1 \cdots dx_N e^{i\int_{t_1}^{t_2} dt \frac{m}{2}\dot{x}^2 - V(x)} . \tag{2.16}$$

The exponent on the right hand side is the time integral of the Lagrangian $L(x, \dot{x})$, namely the classical action S. We write the numerous integrals as a functional integral, utilising the notation $\int dx_1 \cdots dx_N \to$

$\int \mathcal{D}x$, where it is understood that we integrate over all functions $x(t)$ that satisfy the boundary conditions $x(t_1) = x_A$ and $x(t_2) = x_B$. The transition amplitude is then

$$\int \mathcal{D}x e^{i\int_{t1}^{t2} dtL(x,\dot{x})} \equiv \int \mathcal{D}x e^{iS[x]} \tag{2.17}$$

We have now arrived at the basis of the path-integral formalism, and an alluringly simple picture presents itself. The probability amplitude of a system transitioning from one state to another is the result of the interference of all time evolutions (or paths) of the system which leads to the given outcome. Specifically, it is the sum of complex numbers of equal magnitude with phase dictated by the action associated with each path. This description is equivalent to the more usual formulation of quantum mechanics in terms of the Schrödinger equation [46].

Generalising to quantum field theory is usually done by using the Lagrangian density in the action, i.e.

$$S[\phi] = \int d^4x \mathcal{L}[\phi, \partial_\mu \phi]. \tag{2.18}$$

The functional integral is then over all "paths" of the field; all intermittent field configurations which the field may assume.

2.2.1 Expectation values and the N-point function

The path-integral formalism can be used to calculate transition amplitudes of various operators. This is clearest in the Heisenberg picture, where states are time-independent, but eigenvectors of time-dependent operators may be time-dependent. Therefore, let $\hat{x}$ and $\mathcal{O}(\hat{x}, t)$ be Heisenberg picture operators with $\hat{x}$ having eigenvectors $|x, t\rangle$, we then seek to calculate the transition amplitude

$$\langle x_B, t_2 | \mathcal{O}(\hat{x}, t) | x_A, t_1 \rangle . \tag{2.19}$$

We insert two complete sets of states into the above transition amplitude to obtain

$$\langle x_B, t_2 | \mathcal{O}(\hat{x}, t) | x_A, t_A \rangle = \int dx_1 \, dx_2 \, \langle x_B, t_2 | x_2, t \rangle \langle x_2, t | \mathcal{O}(\hat{x}, t) | x_1, t \rangle \langle x_1, t | x_A, t_a \rangle . \tag{2.20}$$

We let $\mathcal{O}(\hat{x}, t)$ operate on $|x_1, t\rangle$, the result is a function $\mathcal{O}(x_1, t)$

$$\begin{aligned}
\langle x_B, t_2 | \mathcal{O}(\hat{x}, t) | x_A, t_A \rangle &= \int dx_1 \, dx_2 \, \langle x_B, t_2 | x_2, t \rangle \mathcal{O}(x_1, t) \langle x_2, t | x_1, t \rangle \langle x_1, t | x_A, t_a \rangle \\
&= \int dx_1 \, dx_2 \mathcal{O}(x_1, t) \langle x_B, t_2 | x_2, t \rangle \delta(x_1 - x_2) \langle x_1, t | x_A, t_a \rangle \\
&= \int dx_1 \mathcal{O}(x_1, t) \int_{x_A}^{x_1} \mathcal{D}x e^{iS[x]} \int_{x_1}^{x_B} \mathcal{D}x' e^{iS[x']} \\
&= \int_{x_A}^{x_B} \mathcal{D}x \mathcal{O}(x) e^{iS[x]}.
\end{aligned} \tag{2.21}$$

From this we may also obtain the vacuum expectation value of $\mathcal{O}$ by requiring normalization and setting appropriate boundary conditions

$$\langle \mathcal{O} \rangle = \frac{\int \mathcal{D}\phi \mathcal{O}(\phi) e^{iS[\phi]}}{\int \mathcal{D}\phi e^{iS[\phi]}}. \tag{2.22}$$

Due to the explicit time-dependence of the path integral formalism, any operator expectation value evaluated is automatically time-ordered [9]. We thus have the general formula

$$\langle T \{\mathcal{O}_1, \mathcal{O}_2, \cdots, \mathcal{O}_N\} \rangle = \frac{\int \mathcal{D}\phi \mathcal{O}_1 \mathcal{O}_2 \cdots \mathcal{O}_N e^{iS[\phi]}}{\int \mathcal{D}\phi e^{iS[\phi]}}. \tag{2.23}$$

T represents time-ordering; the arrangement of operators according to the time at which they operate on the fields. From this we arrive at a simple way of calculating N-point correlation functions; transition amplitudes between field configurations. Let $\hat{\phi_H}(x_i)$ be Heisenberg picture field operators, the time-ordered N-point correlation function is then [9, 10]

$$\langle \Omega | T\{\phi_H(x_1), \phi_H(x_2), \cdots, \phi_H(x_N)\} | \Omega \rangle = \frac{\int \mathcal{D}\phi \phi(x_1) \phi(x_2) \cdots \phi(x_N) e^{iS[\phi]}}{\int \mathcal{D}\phi e^{iS[\phi]}}. \tag{2.24}$$

We therefore define the generating functional $\Phi[J]$

$$\Phi = \int \mathcal{D}\phi e^{iS[\phi]+i\int d^4x J(x)\phi(x)}. \tag{2.25}$$

The purpose of the current term $J(x)$ is to obtain a manner of generating n-point functions of quantum fields by means of functional differentiation. For instance, the probability amplitude of a field transitioning from some state $\phi(x_1)$ to some later state $\phi(x_2)$ is

$$\langle\Omega|T\{\phi_H(x_1),\phi_H(x_2)\}|\Omega\rangle = -\frac{1}{\Phi}\frac{\delta^2\Phi}{\delta J(x_2)\delta J(x_1)}\bigg|_{J(x)=0}. \tag{2.26}$$

This is the two-point correlation function. In a free field theory it is simply the free propagator of the fields. In field theories with interaction terms, the two-point function will usually be the sum of the free propagator, loop corrections to the propagator and various disconnected probability amplitudes. We will discuss the topic of loop corrections in the following section.

2.3 Feynman diagrams by example

We are now ready to introduce the concept of Feynman diagrams. These diagrams are a useful tool in bypassing much of the path-integral formalism and proceeding to directly calculate probability amplitudes. We will introduce these diagrams somewhat indirectly through the example of scalar ϕ^4-theory with one field. The generating functional of this theory is

$$\Phi[J] = \int \mathcal{D}\phi e^{i\int d^4x \frac{1}{2}\phi[\Box-m^2]\phi+\frac{\lambda}{4!}\phi^4+J\phi}. \tag{2.27}$$

$\Box$ is a shorthand for $\partial_\mu\partial^\mu = \frac{\partial^2}{(\partial t)^2} - \nabla^2$. With the exception of the interaction term, the generating functional is Gaussian, and can therefore be evaluated directly. To this end we define the action of the free theory as

$$\begin{aligned} S_F[\phi] &\equiv \frac{1}{2}\int d^4x\left[\phi(x)\left[\Box - m^2\right]\phi(x) + 2J(x)\phi(x)\right] \\ &= \frac{1}{2}\int d^4x\, d^4y\phi(x)\left[\Box - m^2\right]\delta(x-y)\phi(y) + \int d^4x J(x)\phi(x). \end{aligned} \tag{2.28}$$

We now series expand the interaction term and use functional derivatives to replace the field ϕ with the current, thereby obtaining

$$\begin{aligned} \Phi[J] &= \left(1 + i\lambda\int d^4z\frac{\delta^4}{(\delta J(z))^4} + \cdots\right)\int \mathcal{D}\phi e^{iS_F[\phi]} \\ &= e^{i\lambda\int d^4z\frac{\delta^4}{(\delta J(z))^4}}\int \mathcal{D}\phi e^{iS_F[\phi]}. \end{aligned} \tag{2.29}$$

We may now perform the functional integral over ϕ. To do this, we discretise our functional integral into N steps such that $\phi(x) \to \phi_i$ and $J(x) \to J_i$. In so doing, we must discretise the Klein-Gordon operator in the Lagrangian, so let M_{ij} be a Matrix discretisation of $i(-\Box+m^2)\delta(x-y)$. The generating functional becomes

$$\int d\phi_1\, d\phi_2\cdots d\phi_N e^{-\frac{1}{2}\phi_i M_{ij}\phi_j + iJ_i\phi_i}. \tag{2.30}$$

In the above we have utilised the Einstein summation convention for all repeated indices. This integral is a simple product of Gaussian integrals if M_{ij} is diagonal. In general this is not the case, but supposing M_{ij} is orthonormally diagonaliseable we may write $M_{ij} = O_{ki}D_{kl}O_{lj}$, with D a diagonal matrix and O an orthonornormal transformation matrix. We now perform a coordinate transform such that our new variables $\tau_i = O_{ij}\phi_j$ and $K_i = O_{ji}J_j$. If we utilise the diagonal property of $D_{ij} \equiv D_i\delta_{ij}$, our functional integral becomes

$$\int d\tau_1\, d\tau_2\cdots d\tau_N e^{-\frac{1}{2}D_i\tau_i^2 + iK_i\tau_i}. \tag{2.31}$$

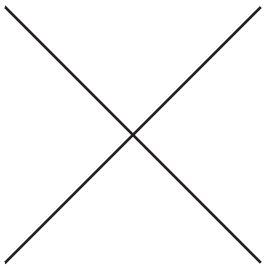

Figure 2.2: The primitive four-point vertex.

This integral can now be separated into N Gaussians and evaluated separately, after which we may transform back to our original coordinates. The result is

$$\prod_{i=1}^{N} \sqrt{\frac{2\pi}{D_i}} e^{-\frac{K_i^2}{2D_i}} = \sqrt{\frac{(2\pi)^N}{\mathrm{Det}M}} e^{-\frac{1}{2} J_i M_{ij}^{-1} J_j}. \tag{2.32}$$

Taking the continuum limit once again, we identify the constant in front of the exponential as $\Phi[J=0]$ and define

$$\Phi_0 \equiv \Phi[J=0] = \sqrt{\frac{(2\pi)^N}{\mathrm{Det}M}}. \tag{2.33}$$

This term represents vacuum energy; it is the sum of all possible interactions in a theory without sources or sinks. The matrix inverse M^{-1} becomes the Green's function of the Klein-Gordon operator in the continuum limit, identified by the relation

$$i(\Box - m^2) M^{-1}(x,y) = \delta(x-y). \tag{2.34}$$

We write the function $M^{-1}(x,y)$ as $D_0(x-y)$ due to Lorentz invariance. It is the propagator of the free Klein-Gordon theory. Examining the generating functional, it can now be written

$$\Phi[J] = \Phi_0 e^{\frac{i\lambda}{4!}\int d^4z \frac{\delta^4}{(\delta J(z))^4}} e^{-\frac{1}{2}\int d^4x\, d^4y J(x) D_0(x-y) J(y)}. \tag{2.35}$$

The two-point function can now be evaluated perturbatively in λ. To zeroth order in the perturbative expansion we obtain the promised free propagator

$$\langle\Omega| T\{\phi_H(x_1), \phi_H(x_2)\} |\Omega\rangle = D_0(x_1 - x_2) \tag{2.36}$$

We will sometimes refer to these lowest-order results as being *tree-level* results. Proceeding to first order in λ we obtain two additional terms in the two-point function,

$$\begin{aligned}\langle\Omega| T\{\phi_H(x_1), \phi_H(x_2)\} |\Omega\rangle = D_0(x_1 - x_2) + i\lambda \int d^4z D_0(x_1 - z) D_0(z-z) D_0(z - x_2) \\ + i\frac{\lambda}{4} \int D_0(x_1 - x_2) D_0(z-z) D_0(z-z) + O(\lambda^2).\end{aligned} \tag{2.37}$$

A pattern is now presenting itself: as we add more powers of λ we obtain more integrals over z, with four functional derivatives leading to four propagator arguments being z. The number of propagators containing terms that are not integrated over is determined by the number of functional derivatives we start with, for instance there are two in the above formula because we were calculating the two-point function. This lends itself well to a diagrammatic representation based on a simple principle, for each propagator $D(x,y)$, draw a line from x to y in your diagram. We see then that each integral over z implies that there are four lines terminating at z, which yields a primitive vertex like the one in Figure 2.2. Each integral over z also comes with a factor λ. If λ is a small parameter, this series expansion lends itself well to perturbation theory.

Such diagrams present a simple and alluring physical interpretation. When conducting an experiment, we are interested in a certain measurable outcome, say a scattering cross-section. Such events would be

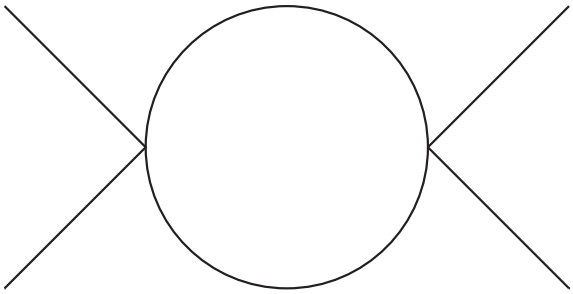

Figure 2.3: The lowest-order correction to the primitive four-point vertex.

the sum of all the terms in the series expansion which has a certain number of external legs, representing the initial and final states of the experiment. What happens between the initial and final state is not directly measured, but can involve any number of interactions. The primitive four-point vertex represents the interaction term in the Lagrangian, and directly describes the ways in which such interactions may take place. Thus we may give a quasi-physical interpretation of these diagrams as being all the possible interactions leading to a specific measurable outcome. It should be noted, however, that even in relatively simple field theories such as our example ϕ^4 theory there exists higher-order terms which are divergent, a topic which will be discussed in the section on renormalisation (2.8). Such divergences are cancelled by similar divergent corrections to the perturbation parameters, forcing the conclusion that both the bare diagrams and the perturbation parameters are non-physical.

Another point worthy of comment is that the perturbation expansion of the two-point function is now a series of *loop corrections*, which should be calculated to all orders in λ to yield exact results. We refer to such loop corrections as *self-energies* and write

$$D^{-1}(x-y) = D_0^{-1}(x-y) + \Pi[D]. \tag{2.38}$$

$\Pi[D]$ is the sum of all such loop- corrections to the propagator, and yields a correction to the the propagator. This correction may be momentum-dependent, but its momentum-independent component may be viewed as a correction to the particle masses. The same is true for all N-point functions, in particular the four-point function yields a perturbative expansion which at lowest order is simply the four-point vertex. Higher order corrections to the four-point function is referred to as *radiative corrections*, the first-order correction is illustrated in Fig. 2.3.

The real power of Feynman diagrams becomes clear with the introduction of drawing rules (or Feynman rules). These rules vary from theory to theory, depending on what interaction terms are present in the Lagrangian. The goal of these rules is to make it so one can draw all the diagrams which represent terms in the perturbation expansion, and no other diagrams. By doing this, we introduce a one-to-one correspondence between Feynman diagrams and terms in the perturbation expansion, allowing one to simply draw the possible diagrams corresponding to a desired outcome rather than calculating this perturbatively. Furthermore, the rules then instruct you on how to read an interaction amplitude from a diagram. For our simple Lagrangian, the Feynman rules are as follows:

- For each incoming or outgoing particle, draw a point.
- Draw all diagrams that connect these points, using lines and the four-point vertex.
- With each line, associate a propagator.
- With each four-point vertex, associate a factor $\frac{\lambda}{4!}\int d^4z$.
- Take care of symmetry factors; multiply an amplitude by the number of ways in which two endpoints can be interchanged without altering the diagram.

The second point above – requiring all points to be connected – is related to normalisation. As an example, observe that one of the terms in Eq. (2.37) contains a disconnected integral, namely a factor $\int d^4z D(0)D(0)$. By going to high enough powers in λ, we can add such terms to any other term in our correlation function. For this reason such disconnected terms add nothing to the probability amplitudes,

as they will simply disappear upon normalisation. This becomes clearer if we illustrate the various terms in (2.37) diagrammatically, as is done in Figure 2.4. The last term is a disconnected diagram corresponding to the vacuum energy from the spontaneous creation and destruction of particle-antiparticle pairs. In most calculations, such diagrams are of little interest, and hence we exclude them in the Feynman rules by requiring that all drawn diagrams are *connected*. In the following chapters we will be resumming large numbers of diagrams systematically. It will therefore be necessary to develop a generating functional for such connected Green's functions. We will elaborate on this concept in the section about effective potentials (2.7).

Figure 2.4: Diagrammatic representation of the two-point function to first order in λ

2.4 The partition function of quantum field theory

There is a remarkable similarity between the partition function of statistical mechanics and the generating functional in the path-integral formalism. Both are essentially summations over all possible states (or paths of states, in the case of the generating functional), weighted by the exponential of a characteristic quantity of the theory. The similarity is even clearer if we restrict ourselves to a finite time interval, the time evolution of a field can then be represented in the path integral formalism as

$$\langle \rho_1 | \, e^{-i\hat{H}(t_2-t_1)} \, | \rho_2 \rangle = \int_{\rho_1}^{\rho_2} \mathcal{D}\phi e^{iS[\phi]}. \tag{2.39}$$

The action now also runs over a finite time interval $S[\phi] = \int_{t_1}^{t_2} dt \int d^3x \mathcal{L}$. We observe how the time interval $i(t_2 - t_1)$ appears to take the role of β from the partition function on the left-hand side above. In order to transform the partition function to a more field-theoretical form, assume that $|\phi\rangle$ is a complete set of field eigenstates. We may then write the partition function as

$$Z = \mathrm{Tr}[e^{-\beta\hat{H}}] = \int d\phi \, \langle \phi | \, e^{-\beta\hat{H}} \, | \phi \rangle \, . \tag{2.40}$$

The integration over ϕ is here an integration over all possible states of the field ϕ. What separates the inner product on the left-hand side of Eq. (2.39) and that of the right-hand side of Eq. (2.40) is simply $i(t_2 - t_1) \neq \beta$. If we perform a Wick rotation to imaginary time in the Lagrangian, and fix $t_1 = 0$ and $t_2 = \beta$, we may insert our path-integral into the partition function, yielding a path-integral representation of the partition function. We call the Wick-rotated action the Euclidean action, denoted S_E as the Wick rotation changes the sign of dt^2, bringing us from Minkowski space to Euclidean space. The Euclidean action S_E and Lagrangian L_E are defined by

$$S_E \equiv \int_0^\beta d\tau L_E, \tag{2.41}$$

$$L_E \equiv -L(t = -i\tau). \tag{2.42}$$

From now we will work exclusively in Euclidean space with both the action and the Lagrangian. The trace in the partition function means that $\phi = \rho_1 = \rho_2$, thus yielding a periodicity requirement in our path integral

$$\begin{aligned} Z &= \int d\phi' \int_{\phi(0,\vec{x})=\phi(\beta,\vec{x})=\phi'} \mathcal{D}\phi e^{S_E[\phi]} \\ &= \int_{\phi(0,\vec{x})=\phi(\beta,\vec{x})} \mathcal{D}\phi e^{S_E[\phi]}. \end{aligned} \tag{2.43}$$

The last line above is the partition function of quantum field theory. Quantities from statistical mechanics carry over to thermal field theory. For instance, the Helmholtz free energy density is given by

$$\mathcal{F} = -\frac{1}{\beta V} \ln Z. \tag{2.44}$$

In a manner completely analogous to that of Φ, the two-point function in thermal field theory is [47]

$$D(x-y) = \frac{1}{Z}\int \mathcal{D}\phi\phi(x)\phi(y)e^{-S_E[\phi]}. \tag{2.45}$$

Like the two-point function from the previous section, the thermal two-point function also includes disconnected diagrams which we will often need to discard prior to calculating the quantities we are interested in.

2.5 Matsubara sums

As we saw in the previous section, the temperature scale of the partition function is determined by the periodicity of the fields. We achieve this periodicity by writing the fields as a Fourier sum of so-called Matsubara frequencies in energy-momentum space, i.e.

$$\phi = \sum_n \int d^3p c_n(\vec{p})e^{i\omega_n t} \tag{2.46}$$

We usually abbreviate the summation and integration using the sum-integral sign $\not\int$, and the shorthand $\omega_n = -i\omega = -ip_0$. The sum-integral sign is defined in Eq. (1), and includes some prefactors necessary for dimensional regularisation, which we will discuss in the section on renormalisation (2.8). Due to symmetry requirements, $\omega_n = 2\pi nT$ for bosons and $\omega_n = \pi(2n+1)T$ for fermions. To see this we follow Ref. [47] and look once more at the thermal two-point function

$$D(x-y) = \frac{1}{Z}\mathrm{Tr}\left[e^{-\beta\hat{H}}T\left[\hat{\phi}(x),\hat{\phi}(y)\right]\right]. \tag{2.47}$$

The time-ordering operator T is different for fermions and bosons, due to the anticommutation relation of fermion fields. For bosons, the time-ordering operator takes the form

$$T\left(\hat{\phi}(x),\hat{\phi}(y)\right) = \begin{cases}\hat{\phi}(x)\hat{\phi}(y) \text{ if } x^0 > y^0\\ \hat{\phi}(y)\hat{\phi}(x) \text{ if } x^0 < y^0\end{cases} \tag{2.48}$$

Assuming that $x^0 = 0$ and $0 < y^0 = t < \beta$, we now attempt to arrive at an expression where $x^0 = \beta$. It is convenient to express the time component separately, so we write $D(x-y) = D(\vec{x},\vec{y},x^0,y^0)$. By exploiting the cyclic property of the trace we find

$$\begin{aligned} D(\vec{x},\vec{y},0,t) &= \frac{1}{Z}\mathrm{Tr}\left[e^{-\beta\hat{H}}\hat{\phi}(y)\hat{\phi}(x)\right]\\ = \frac{1}{Z}\mathrm{Tr}\left[\hat{\phi}(x)e^{-\beta\hat{H}}\hat{\phi}(y)\right] &= \frac{1}{Z}\mathrm{Tr}\left[e^{-\beta\hat{H}}e^{\beta\hat{H}}\hat{\phi}(x)e^{-\beta\hat{H}}\hat{\phi}(y)\right]\\ = \frac{1}{Z}\mathrm{Tr}\left[e^{-\beta\hat{H}}\hat{\phi}(x)_{x_0=\beta}\hat{\phi}(y)\right] &= D(\vec{x},\vec{y},\beta,t). \end{aligned} \tag{2.49}$$

In the above we have used the identity

$$e^{\beta\hat{H}}\hat{\phi}(0,\vec{x})e^{-\beta\hat{H}} = \hat{\phi}(\beta,\vec{x}), \tag{2.50}$$

which stems from transforming the equation

$$|x_A, t=\beta\rangle = e^{i\beta\hat{H}}|x_A, t=0\rangle \tag{2.51}$$

to the Heisenberg picture and imaginary time formalism. We see therefore that the two-point function for bosons is periodic with period β. Thus we can only allow the even Matsubara frequencies in the wave function, namely $\omega_n = 2\pi nT$. For fermions the time-ordering operator is subtly different due the anticommutation relation, namely

$$T\left(\hat{\psi}(x),\hat{\psi}(y)\right) = \begin{cases}\hat{\psi}(x)\hat{\psi}(y) \text{ if } x^0 > y^0\\ -\hat{\psi}(y)\hat{\psi}(x) \text{ if } x^0 < y^0\end{cases} \tag{2.52}$$

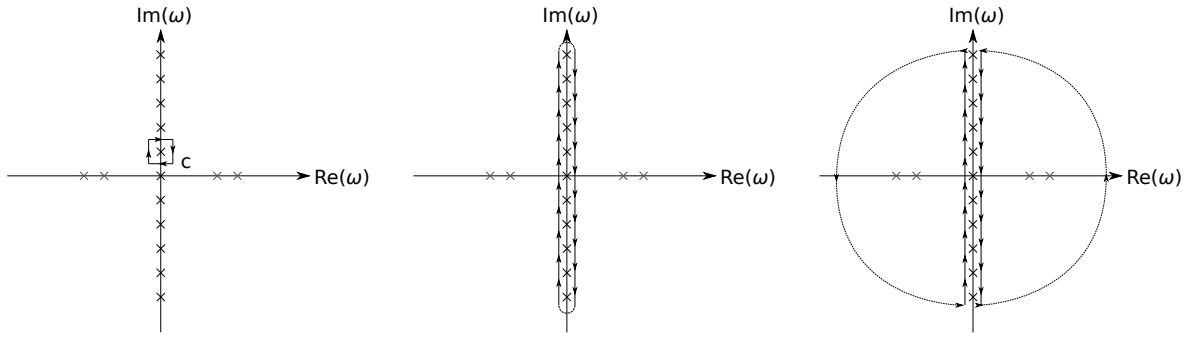

(a) A single contour, indexed by c.

(b) Summing all the single contours yields two infinite line integrals.

(c) We close the line integrals separately around the real poles of the dispersion relation.

Figure 2.5: Diagrammatic illustration of Matsubara sums as contour integrals. The crosses indicate poles in our integrand.

Through an entirely analogous calculation, this leads us to the conclusion that the fermion two-point function fulfils

$$D(\vec{x},\vec{y},0,t) = -D(\vec{x},\vec{y},\beta,t). \tag{2.53}$$

And thus $\omega_n = \pi(2n+1)T$ for fermions.

In computing the partition function, we will often encounter functional traces involving the propagator. This usually takes the form

$$\Pi \equiv \sum\!\!\!\!\!\!\int_p \frac{f(\omega,p)}{d(\omega,p)}. \tag{2.54}$$

In the above $d(\omega,p)$ is the determinant of the inverse propagator, and takes the form of an even polynomial in ω with real roots which represent the dispersion relations $\epsilon_i(p)$. $f(\omega,p)$ is a polynomial which is two orders lower in ω than ϵ. We will restrict ourselves to bosons in what follows, we must therefore evaluate the sum

$$T\sum_{\omega=2\pi i n T} \frac{f(\omega,p)}{d(\omega,p)}. \tag{2.55}$$

We will now calculate this general sum following a procedure which can be found in most textbooks on thermal field theory [47, 48]. In order to do this, we observe the following: the hyperbolic cotangent $\coth x$ has simple poles with residue 1 at the points $2\pi n i$ where n is an integer. Since $d(\omega,p)$ has only has real, nonzero roots, we may write our sum as

$$T\sum_{\omega=i2\pi n T} \frac{f(\omega,p)}{d(\omega,p)} = \frac{1}{4\pi i}\sum_c \oint_c \frac{f(\omega,p)}{d(\omega,p)} \coth\frac{\omega}{2T}. \tag{2.56}$$

c indexes a rectangular contour around a single pole in the complex ω-plane, as illustrated in Fig. 2.5a. The overlapping parts of the rectangular contours cancel, leaving only the lines in the imaginary direction. We now close the two line integrals separately as illustrated in Figure 2.5c The new contours enclose the poles of the dispersion relation on the real axis. For large ω, the extra orders of ω in $d(\omega,p)$ as compared to $f(\omega,p)$ lead to the summand going to zero as $\frac{1}{\omega^2}$. The contributions from the semicircles are therefore suppressed by a factor $\frac{1}{\omega}$, which is sufficient to ensure that they go to zero in the limit of large ω. We must now sum over the residues due to the roots of d. As stated earlier, the roots are given by $\omega^2 = \epsilon_i(p)^2$, the residue theorem therefore yields

$$T\sum_{\omega=i2\pi n} \frac{f(\omega,p)}{d(\omega,p)} = \frac{1}{2}\sum_i \lim_{\omega\to\epsilon_i} \frac{1}{\omega}\frac{(\omega^2-\epsilon_i^2)f(\omega,p)}{d(\omega,p)} \coth\frac{\omega}{2T}. \tag{2.57}$$

As a simple example, we consider the sum

$$\sigma = T\sum_n \frac{1}{\omega_n^2 + p^2 + m^2}. \tag{2.58}$$

We Wick rotate by defining $\omega = i\omega_n$, thereby obtaining

$$\sigma = -T\sum_{\omega=2\pi n T i} \frac{1}{\omega^2 - p^2 - m^2}. \tag{2.59}$$

Using the aforementioned trick, we may now write the sum as a contour integral around the contour illustrated in Fig. 2.5b

$$\sigma = -\frac{1}{4\pi i}\oint d\omega \frac{1}{\omega^2 - p^2 - m^2}\coth\frac{1}{2}\beta\omega. \tag{2.60}$$

Apart from the poles of $\coth\frac{1}{2}\beta\omega$ on the imaginary axis, there are simple poles at $\omega = \pm\sqrt{p^2+m^2}$. We now close the contours as illustrated in Fig 2.5c in stead, this yields a minus sign as the orientation of the semicircles is now counter-clockwise. The residue at $\omega = \pm\sqrt{p^2+m^2}$ is calculated by the formula valid for all simple poles c

$$\mathrm{Res}\,(f(z), c) = \lim_{z\to c}(z-c)f(z). \tag{2.61}$$

Thus our sum-integral becomes

$$\sigma = \frac{1}{2}\left(\frac{\coth\left(\frac{\sqrt{p^2+m^2}}{2T}\right)}{2\sqrt{p^2+m^2}} - \frac{\coth\left(-\frac{\sqrt{p^2+m^2}}{2T}\right)}{2\sqrt{p^2+m^2}}\right). \tag{2.62}$$

We now use the identities

$$\coth(-x) = -\coth(x), \tag{2.63}$$

$$\coth\left(\frac{x}{2}\right) = 1 + \frac{2}{e^x - 1}. \tag{2.64}$$

To write our final result

$$\sigma = \frac{1}{\sqrt{p^2+m^2}}\left(\frac{1}{2} + \frac{1}{e^{\sqrt{p^2+m^2}/T} - 1}\right). \tag{2.65}$$

This matches what one obtains by insertion into Eq. (2.57). The last term in the brackets is the thermal distribution function for bosons,

$$n(E) = \frac{1}{e^{E/T} - 1}. \tag{2.66}$$

We have thus obtained a thermal distribution of bosons in addition to a vacuum term which is present also at $T \to 0$, matching what one would obtain by performing the integral

$$\int_{-\infty}^{\infty}\frac{d\omega}{2\pi}\frac{1}{\omega^2 + p^2 + m^2} = \frac{1}{2\sqrt{p^2+m^2}}. \tag{2.67}$$

2.6 Chemical potential

As was mentioned briefly in the section on statistical mechanics, when the number of particles in an ensemble is unknown it is necessary to introduce a second parameter – the chemical potential – to fully characterise a system. This is also the case in thermal field theory, although the chemical potential is a somewhat more general concept. A chemical potential introduces a statistical preference in the system for a certain type of charge, this charge can be particle number, electric charge, isospin, hypercharge,

colour charge or indeed any other form of conserved quantity. The basis for this generalisation is the aforementioned Noether's theorem, giving rise to a conserved charge $Q_i \equiv \int d^4x j_i^0$. A chemical potential is introduced in a manner analogous to that of statistical mechanics, we modify the partition function by making the replacement $E \to E - \mu_i N_i$ where N_i is a particle number. We may similarly modify the Hamiltonian of our quantum field theory, making the replacement

$$\hat{H} \to \hat{H} - \mu_i \hat{Q}_i. \tag{2.68}$$

Q_i is here some generalised charge, which we derive from Noether's theorem.

$$Q_i = \int d^4x j^0. \tag{2.69}$$

In practice, since we normally operate with the Hamiltonian and Lagrangian densities, we simply introduce a term $\mu_i j_i^0$ in the Hamiltonian density. There is a limit to how many of these potentials we may introduce. We must require that the symmetries from whence we derive the charges commute. The reason for this is simply so as not to overdetermine the chemical potentials. Adding more chemical potentials would be redundant due to the symmetry of the system, and lead to extra equations relating the various chemical potentials. Equivalently, we may only introduce as many currents as can be simultaneously diagonalised.

2.7 Effective potential

As we have seen in the section on path-integrals, the generating functional gives rise to a large number of disconnected diagrams of little importance to most calculations. We will be concerning ourselves with systematic methods of resumming and renormalising large classes of Feynman diagrams in this thesis, and it is therefore important to exclude these diagrams from our equations a priori. The effective potential is a generating functional for the connected Green's functions in quantum field theory. It is a Legendre transform of the generating functional from the chapter on path-integrals (2.2), and can with no modification be used in conjunction with the partition function derived in Sec. 2.4. We will be using the *two-particle irreducible* (2PI) effective potential, a generating functional which yields gap equations for both the dressed propagator and mean-field expectation values. The term two-particle irreducible stems from the role of the class of Feynman diagrams of the same name – all diagrams in which one may cut any two propagator lines and the diagram remains connected – which play an important role in this formalism, as we shall see later. The formalism was developed for relativistic field theory by Cornwall, Jackiw and Tomboulis [49], and has been used extensively in studies of all-order renormalisation [43, 50–54]. We will follow the derivation of Cornwall *et al.* [49] in what follows. We start from the generating functional $\Phi[J]$, and modify it to contain a two-field current $K(x,y)$, such that

$$\Phi[J,K] = e^{iW[J,K]} = \int \mathcal{D}\phi e^{iS[\phi] + \int d^4x J(x)\phi(x) + \int d^4x\, d^4y \phi(x) K(x,y) \phi(y)}. \tag{2.70}$$

Note the implicit definition of $W[J,K] \equiv -i \ln \Phi[J,K]$. Next we define the new quantities $\rho(x)$ and $D(x,y)$

$$\frac{\delta W[J,K]}{\delta J(x)} = \rho(x), \tag{2.71}$$

$$\frac{\delta W[J,K]}{\delta K(x,y)} = \frac{1}{2}\left[\rho(x)\rho(y) + D(x,y)\right]. \tag{2.72}$$

The above definitions are not arbitrary. Our definition of $\rho(x)$ is such that $\rho(x) = \frac{1}{\Phi}\frac{\delta \Phi}{\delta J(x)} = \langle \phi \rangle$. It is in this manner that we incorporate spontaneous symmetry breaking in the theory; $\rho(x)$ is a classical field representing the expectation value of the ground state, the value of which is subject to an effective potential yet to be determined. Furthermore, the definition of $D(x,y)$ is such that the disconnected diagrams of the two-point function are not present in D. The reason for this is that we have explicitly extracted the term $\rho(x)\rho(y)$ from the two-point function, thereby removing the disconnected diagrams. In other words, $D(x,y)$ is the sought-after connected two-point function. We may now determine the effective potential by Legendre transforming the generating functional $W[J,K]$ to a pure functional of

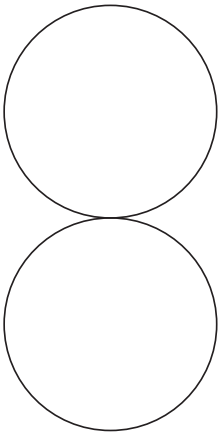

Figure 2.6: The double-bubble diagram, central to the Hartree and Large-N approximation

$\rho(x)$ and $D(x,y)$, we define $\Gamma[\rho, D]$:

$$\Gamma[\rho, D] = W[J,K] - \int d^4x J(x)\rho(x) - \frac{1}{2}\int d^4x\, d^4y \rho(x)K(x,y)\rho(y) - \frac{1}{2}\int d^4x\, d^4y D(x,y)K(y,x) \tag{2.73}$$

It is apparent that

$$\frac{\delta\Gamma[\rho(x),D]}{\delta\rho(x)} = -J(x) - \int d^4y K(x,y)\rho(y) \tag{2.74}$$

$$\frac{\delta\Gamma[\rho(x),D]}{\delta D(x,y)} = K(y,x) \tag{2.75}$$

The purpose of $J(x)$ and $K(x,y)$ are simply to generate N-point functions, after which we set them to zero. By doing so, we choose to evaluate the effective potential in the classical minimum, with $\rho(x)$ being the expectation value of the fields and the quantum fields being quantum fluctuations around this expectation value. Cornwall *et al.* derived that $\Gamma[\rho, D]$ is given by [49]

$$\Gamma[\rho(x), D] = I[\rho] + \frac{1}{2}\mathrm{Trln}\, D^{-1} + \frac{1}{2}\mathrm{Tr}D_0^{-1}D + \Phi[D]. \tag{2.76}$$

Here, $I[\rho]$ is the classical action one obtains when shifting the field $\phi(x) \to \phi(x) + \rho(x)$, thus incorporating symmetry breaking, and $\Phi[D]$ is the sum of all vacuum diagrams that are still connected after cutting two propagator lines, the aforementioned two-particle irreducible diagrams. If we now recall the definition of the self-energy matrix $\Pi[D] = D^{-1} - D_0^{-1}$, we may write the stationarity condition in Eq. (2.75) in the absence of sources as

$$\Pi[D] = 2\frac{\delta\Phi[D]}{\delta D}. \tag{2.77}$$

Thus the 2PI effective potential yields a set of self-consistent equations for the self-energy, which we refer to as the *gap equations*. By solving these gap equations, we can in principle find the dressed propagator to all orders in perturbation theory. In practice, however, these depend on an infinite number of increasingly complex 2PI diagrams. A number of different approximation schemes exist which incorporate a subset of such 2PI diagrams. We will be concerned with two such approximation schemes in our treatment of the linear sigma model, namely the large-N approximation and the Hartree-approximation. These approximations include some or all of the double-bubble diagrams illustrated in Fig 2.6, and offer a tractable set of gap equations and the opportunity to incorporate a large number of corrective terms to the self-energy of the fields. They are, however, incomplete descriptions of the model, and as such do not possess all the symmetries and characteristics of the complete model. For instance, the Hartree approximation is known to violate Goldstone's theorem, giving mass to fields which are massless in

the exact results [55]. However, attempts have been made to rectify this by studying various modified versions of the Hartree approximations, notably by Ivanov *et al.* [56, 57], Nemoto *et al.* [58], and Roh and Matsui [59].

2.8 Renormalisation

The procedure of renormalisation is a systematic way to remove divergences arising in perturbative expansions. A good introduction to the subject can be found in Ref. [60]. Historically renormalisation was born when Hans Bethe calculated the Lamb shift of the 2p state of hydrogen in 1947 [61]. It was believed at the time that the shift – which was not predicted by Dirac theory – was due to the electron interacting with its own electric field. However, calculations of this self-interaction always turned up a linearly divergent integral. The spirit of renormalisation is nicely summarised in Bethe's 1947 paper.

> It is possible to identify the most strongly (linearly) divergent term in the level shift with an electromagnetic *mass* effect which must exist for a bound as well as for a free electron. This effect should properly be regarded as already included in the observed mass of the electron, and we must therefore subtract from the theoretical expression, the corresponding expression for a free electron of the same average kinetic energy.

In other words the divergent term is part of a physical observable (in this case the mass of the electron), which is known to be finite. Hence the observed divergence must be cancelled by some other term, leading to a finite, observed physical mass. Bethe therefore subtracted the same term calculated for a free electron to obtain a finite correction and the procedure of renormalisation was born[1].

Renormalisation is thus a systematic way of removing divergences from quantum field theory, by comparing the physical observables with experiment. The divergences are viewed as being due to the fact that the perturbative expansions usually made in quantum field theory are around large, non-physical quantities. The bare mass of a particle is not directly observable, and similarly the coupling constant is only measured with all its radiative corrections included. Therefore, if we encounter divergent terms in the perturbative expansion this is due to our series expanding around a non-physical quantity, and this quantity must be corrected to account for the divergence.

The procedure of renormalisation is a series of steps to systematically remove divergences by introducing counterterms in the perturbation parameters. The algorithm is as follows

- Introduce counterterms: if g is a perturbation parameter, let $g \to g + \delta g$, where δg is a correction, typically of order g^2.
- Regularise the divergence: find some method by which you might make sense of the divergence I by modifying it $I \to I(\Lambda)$, such that I becomes finite except in some limit, typically $\Lambda \to \infty$ in which you recover the original divergence.
- Adjust the counterterm δg such that the perturbation expansion matches some observable. The result is a scale-dependent, but finite expression.
- If necessary, repeat the procedure to higher order.

The choice of method of regularisation is a free one, and how exactly divergences are parametrised vary greatly. However, all methods of regularisation must yield the same results in the limit in which we recover the original divergence. Perhaps the simplest method of regularisation is cutoff regularisation, in which an infinite divergent integral is converted to a finite one simply by introducing a finite integration limit. For instance we might define

$$I = \int_0^\infty dx f(x) \tag{2.78}$$

$$I(\Lambda) = \int_0^\Lambda dx f(x) \tag{2.79}$$

[1] This was not the only divergence, however. After removing the linear term, there remained a logarithmic divergence which needed to be treated by the introduction of a *renormalisation scale* Λ, which we will discuss shortly.

This works if the integral is divergent for large x, which we refer to as *ultraviolet (UV) divergence*. Conversely, a divergence at small x is referred to as an *infrared (IR) divergence*. Even if $f(x)$ diverges for $x \to \infty$, $I(\Lambda)$ will be finite for all finite Λ if the only divergence is a UV divergence. This mode of regularisation is simple and illustrative of the general idea of regularisation, but we will not be utilising it in this thesis. Instead we will use dimensional regularisation, a widely used regularisation scheme which preserves Lorentz- and gauge symmetries [60, 62]. The scheme was initially proposed by 't Hooft and Veltman [63], and is based on the following idea. We perform all calculations in $d = n + 2\epsilon$ dimensions where n is an integer and ϵ is a small parameter – thus making an analytical continuation to non-integer dimensions – the divergences then appear as poles when $\epsilon \to 0$, and we may remove the divergences before taking said limit. The concept of performing integration in a general number of dimensions involves the use of some unusual identities. As an example, consider the general integral

$$I(\Delta, n, m) = \int \frac{d^d p}{(2\pi)^d} \frac{|p|^n}{(p^2 + \Delta)^m}. \tag{2.80}$$

The integrand is rotationally invariant, so we transform to polar coordinates

$$I(\Delta, n, m) = \frac{1}{(2\pi)^d} \int d\Omega_d \int_0^\infty dp \frac{p^{n+d-1}}{(p^2 + \Delta)^m} \tag{2.81}$$

We will need to use the Gamma and Beta functions to evaluate these integrals, namely

$$\Gamma(z) = \int_0^\infty dt t^{z-1} e^{-t}, \tag{2.82}$$

$$\mathrm{B}(x, y) = \frac{\Gamma(x)\Gamma(y)}{\Gamma(x + y)} = \int_0^\infty dt \frac{t^{x-1}}{(1 + t)^{x+y}}. \tag{2.83}$$

We find the angular integral by using the following trick

$$\begin{aligned} (\sqrt{\pi})^d &= \left(\int_{-\infty}^\infty dx e^{-x^2} \right)^d = \int d^d x e^{-\sum_{i=1}^d x_i^2} \\ &= \int d\Omega_d \int_0^\infty dx x^{d-1} e^{-x^2} = \int d\Omega_d \int_0^\infty dx^2 \frac{1}{2} x^{\frac{d}{2}-1} e^{-x^2}. \\ &= \frac{\Gamma(\frac{d}{2})}{2} \int d\Omega_d. \end{aligned} \tag{2.84}$$

And thus

$$\Omega_d \equiv \int d\Omega_d = \frac{2\pi^{\frac{d}{2}}}{\Gamma(\frac{d}{2})}. \tag{2.85}$$

The second integral is carried out by the substitution $u = \frac{p^2}{\Delta}$

$$\begin{aligned} \int_0^\infty dp \frac{p^{n+d-1}}{(p^2 + \Delta)^m} &= \frac{\Delta^{\frac{n+d}{2}-m}}{2} \int_0^\infty \frac{u^{\frac{n+d}{2}-1}}{(u+1)^m} \\ = \frac{\Delta^{\frac{n+d}{2}-m}}{2} B(\tfrac{n+d}{2}, m - \tfrac{n+d}{2}) &= \frac{\Delta^{\frac{n+d}{2}-m}}{2} \frac{\Gamma(\frac{n+d}{2})\Gamma(m - \frac{n+d}{2})}{\Gamma(m)} \end{aligned} \tag{2.86}$$

Thus our original integral becomes

$$I(\Delta, n, m) = \frac{\Delta^{\frac{n+d}{2}-m}}{(4\pi)^{\frac{d}{2}}} \frac{\Gamma(\frac{n+d}{2})\Gamma(m - \frac{n+d}{2})}{\Gamma(\frac{d}{2})\Gamma(m)}. \tag{2.87}$$

Two cases of particular interest are

$$I(\Delta, 0, m) = \int \frac{d^d p}{(2\pi)^d} \frac{1}{(p^2 + \Delta)^m} = \frac{\Delta^{\frac{d}{2}-m}}{(4\pi)^{\frac{d}{2}}} \frac{\Gamma(m - \frac{d}{2})}{\Gamma(m)}. \tag{2.88}$$

$$I(\Delta, 2, m) = \int \frac{d^d p}{(2\pi)^d} \frac{p^2}{(p^2 + \Delta)^m} = \frac{\Delta^{\frac{d}{2}-m+1}}{(4\pi)^{\frac{d}{2}}} \frac{d}{2} \frac{\Gamma(m - 1 - \frac{d}{2})}{\Gamma(m)}. \tag{2.89}$$

For instance, consider the sum-integral

$$\not\sum\!\!\!\!\!\!\int \frac{1}{\omega_n^2 + p^2 + m^2}. \tag{2.90}$$

We have already evaluated the Matsubara sum in Sec. 2.5, what remains is the integral

$$\left(\frac{\Lambda^2 e^\gamma}{4\pi}\right)^\epsilon \int \frac{d^d p}{(2\pi)^d} \frac{1}{\sqrt{p^2+m^2}} \left(\frac{1}{2} + \frac{1}{e^{\sqrt{p^2+m^2}/T} - 1}\right). \tag{2.91}$$

The last term in the brackets is exponentially suppressed and hence convergent at high p, but the first term is quadratically divergent for $d = 3$. We can calculate the first term using Eq. (2.88) with $m = \frac{1}{2}$

$$\frac{1}{2}\left(\frac{\Lambda^2 e^\gamma}{4\pi}\right)^\epsilon \int \frac{d^d p}{(2\pi)^d} \frac{1}{\sqrt{p^2+m^2}} = \left(\frac{\Lambda^2 e^\gamma}{m^2}\right)^\epsilon \frac{m^2}{16\pi^{\frac{3}{2}}} \frac{\Gamma(\epsilon-1)}{\Gamma(\frac{1}{2})} \tag{2.92}$$

We now insert the known value $\Gamma(\frac{1}{2}) = \sqrt{\pi}$ and use the series expansion $\Gamma(\epsilon-1) = -\frac{1}{\epsilon} - 1 + \gamma + O(\epsilon)$ to write

$$\frac{1}{2}\left(\frac{\Lambda^2 e^\gamma}{4\pi}\right)^\epsilon \int \frac{d^d p}{(2\pi)^d} \frac{1}{\sqrt{p^2+m^2}} = -\frac{m^2}{(4\pi)^2}\left(\frac{\Lambda^2}{m^2}\right)^\epsilon \left[\frac{1}{\epsilon} + 1 + O(\epsilon)\right]. \tag{2.93}$$

By Taylor expanding $\left(\frac{\Lambda^2}{m^2}\right)^\epsilon$ around $\epsilon = 0$, we obtain

$$-\frac{m^2}{(4\pi)^2}\left[\frac{1}{\epsilon} + \ln\left(\frac{\Lambda^2}{m^2}\right) + 1 + O(\epsilon)\right]. \tag{2.94}$$

Peculiarly, the divergence that remains is logarithmic. This is a general property of dimensional regularization: power divergences are automatically regularised away, and what remains is a logarithmic divergence in ϵ. The above expansion allows us to add a divergent term $\frac{m^2}{(4\pi)^2\epsilon}$ to the regularised integral, thereby renormalising it. We will use this integral later when renormalising the large-N approximation in Chapter 3.4.

Chapter 3

The linear sigma model

Along with effective models such as the Nambu-Jona-Lassinio (NJL) [64–66] model and chiral perturbation theory [6, 7, 67], the linear sigma model has garnered a lot of attention in recent years as an effective theory for studying QCD [43, 51–53, 58, 59, 66, 68–72]. The literature on the linear sigma model is vast, and goes back to the work of Gell-Mann and Levy [73] in 1960. The relative simplicity of the model, along with its applicability to the study of spontaneous symmetry breaking - as we have already seen an example of in the chapter on Goldstones' theorem (1.1.3) - makes it well-suited for the study of phase transitions. For this reason, the linear sigma model has been applied to the study of pion condensation and chiral symmetry breaking, as well as kaon condensation [52, 53, 74]. The latter two condensates are relevant to the study of colour-flavour locking at high baryon density, whereas pion condensates are useful for study of the normal quark matter phase discussed in Sec. 1.2.5, as well as for chiral symmetry breaking at low baryon density.

With regards to chiral symmetry breaking, a major hindrance in studying the chiral phase transition at finite baryon density is posed by the fact that at nonzero baryon densities, the Euclidean path-integral is not positive definite [6, 45]. This lack of positivity makes the treatment of QCD at finite baryon density untractable by lattice gauge theories. However, the introduction of an isospin chemical potential μ_I does not violate the aforementioned positivity, and is therefore accessible both to lattice QCD and various effective field theories. In this manner, QCD at zero baryon chemical potential and finite isospin chemical potential offers us an opportunity to study the validity of various approximate analytical calculations.

The isospin chemical potential introduces a nonzero electric charge by inducing a statistical preference for either up or down quarks. Expressed in terms of up and down quark number densities (n_u and n_d, respectively), the baryon number density is $n_B = \frac{1}{3}(n_u + n_d)$, and the isospin density is $n_I = n_d - n_u$. Thus the isospin chemical potential introduces another axis to the phase diagram of QCD, and allows the study of electrically charged matter in the context of QCD. We will therefore study an idealised model in which $\mu_B = 0$ for varying temperatures and isospin chemical potential.

Fig. 3.1 shows our current understanding of this phase-diagram. At low isospin chemical potential and temperature, we have a chiral condensate. Due to the explicit chiral symmetry breaking imposed by the nonzero quark masses, the chiral condensate never fully evaporates, but rather crosses over to an approximately deconfined phase for high T. It is possible that for sufficiently high μ_I, this transition ceases to be a cross-over [75]. Increasing the isospin chemical potential to a critical value of $\mu_c = m_\pi$ allows the excitation of the pion mode, and we obtain a Bose-Einstein condensate of pions [6, 7]. The phase transition between a chiral condensate and a pion condensate is second order in the pion condensate, with the global minimum of the effective potential rotating in the direction of the pion mode. In the nonlinear sigma model, this crossover is a simple rotation of the condensate, however at next-to-leading order calculations the transition is both a rotation and slight rescaling of the condensates [75]. The deconfinement transition and the pion condensate transition meet at a tricritical point marked by a dot in Fig. 3.1, beyond which the pion condensate dominates. In this region, the deconfinement transition and the evaporation of the pion condensate appear to coincide. Recent studies in lattice QCD indicate that this high-density melting of the pion condensate might be first order [75], whereas mean-field studies in various models indicate a second-order transition [6, 7, 76].

Since we will restrict ourselves to pion condensation, we are only considering bound states of up and down quarks; two-flavour QCD. For higher densities, the strange quark may also participate in

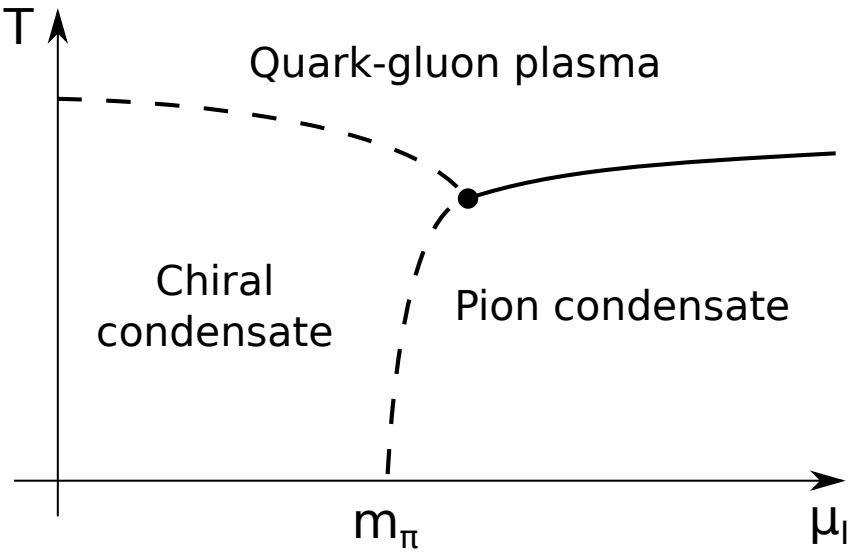

Figure 3.1: Sketch of the phase diagram of QCD at finite isospin chemical potential and $\mu_b = 0$

condensation, forming a kaon condensate. This can be studied by adding a third chemical potential μ_s, which has been done – among others – in the NJL model [64]. The study of kaon condensation is a key part of the study of colour-flavour-locking.

The linear sigma model describes the behaviour of N bosonic fields through the Lagrangian of an $O(N)$-symmetric ϕ^4-theory. In the case of pions, we recall from the Introduction that pions are the Goldstone bosons of the spontaneous symmetry breaking of the $SU(2)_L \times SU(2)_R$ chiral symmetry down to an $SU(2)_I$. We exploit that $SU(2) \times SU(2)$ is locally isomorphic to $O(4)$, and that $SU(2) \equiv O(3)$ to describe the dynamics of the up and down quark in terms of four bound states: the pions and the sigma meson [77]. The Euclidean Lagrangian density is

$$\mathcal{L} = \frac{1}{2}(\partial_\mu \phi_i)(\partial^\mu \phi_i) + \frac{1}{2}m^2(\phi_i \phi_i) + \frac{\lambda}{4N}(\phi_i \phi_i)^2 - H\phi_1. \tag{3.1}$$

In the above Lagrangian density, ϕ_i describes N scalar fields. H breaks the $O(N)$ symmetry explicitly, ensuring that all fields obtain a mass, rather than producing $N-1$ massless Goldstone bosons. In addition, in order to allow for a chiral condensate in the ground state, m^2 is negative, producing a Mexican hat-shape akin to what we saw in the chapter on Goldstone's theorem (1.1.3). We should expect to recover these massless Goldstone bosons in the limit $H \to 0$, which we refer to as the chiral limit.

The massive particle of the theory is called the sigma meson, its mass is believed to be in the range $400 - 1200$ MeV and its main decay mode is $\sigma \to \pi\pi$. The interpretation of the sigma field is somewhat uncertain. It is a resonance observed in the spectrum of the pions, and has has been taken to be the s-wave interaction of two pions [47], however Lin and Serot have argued that its mass should be larger than $1GeV$ [78], which would rule out this possibility.

Renormalisation of the linear sigma model at finite temperature is nontrivial, as a naïve perturbative expansion in the coupling constant becomes unstable at high temperatures [79, 80]. For this reason, several methods have been applied which involve the resummation of some class of diagrams to all orders in perturbation theory, including the aforementioned 2PI effective potential of Cornwall *et.al.* [43, 50–54], optimised perturbation theory [80] and screened perturbation theory [81]. Such techniques provide more reliable solutions in the high-T limit, but tend to complicate renormalisation. In particular, one is not guaranteed order-by-order renormaliseability or divergences independent of temperature and chemical potential. Thus, the renormaliseability of the linear sigma model has been the subject of several studies, see for instance [50, 82]. We will be utilising the renormalisation scheme proposed by Fejos *et.al.* [50], which involves all-order renormalisation through the separate handling of divergences and subdivergences. The method is equivalent to iterative renormalisation, but offers a simple one-step procedure to determine the end result of summing counterterms of all orders in the coupling.

The layout of this chapter is as follows: first we will introduce a chemical potential and derive the 2PI effective potential for the model. Following this, we will study two simplified versions of the full

$O(4)$ linear sigma model: the large-N approximation and the $O(2)$ linear sigma model in the Hartree approximation. In the large-N approximation, the particle masses receive thermal loop corrections in which the neutral pions propagate in the self-energy loops. The $O(2)$ model enables us to study in detail loop corrections with the charged pions propagating in the loops. Finally, we will combine these two models into an $O(N)$ model in the chiral limit Hartree approximation and perform some numerics to study pion condensation at low temperatures and finite isospin chemical potential.

These approximations have already been studied in the case of $\mu_I = 0$ by Lenaghan and Rischke [51], we will extend these studies to finite isospin chemical potential. In addition, the large-N approximation has been studied at finite isospin chemical potential in the 2PI formalism by Andersen [53], and the Hartree approximation at finite isospin chemical potential was considered by Mao *et al.* [43] without renormalisation. These studies, along with results from other effective theories and lattice calculations will be used for comparison with the results found for the Hartree approximation.

3.1 Introducing a chemical potential

An $O(N)$-symmetric model is invariant under rotations among its fields. There are $N(N-1)/2$ generators of the group $O(N)$, and to each there corresponds a conserved Noether current. However, only $N/2$ generators of the group may be chosen such that they commute, we can therefore at most introduce $\frac{N}{2}$ currents in our model. One way of choosing these generators is to choose rotations between neighbouring fields, i.e.

$$\begin{pmatrix} \phi_{2i-1} \\ \phi_{2i} \end{pmatrix} \to \begin{pmatrix} \cos\theta & \sin\theta \\ -\sin\theta & \cos\theta \end{pmatrix} \cdot \begin{pmatrix} \phi_{2i-1} \\ \phi_{2i} \end{pmatrix} \tag{3.2}$$

This is equivalent to a phase transformation with complex fields $\Phi_i = \frac{1}{\sqrt{2}}(\phi_{2i-1} + i\phi_{2i})$, as studied in the Sec. 1.1.1 on $U(1)$ symmetry. It is in this manner that we introduce a chemical potential which couples to isospin. Recall that the $U(1)$ gauge symmetry introduces an electrical charge to the fields Φ and $\Phi^\dagger$. By introducing a chemical potential which couples to the Noether current associated with this electrical charge, we thus induce a statistical preference for one of the charged pions over the other. Since the pions form an isospin triplet according to their charge, the chemical potential induces a statistical preference for a certain isospin. Noether's theorem gives us the conserved currents

$$j_k^\mu \equiv \frac{\partial \mathcal{L}}{\partial(\partial_\mu \phi_i)} \delta\phi_i = \phi_{2k}(\partial^\mu \phi_{2k-1}) - \phi_{2k-1}(\partial^\mu \phi_{2k}). \tag{3.3}$$

We may introduce a chemical potential associated with a current like this, we do so by modifying the Hamiltonian density

$$\mathcal{H} \to \mathcal{H} - \mu j_k^0. \tag{3.4}$$

We could in principle introduce several chemical potentials at once, but we will restrict ourselves to introducing one. The way we have chosen our $O(N)$ generators is such that the introduction of several chemical potentials would affect separate pairs of fields, and thus our Lagrangian with one chemical potential can easily be generalised to as much as $\frac{N}{2}$ separate chemical potentials. Should we wish for some different combination of these potentials we may utilise the original $O(N)$ symmetry and rotate the fields to some more desired configuration. In order to obtain the Hamiltonian density, we perform a Legendre transform of the Lagrangian.

$$\mathcal{H} = \pi_i(\partial^0 \phi_i) - \mathcal{L}, \tag{3.5}$$

π_i is the canonical momentum, defined by

$$\pi_i \equiv \frac{\partial \mathcal{L}}{\partial(\partial_0 \phi_i)} = \partial^0 \phi_i. \tag{3.6}$$

We obtain the Hamiltonian and subtract the density term in order to introduce the chemical potential, this yields

$$\mathcal{H} = \frac{1}{2}\pi_i\pi_i - \frac{1}{2}(\nabla\phi_i)\cdot(\nabla\phi_i) - \frac{1}{2}m^2(\phi_i\phi_i) - \frac{\lambda}{4N}(\phi_i\phi_i)^2 - \mu(\phi_{2k-1}\pi_{2k} - \phi_{2k}\pi_{2k-1}). \tag{3.7}$$

We can now find the new canonical momenta from Hamilton's equation

$$\partial_0 \phi_i = \frac{\partial \mathcal{H}}{\partial \pi_i}. \tag{3.8}$$

This yields

$$\pi_{2k-1} = \partial_0 \phi_{2k-1} - \mu \phi_{2k}, \tag{3.9}$$
$$\pi_{2k} = \partial_0 \phi_{2k} + \mu \phi_{2k-1}, \tag{3.10}$$
$$\pi_i = \partial_0 \phi_i, \text{ if } i \neq (2k-1), 2k. \tag{3.11}$$

Performing the inverse Legendre transform, we obtain the Lagrangian

$$\begin{aligned}\mathcal{L} = &\frac{1}{2}(\partial_\mu \phi_i)(\partial^\mu \phi_i) + \frac{1}{2}m^2(\phi_i \phi_i) - \frac{1}{2}\mu^2(\phi_{2k-1}^2 + \phi_{2k}^2) \\ &+ \frac{\lambda}{4N}(\phi_i \phi_i)^2 - H\phi_1 + \mu(\phi_{2k-1}\partial_0 \phi_{2k} - \phi_{2k}\partial_0 \phi_{2k-1}).\end{aligned} \tag{3.12}$$

The introduction of a chemical potential has added new terms to the Lagrangian which, upon inspection could be obtained by the transformations

$$\partial_0 \phi_{2k-1} \to (\partial_0 \pm \mu)\phi_{2k-1}, \tag{3.13}$$
$$\partial_0 \phi_{2k} \to (\partial_0 \pm \mu)\phi_{2k}. \tag{3.14}$$

The substitution above is made such that the product $(\partial_\mu \phi_i)(\partial^\mu \phi_i)$ contains both one term where μ is added and one where it is subtracted. The significance of this transformation is somewhat clearer in terms of a complex scalar field $\Phi = \frac{1}{\sqrt{2}}(\phi_{2k-1} + i\phi_{2k})$, where it is simply

$$\partial_0 \Phi \to (\partial_0 + i\mu)\Phi \tag{3.15}$$
$$\partial_0 \Phi^\dagger \to (\partial_0 - i\mu)\Phi^\dagger \tag{3.16}$$
$$\tag{3.17}$$

Recalling our discussion of gauge symmetries and gauge fields in Sec. 1.1.2, we thus see that we may interpret the chemical potential as a constant gauge field $A_\mu = (\mu, \vec{0})$, inducing a statistical preference for a certain charge. For our $O(4)$ model, we introduce the chemical potential corresponding to the conserved current given by

$$j^\mu = \phi_3 \partial^\mu \phi_2 - \phi_2 \partial^\mu \phi_3. \tag{3.18}$$

In terms of a complex field $\Phi = \frac{1}{\sqrt{2}}(\phi_2 + i\phi_3)$, the Noether current corresponds to the one found in the chapter on $U(1)$ symmetry (1.1.1), namely

$$j^\mu = i\left(\Phi^\dagger(\partial^\mu \Phi) - (\partial^\mu \Phi)^\dagger \Phi\right). \tag{3.19}$$

These fields couple to a gauge field as particles and antiparticles, as can be seen from Eq. (1.27). We therefore identify the charged pions as

$$\pi^\pm = \frac{\phi_2 \pm i\phi_3}{\sqrt{2}}. \tag{3.20}$$

As promised, the recently introduced chemical potential therefore couples to the charge of the pions and we label the *isospin chemical potential* μ_I.

3.2 Propagator and effective potential

The $O(N)$ symmetry of the original Lagrangian is now broken explicitly in two ways. The term $H\phi_1$, present to ensure physical pion masses breaks down the $O(N)$ symmetry to $O(N-1)$. Furthermore, the introduction of a chemical potential has added several terms coupling to ϕ_2 and ϕ_3 in the Lagrangian, isolating them in their own internal $O(2)$-symmetry. What remains is an $O(2) \times O(N-3)$ symmetry,

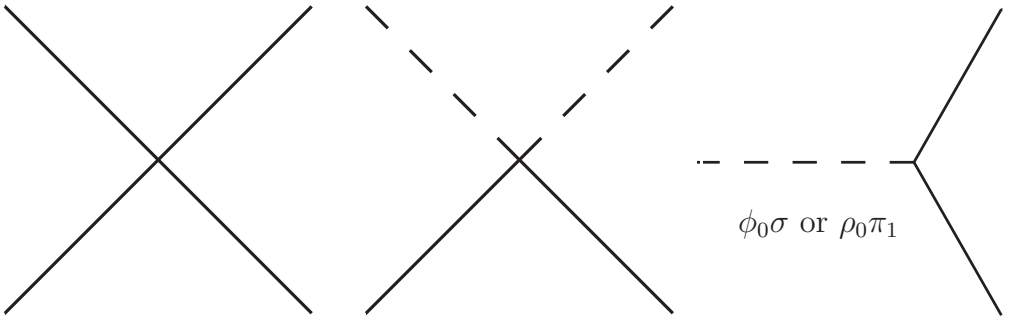

(a) Same-particle four point vertex (b) Mixed four-point vertex (c) Three-point vertex, the incoming particle must be a ϕ_1 or ϕ_2

Figure 3.2: The primitive interaction vertices after symmetry breaking. The different types of lines indicate that different particles are allowed for these vertices. The single leg in the three-point vertex must be a ϕ_1 or ϕ_2

which in the case of $N = 4$ is simply an $O(2)$ symmetry. We therefore allow for the breaking of the $O(N)$ symmetry by introducing the classical, constant fields ϕ_0 and ρ_0. The global minimum of the potential these fields will be subject to is governed by the symmetry-breaking terms in the Lagrangian. H and μ_I serve to shift the global minimum in the directions of ϕ_1 and the $O(2)$-invariant group of ϕ_2 and ϕ_3, respectively. Thus we make the substitutions

$$\phi_1 \quad \to \phi_0 + \phi_1, \tag{3.21}$$

$$\phi_2 \quad \to \rho_0 + \phi_2. \tag{3.22}$$

The field ϕ_0 now represents the chiral condensate, which is present in the vacuum state at $T = \mu_I = 0$, and yields a nonzero mass for the σ particle in the vacuum. ρ_0 is related to the symmetry breaking induced by μ_I, and thus represents a Bose condensate of charged pions. What mixture of ρ_0 and ϕ_0 is present at tree-level is thus decided by a tug-of-war between H and μ_I^2, shifting the direction of the global minimum. Furthermore, the presence of either condensate implies the breaking of chiral symmetry. We thus take ρ_0 and ϕ_0 to be order parameters of chiral symmetry breaking, and identify the field ϕ_1 with the σ particle and the fields $\phi_4, \phi_5, \cdots$ with neutral pions.

The full Lagrangian is now

$$\begin{aligned}\mathcal{L} = &\frac{1}{2}(\partial_\mu\phi_i)(\partial^\mu\phi_i) + \frac{1}{2}m_i^2\phi_i^2 + \frac{2\lambda}{N}\rho_0\phi_0\phi_1\phi_2 \\ &+ \frac{\lambda}{4N}(\phi_i\phi_i)^2 - H\phi_1 + \mu_I(\phi_3\partial_0\phi_2 - \phi_2\partial_0\phi_3) \\ &+ \mathcal{L}_c + \mathcal{L}_I + \mathcal{L}_T.\end{aligned} \tag{3.23}$$

$$\mathcal{L}_c \equiv \frac{1}{2}m^2(\phi_0^2 + \rho_0^2) - \frac{1}{2}\mu_I^2\rho_0^2 + \frac{\lambda}{4N}(\phi_0^2 + \rho_0^2)^2 - H\phi_0 \tag{3.24}$$

$$\mathcal{L}_I \equiv \frac{\lambda}{N}\phi_0\phi_1(\phi_i\phi_i) + \frac{\lambda}{N}\rho\phi_2(\phi_i\phi_i) \tag{3.25}$$

$$\mathcal{L}_T \equiv \left(m^2 + \frac{\lambda}{N}\phi_0^2\right)\phi_0\phi_1 + \left(m^2 + \frac{\lambda}{N}\rho_0^2\right)\rho_0\phi_2 \tag{3.26}$$

We have introduced new mass terms m_i in order to simplify notation, they are

$$m_1^2 = m^2 + \frac{3\lambda}{N}\phi_0^2 + \frac{\lambda}{N}\rho_0^2, \tag{3.27}$$

$$m_2^2 = -\mu_I^2 + m^2 + \frac{\lambda}{N}\phi_0^2 + \frac{3\lambda}{N}\rho_0^2, \tag{3.28}$$

$$m_3^2 = -\mu_I^2 + m^2 + \frac{\lambda}{N}\phi_0^2 + \frac{\lambda}{N}\rho_0^2, \tag{3.29}$$

$$m_4^2 = m^2 + \frac{\lambda}{N}\phi_0^2 + \frac{\lambda}{N}\rho_0^2. \tag{3.30}$$

By introducing the symmetry breaking terms, we have obtained the classical Lagrangian, $\mathcal{L}_c$, which provides the classical action $I[\rho]$ in the 2PI effective potential. In addition, we have obtained two new primitive interactions – codified in $\mathcal{L}_\mathcal{I}$ – from the cross terms between the newly introduced classical fields and their corresponding quantum fluctuations. All the primitive interaction vertices are illustrated in Fig. 3.2. We have obtained tadpoles, one-point interaction functions as given by $\mathcal{L}_T$. When evaluating ϕ_0 and ρ_0 at the classical minimum, the tadpoles vanish, as can easily be seen at the tree level. Thus we take the vanishing of these terms as a resummation condition. The terms quadratic in the fields yield the inverse tree-level Euclidean propagator $D_0^{-1}(\omega_n, p)$

$$D_0^{-1} = \begin{pmatrix} \omega_n^2 + p^2 + m_1^2 & \frac{2\lambda}{N}\phi_0\rho_0 & 0 & 0 \\ \frac{2\lambda}{N}\phi_0\rho_0 & \omega_n^2 + p^2 + m_2^2 & -2\mu_I\omega_n & 0 \\ 0 & 2\mu_I\omega_n & \omega_n^2 + p^2 + m_3^2 & 0 \\ 0 & 0 & 0 & \omega_n^2 + p^2 + m_4^2 \end{pmatrix}, \tag{3.31}$$

where $\omega_n = 2\pi nT$ is the nth Matsubara frequency. The 2PI effective potential can now be extracted from the Lagrangian, following the steps in Chapter 2.7 we find

$$\begin{aligned} \Gamma[\phi_0, \rho_0, D] &= \frac{1}{2}m^2(\phi_0^2 + \rho_0^2) + \frac{\lambda}{4N}(\phi_0^2 + \rho_0^2)^2 \\ &\quad -\frac{1}{2}\mu_I^2\rho_0^2 - H\phi_0 + \frac{1}{2}\mathrm{Tr}\ln D^{-1} \\ &\quad +\frac{1}{2}\mathrm{Tr}D_0^{-1}D + \Phi[D]. \end{aligned} \tag{3.32}$$

As before, $\Phi[D]$ is the sum of all 2PI vacuum diagrams, and we will later restrict ourselves to approximations of $\Phi[D]$ by including only a selection of these. The stationarity conditions from Eqs. (2.74) and (2.75) become

$$\frac{\delta\Gamma[\phi_0, \rho_0, D]}{\delta\phi_0} = 0, \tag{3.33}$$

$$\frac{\delta\Gamma[\phi_0, \rho_0, D]}{\delta\rho_0} = 0, \tag{3.34}$$

$$\frac{\delta\Gamma[\phi_0, \rho_0, D]}{\delta D} = 0. \tag{3.35}$$

The thermal behaviour of the linear sigma model is incorporated through calculating self-energies $\Pi[D]$ emerging from the above stationarity conditions $\Phi[D]$. Once more, using that $\Pi[D] \equiv D^{-1} - D_0^{-1}$, it is desirable to rewrite Eq. (3.35) as

$$\Pi[D] = 2\frac{\delta\Phi[D]}{\delta D}. \tag{3.36}$$

Thus the self-energy can be found by cutting one propagator line in $\Phi[D]$, this yields an efficient way of constructing the mass corrections diagrammatically without taking a detour via functional differentiation. The upshot of the stationarity condition for D is thus a set of self-consistent gap equations which can be solved for the dressed propagator.

3.3 Tree-level masses

Before taking loop corrections into account in our calculations, we can evaluate the tree-level masses. Upon differentiation, the stationarity conditions of Eqs. (3.33) and (3.34) become

$$\phi_0\left[m^2 + \frac{\lambda}{N}(\phi_0^2 + \rho_0^2)\right] = H, \tag{3.37}$$

$$\rho_0\left[m^2 + \frac{\lambda}{N}(\phi_0^2 + \rho_0^2) - \mu_I^2\right] = 0. \tag{3.38}$$

For large enough μ_I, the global minimum will lie in the direction of ϕ_2, if we therefore assume $\rho_0 \neq 0$, the expression within the bracket of Eq. (3.38) must be zero. Identifying this expression as m_3^2, we thus obtain the condition

$$m_3^2 = 0. \tag{3.39}$$

Applied to the other mass modes, we similarly obtain

$$m_1^2 = \frac{2\lambda}{N}\phi_0^2 + \mu_I^2, \tag{3.40}$$

$$m_2^2 = \frac{2\lambda}{N}\rho_0^2. \tag{3.41}$$

Inserting (3.39) into (3.37), we see that

$$\phi_0 = \frac{H}{\mu_I^2}, \tag{3.42}$$

$$\rho_0^2 = \frac{N}{\lambda}(\mu_I^2 - m^2) - \frac{H^2}{\mu_I^4}. \tag{3.43}$$

The charged pions are linear combinations of ϕ_2 and ϕ_3. To find their masses, we utilise the dispersion relations ϵ_i. We find the dispersion relation by analytical continuation $\omega_n \to i\omega$, and then solving the equation $\mathrm{Det}[D_0^{-1}(\omega, p)] = 0$ with respect to ω. The roots of this equation are the dispersion relations $\epsilon_i(p)$, yielding the quasiparticle masses m_{ip} at $p = 0$ through the identity

$$\epsilon_i(p) \equiv \sqrt{p^2 + m_{ip}^2}. \tag{3.44}$$

Doing this we find the quasiparticle masses

$$m_{1p,2p} = \sqrt{\frac{7}{2}\mu_I^2 - m^2 \pm \frac{1}{2}\sqrt{(2m^2 - 5\mu_I^2)^2 - 24\frac{\lambda}{N}\frac{H^2}{\mu_I^2}}}, \tag{3.45}$$

$$m_{3p} = 0, \tag{3.46}$$

$$m_{4p} = \mu_I. \tag{3.47}$$

The π^+ is thus a massless Goldstone mode, as we expect since ρ_0 breaks the $O(2)$ symmetry of ϕ_2 and ϕ_3. As a check, for $H = \mu_I = 0$, the masses become

$$m_{1p}^2 = -2m^2, \tag{3.48}$$

$$m_{2p}^2 = 0, \tag{3.49}$$

$$m_{3p}^2 = 0, \tag{3.50}$$

$$m_{4p}^2 = 0. \tag{3.51}$$

In this limit we have a three-fold mass degeneracy, as we found when discussing Goldstone's theorem in Sec. (1.1.3).

3.4 Large-N approximation

Whilst not at all valid for the case of pions – where $N = 4$ – it is illustrative to study the case where $N \gg 1$. This mode of approximation, a series expansion in powers of $\frac{1}{N}$ has the virtue of retaining the symmetries associated with the $O(N)$ group for each order in the perturbation theory, thus preserving Goldstone's theorem. We will limit our discussion to leading order, yielding a relatively simple derivation of the self-energy associated with the diagonal elements of the inverse propagator.

For large N, we have $N - 3$ diagonal terms in the inverse propagator with mass m_4^2. These terms dominate the self-energy of all the particles in the limit of large N. To leading order in N, the dominating contribution to the self-energy will thus be N diagrams like those in Fig. 3.3. The dressed propagator of the particles propagating in the loop of Fig. 3.3 can be written as

$$D^{-1}(\omega_n, p) = P^2 + m_4^2 + \Pi[D], \tag{3.52}$$

where $\Pi[D]$ is the self energy of the same particle. Since this loop correction is independent of external momentum, it must be a constant. We can therefore write the inverse propagator as

$$D^{-1}(\omega_n, p) = P^2 + M^2, \tag{3.53}$$

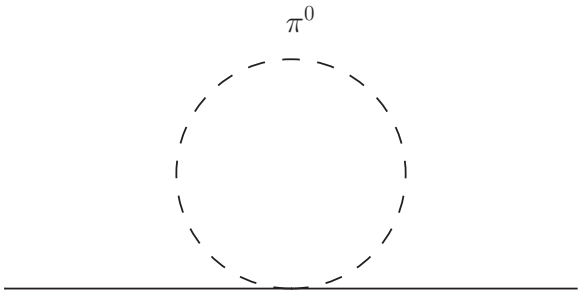

Figure 3.3: Leading-order contribution to the sigma particle self-energy in the large-N approximation. The particle propagating in the loop is the π^0.

where M is a constant yet to be determined. The inverse propagator is diagonal to this order in $\frac{1}{N}$, and so inversion is trivial, we find a diagonal self-energy matrix

$$\Pi[D]_{ii} = \lambda \sum\!\!\!\!\!\!\int_Q \frac{1}{Q^2 + M^2}. \tag{3.54}$$

In the above, no summation is implied over i. Using the relation $M^2 = m_4^2 + \Pi[D]_{44}$, we thus obtain a gap equation for M

$$M^2 = m_4^2 + \lambda \sum\!\!\!\!\!\!\int_Q \frac{1}{Q^2 + M^2}. \tag{3.55}$$

We have already calculated the Matsubara sum in Chapter 2.5, and regularised the remaining integral in Chapter 2.8. Further to the regularisation, what remains is fixing the counterterms necessary to remove divergences to all orders, see Appendix A for details on how this is carried out. We end up making the substitutions

$$m^2 \to \frac{m^2}{1 - \frac{\lambda}{16\pi^2\epsilon}}, \tag{3.56}$$

$$\lambda \to \frac{\lambda}{1 - \frac{\lambda}{16\pi^2\epsilon}}. \tag{3.57}$$

What remains is the renormalised gap equation

$$\begin{aligned} M^2 &= m^2 + \lambda I_{Nf}(M^2) \\ &= m^2 + \frac{\lambda}{2N}(\phi_0^2 + \rho_0^2) - \frac{\lambda M^2}{16\pi^2}\left(1 + \ln\frac{\Lambda^2}{M^2}\right) \\ &\quad + \lambda \int \frac{d^3q}{(2\pi)^3}\frac{1}{\sqrt{q^2+M^2}}\frac{1}{e^{\sqrt{q^2+M^2}/T} - 1}. \end{aligned} \tag{3.58}$$

The integral $I_{Nf}(M^2)$ is defined in Eq. (A.10). The self-energy matrix $\Pi[D]$ is now a diagonal matrix with entries

$$\Pi[D]_{ii} = \lambda I_{Nf}(M^2). \tag{3.59}$$

The stationarity conditions are altered by the inclusion of loop corrections. By using the identity $D = D_0^{-1} + \Pi[D]$, the term $\frac{1}{2}\mathrm{Tr}\,[D_0^{-1}D]$ in the effective potential can be written

$$\frac{1}{2}\mathrm{Tr}\,[D_0^{-1}D] = \frac{1}{2}\mathrm{Tr}\,[\mathbb{1}] + \frac{1}{2}\mathrm{Tr}\,[D_0^{-1}\Pi[D]]. \tag{3.60}$$

The masses in D_0 depend on ϕ_0 and ρ_0 and thus the self-energy matrix $\Pi[D]$ enter the stationarity conditions for the condensates

$$\phi_0\left[m^2 + \frac{\lambda}{N}(\phi_0^2 + \rho_0^2) + \lambda\Pi[D]_{11}\right] = \phi_0 M^2 = H, \tag{3.61}$$

$$\rho_0\left[m^2 + \frac{\lambda}{N}(\phi_0^2 + \rho_0^2) + \Pi[D]_{22} - \mu_I^2\right] = \rho_0(M^2 - \mu_I^2) = 0. \tag{3.62}$$

The stationarity conditions yield two different sets of solutions, corresponding to different phases. If $\rho_0 \neq 0$, this implies

$$M^2 = \mu_I^2 \tag{3.63}$$

$$\phi_0 = \frac{H}{\mu_I^2} \tag{3.64}$$

$$\rho_0 = \sqrt{\frac{N}{\lambda}(\mu_I^2 - m^2) - \frac{H^2}{\mu_I^4} - NI_{Nf}(\mu_I^2)} \tag{3.65}$$

Since the fields ϕ_i, ρ_0 and ϕ_0 are real fields, this solution is only consistent as long as Eq. (3.65) yields a real ρ_0. If the expression within the square root becomes negative, we are forced to conclude that $\rho_0 = 0$. In that case, we are obliged to solve the gap equation to find M and ϕ_0. We may now once again evaluate the quasiparticle masses as we did at tree level in Eqs. (3.45), (3.46), and (3.47). However, the inverse dressed propagator is given by $D^{-1} = D_0^{-1} + \Pi[D]$. Since we know the structure of the self-energy matrix, we see that for every instance of m^2 in the tree-level propagator we now find an instance of $m^2 + \lambda I_{Nf}(M^2)$ in the dressed propagator. We can therefore immediately write the new quasiparticle masses in the phase $\rho_0 \neq 0$ as

$$M_{1p,2p} = \sqrt{\frac{7}{2}\mu_I^2 - m^2 - \lambda I_{Nf}(M^2) \pm \frac{1}{2}\sqrt{(2m^2 + 2\lambda I_{Nf}(M^2) - 5\mu_I^2)^2 - 24\frac{\lambda}{N}\frac{H^2}{\mu_I^2}}}, \tag{3.66}$$

$$M_{3p} = 0, \tag{3.67}$$

$$M_{4p} = \mu_I. \tag{3.68}$$

If $\rho_0 = 0$, the off-diagonal terms $\frac{\lambda}{N}\phi_0\rho_0$ in the dressed propagator are zero and hence there is no mixing between the modes of M_1 and M_2. In this limit, we find the quasiparticle masses

$$M_{1p} = \sqrt{M^2 + \frac{2\lambda}{N}\frac{H^2}{M^4}}, \tag{3.69}$$

$$M_{2p,3p} = M \pm \mu_I, \tag{3.70}$$

$$M_{4p} = M. \tag{3.71}$$

Note that whereas M_{3p} was massless when $\rho_0 \neq 0$, all particles are now massive. The reason for this is Goldstone's theorem, which provides that when the residual $O(2)$ symmetry is spontaneously broken by a pion condensate, the π^+ becomes a massless Goldstone mode. When $\rho_0 = 0$ the $O(2)$ symmetry is restored and thus all the particles become massive, and we have a three-fold mass degeneracy in the pion modes.

Before proceeding, we may at this point determine the critical potential μ_c, defined as the minimum isospin chemical potential for which there is a nonzero pion condensate in the equilibrium state. To see this, observe that at $\mu_I = 0$, the stationarity condition for ρ in Eq. (3.62) reduces to the requirement

$$\rho_0 M^2 = 0. \tag{3.72}$$

Thus, for $M \neq 0$ we conclude that $\rho_0 = 0$. Since $\mu_I = 0$, M can only be zero when $H = 0$, namely in the chiral limit. At the physical point we choose H such that $M = m_\pi$ in the vacuum. Next we observe that $I_{Nf}(M^2)$ increases monotonically with T, Eq. (3.65) implies that ρ_0 decreases monotonically with increasing T. This gives rise to a second order phase transition at some critical temperature $T_c(\mu_I)$, determined by the equation

$$\frac{N}{\lambda}(\mu_I^2 - m^2) - \frac{H^2}{\mu_I^4} - NI_{Nf}(\mu_I^2, T_c) = 0. \tag{3.73}$$

In addition to implying the condition for T_c, we conclude that μ_c is found at $T = 0$. Finally, we observe that in the phase where $\rho_0 = 0$, I_{Nf} is independent of chemical potential. Thus the region of $T = 0$ and $\mu_I < \mu_c$ is governed by the same gap equation, and hence $M = m_\pi$ in the entirety of this region. The stationarity condition for ρ_0 in this domain is then simply

$$\rho_0(m_\pi^2 - \mu_I^2) = 0 \tag{3.74}$$

Nonzero ρ_0 is therefore first allowed at $\mu_c = m_\pi$. This is in accordance with theoretical predictions, and stems from the fact that it first becomes energetically favourable to excite the pion condensate when μ_I surpasses the minimum excitation quantum, m_π [6].

3.5 $O(2)$ Model with chemical potential

In the preceding section we handled the renormalisation of the diagonal terms in the propagator. We now turn our attention to the fields ϕ_2 and ϕ_3, the $O(2)$ doublet connected to the isospin chemical potential. To this end, we isolate this doublet in a simplified $O(2)$ model and study its renormalisation. In this model, we set $H = 0$, and introduce a chemical potential by coupling to the current $j_1^\mu = \phi_2\partial^\mu\phi_1 - \phi_1\partial^\mu\phi_2$. Letting $\phi_1 \to \phi_0 + \phi_1$, where ϕ_0 is a classical field, we obtain the 2PI effective potential

$$\Gamma[\phi_0, D] = \frac{1}{2}(m^2 - \mu_I^2)\phi_0^2 + \frac{\lambda}{8}\phi_0^4 + \frac{1}{2}\mathrm{Tr}\ln D^{-1} + \frac{1}{2}\mathrm{Tr}D_0^{-1}D + \Phi[D], \tag{3.75}$$

and the tree-level masses

$$m_1^2 = m^2 - \mu_I^2 + \frac{3\lambda}{2}\phi_0, \tag{3.76}$$

$$m_2^2 = m^2 - \mu_I^2 + \frac{\lambda}{2}\phi_0. \tag{3.77}$$

At tree-level, ϕ_0 must satisfy the stationarity condition

$$\phi_0\left[(m^2 - \mu_I^2) + \frac{\lambda}{2}\phi_0^2\right] = 0. \tag{3.78}$$

For $\mu_I > m^2$, the solution $\phi_0 = 0$ is a local maximum of the potential and so the lowest-energy solution to the stationarity condition is

$$\phi_0 = \begin{cases} 0 & \text{if } m^2 > \mu_I^2, \\ \sqrt{\frac{2(\mu_I^2 - m^2)}{\lambda}} & \text{if } m^2 \le \mu_I^2. \end{cases} \tag{3.79}$$

We see that as μ_I increases, it drives the minimum of the effective potential away from the origin in a continuous manner, transforming the shape of the potential from an increasing curve to a Mexican hat-shape like the potential encountered in the section on Goldstone's theorem, Sec. 1.1.3. This behaviour starts when $\mu_I^2 = m^2$, changing the sign of the quadratic term in the effective potential. We recall from our treatment of the large-N approximation that the onset of pion condensation was found to be at $\mu_I = m_\pi$ at the physical point. Similarly we here see that when $m^2 > 0$, the mass at $\mu_I = 0$ is m^2, and a condensate forms when $\mu_I^2 > m^2$, indicating a density-driven phase transition. Fig. 3.4 illustrates this μ_I-dependence. For $\phi_0 = 0$, the inverse tree-level propagator is

$$D_0^{-1} = \begin{pmatrix} -\omega^2 + m^2 - \mu_I^2 & -2\mu_i\omega \\ 2i\mu_i\omega & -\omega^2 + m^2 - \mu_I^2 \end{pmatrix}. \tag{3.80}$$

From this we obtain the tree-level masses as we did in Sec. 3.3

$$m_1 = m + \mu_I, \tag{3.81}$$

$$m_2 = m - \mu_I. \tag{3.82}$$

For $m \le \mu_I$, ϕ_0 is nonzero, this gives the inverse tree-level propagator

$$D_0^{-1} = \begin{pmatrix} -\omega^2 - 2(m^2 - \mu_I^2) & -2i\mu_I\omega \\ 2i\mu_I\omega & -\omega^2 \end{pmatrix}. \tag{3.83}$$

This leads to the tree-level quasiparticle masses

$$m_1 = \sqrt{6\mu_I^2 - 2m^2}, \tag{3.84}$$

$$m_2 = 0. \tag{3.85}$$

Fig. 3.5 shows that ϕ_0 is continuous, but has a discontinuous second derivative at $\mu_I^2 = m^2$. Thus, we conclude that at tree level, we have a second order density-driven phase transition at this point. As we saw with the large-N approximation, $\phi_0 \neq 0$ breaks the $O(2)$ symmetry of the charged pions, and thus Goldstone's theorem provides that $m_2^2 = 0$.

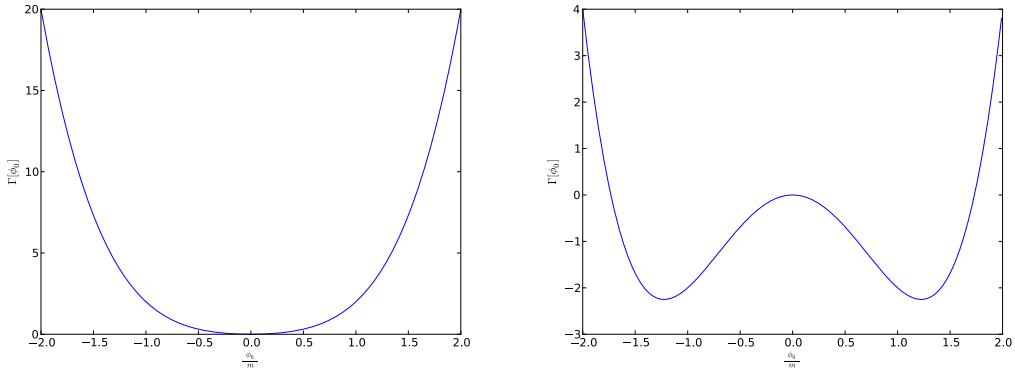

(a) $\mu_I^2 = 0$ (b) $\mu_I^2 = 4m^2$

Figure 3.4: Plots of $\Gamma[\phi_0]$ at tree level with $\lambda = 4$ for two different values of μ_I.

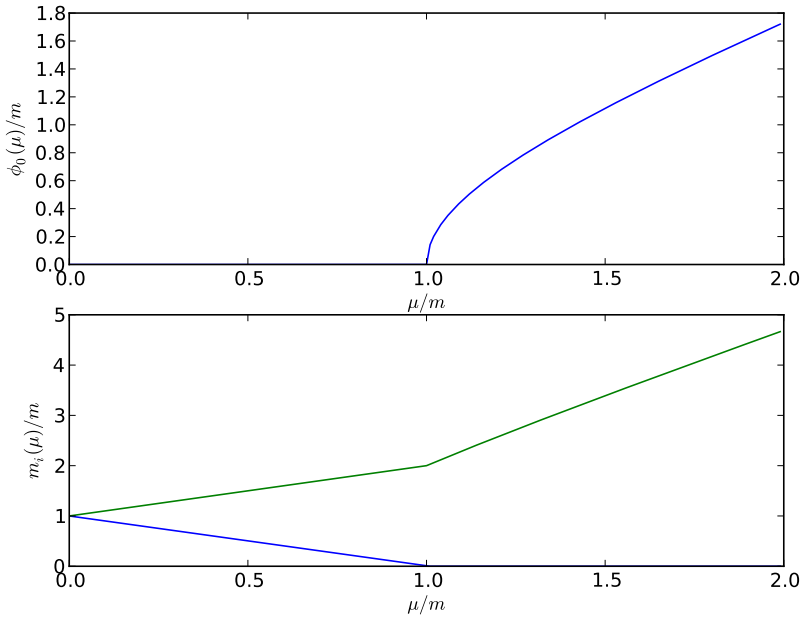

Figure 3.5: Plot of m_i and ϕ_0 at tree level as a function of chemical potential, everything is in units of m, and $\lambda = 1$.

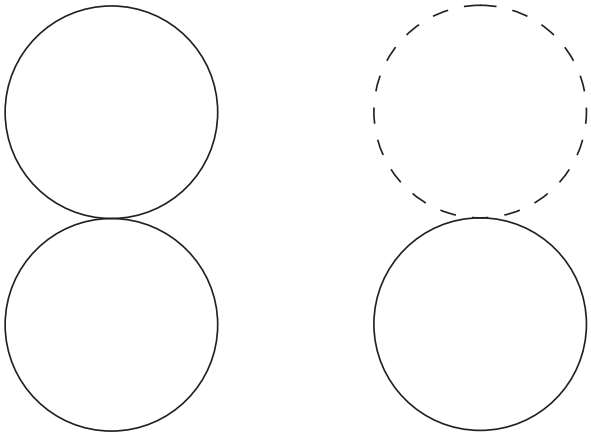

(a) Double bubble. (b) Mixed double bubble.

Figure 3.6: Two diagrams contributing to $\Phi[D]$ in the Hartree approximation.

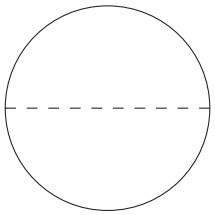

Figure 3.7: The setting-sun diagram, excluded from the Hartree approximation.

3.5.1 Hartree approximation

The Hartree approximation is defined by including all the double-bubble diagrams (Fig. 3.6) in $\Phi[D]$. We thus include all diagrams from the large-N approximation, along with loop diagrams containing the charged pions and the sigma meson. As was the case in the large-N approximation, these diagrams have the virtue of being independent of external momenta, thus making the mass correction a constant. However, while Goldstone's theorem is fulfilled order-by-order in the $\frac{1}{N}$ expansion [54], the Hartree approximation may violate Goldstone's theorem. This is due to the exclusion of some diagrams necessary to fulfil the symmetry, such as the so-called setting sun diagram, illustrated in Fig. 3.7 [58,72,83]. Nemoto *et. al.* have suggested that this violation is not a consequence of the effective potential, but rather by the definition of the quasiparticle masses in a manner which breaks the $O(N)$ symmetry [58], however we will not be utilising their approach in this thesis.

Using the primitive four-point vertices to construct $\Phi[D]$, we arrive at

$$\Phi[D] = \frac{\lambda}{8}(\delta_{ab}\delta_{cd} + \delta_{ac}\delta_{bd} + \delta_{ad}\delta_{bc})D_{ab}D_{cd} \tag{3.86}$$

Each product of two Kronecker deltas in Eq. (3.86) correspond to an O(2) invariant. Like the $O(4)$ case, the self-energy loops are independent of external momentum, which means that the self-energies must be constant. Thus we can write the inverse dressed propagator as

$$D^{-1}(\omega_n, p) = \begin{pmatrix} \omega_n^2 + p^2 + m_1^2 + \Pi_{11} & -2\mu_I\omega_n + \Pi_{12} \\ 2\mu_I\omega_n + \Pi_{21} & \omega_n^2 + p^2 + m_2^2 + \Pi_{22} \end{pmatrix}. \tag{3.87}$$

Π_{ij} is the sum of loop corrections to the inverse propagator, arising from cutting a propagator line in the diagrams contributing to $\Phi[D]$, as prescribed by Eq. (3.36). The sigma meson corrections are illustrated in Fig. 3.8. We invert (3.87) and obtain the dressed propagator

$$D(\omega_n, p) = \frac{1}{\mathrm{Det}[D^{-1}(\omega_n, p)]} \begin{pmatrix} \omega_n^2 + p^2 + m_2^2 + \Pi_{22} & 2\mu_I\omega_n - \Pi_{12} \\ -2\mu_I\omega_n - \Pi_{21} & \omega_n^2 + p^2 + m_1^2 + \Pi_{11} \end{pmatrix}, \tag{3.88}$$

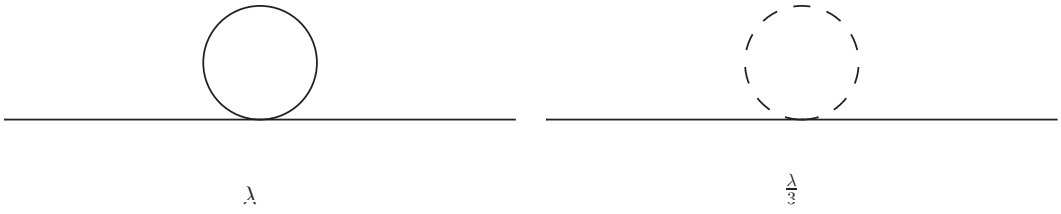

(a) Sigma particle propagating in the loop. (b) Pion propagating in the loop.

Figure 3.8: Loop corrections to the self-energy of the sigma particle derived from the double-bubble diagrams in Fig. 3.6

The above determinant is

$$\mathrm{Det}[D^{-1}(\omega_n,p)] = (\omega_n^2+p^2+M_1^2)(\omega_n^2+p^2+M_2^2) + (2\mu_I\omega_n - \Pi_{12})(2\mu_I\omega_n+\Pi_{21}). \tag{3.89}$$

We have introduced the notation

$$M_i^2 = m_i^2 + \Pi_{ii}, \tag{3.90}$$

with no summation over the index i in the self-energy term. M_i is thus the corrected mass of mode i. Turning now to Π_{12} and Π_{21}, we get contributions from two terms in $\Phi[D]$, namely $D_{ab}D_{ab}$ and $D_{ab}D_{ba}$. Thus we only get contributions to these self-energies from the off-diagonal terms in the inverse propagator of Eq. (3.87). This leads to the gap equations

$$\Pi_{12} = -\frac{\lambda}{4}\,\not\!\!\sum\!\!\!\!\!\!\int \frac{\Pi_{12}+\Pi_{21}}{\mathrm{Det}[D^{-1}(\omega_n,p)]}, \tag{3.91}$$

$$\Pi_{21} = -\frac{\lambda}{4}\,\not\!\!\sum\!\!\!\!\!\!\int \frac{\Pi_{21}+\Pi_{12}}{\mathrm{Det}[D^{-1}(\omega_n,p)]}. \tag{3.92}$$

The equations are symmetric, since they get equal contributions from the two diagrams in Fig. 3.6. This should be expected, since the two diagrams are essentially equivalent, the choice of direction in the loop is arbitrary. More fundamentally, this stems from the $O(2)$ symmetry of the Lagrangian. We conclude that

$$\Pi_{21} = \Pi_{12}. \tag{3.93}$$

Isolating the terms proportional to Π_{12} in Eq. (3.91) yields

$$\Pi_{12}\left(1 + \frac{\lambda}{2}\,\not\!\!\sum\!\!\!\!\!\!\int \frac{1}{\mathrm{Det}[D^{-1}(\omega_n,p)]}\right) = 0 \tag{3.94}$$

The expression in the brackets can not generally be expected to be zero, especially not as it depends on temperature and isospin chemical potential. We conclude that

$$\Pi_{12} = \Pi_{21} = 0. \tag{3.95}$$

This can be intuitively understood from considering the perturbative expansion in λ. In order to simplify the notation somewhat, let $\epsilon_0(\omega_n,p)$ be the determinant of the dressed propagator evaluated at $\Pi_{12}=0$. If we Taylor expand the right-hand side of Eq. (3.91) around $\Pi_{12}=\Pi_{21}=0$, we obtain

$$\Pi_{12} = -\frac{\lambda}{2}\Pi_{12}\,\not\!\!\sum\!\!\!\!\!\!\int \frac{1}{\epsilon_0(\omega_n,p)}\left(1+\frac{\Pi_{12}^2}{\epsilon_0(\omega_n,p)}+\frac{\Pi_{12}^4}{\epsilon_0(\omega_n,p)^2}+\cdots\right). \tag{3.96}$$

We now expand Π_{12} in powers of λ

$$\Pi_{12} = \Pi_{12}^{(1)} + \Pi_{12}^{(2)} + \Pi_{12}^{(3)} + \cdots. \tag{3.97}$$

To lowest order in λ, we obtain the following equation

$$\Pi_{12}^{(1)} = 0. \tag{3.98}$$

Figure 3.9: Feynman diagrams contributing to the lowest-order off-diagonal self-energies.

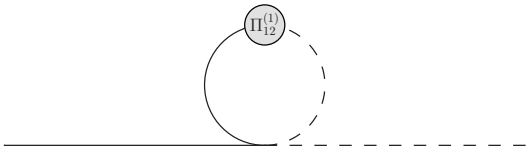

Figure 3.10: Feynman diagram corresponding to Eq. (3.99).

We might also derive the above equation directly by applying the Feynman rules to the diagrams in Fig. 3.9. To second order in λ, we obtain the equation

$$\Pi_{12}^{(2)} = -\frac{\lambda}{2}\Pi_{12}^{(1)} \oint\!\!\!\!\!\!\int \frac{1}{\epsilon_0(\omega_n, p)} = 0. \tag{3.99}$$

$\Pi_{12}^{(2)}$ is proportional to $\Pi_{12}^{(1)}$, and therefore zero. Any subsequent iteration to higher order would also be proportional to the lower-order corrections, again leading to the conclusion that $\Pi_{12} = 0$. If we examine this diagrammatically, Eq. (3.99) corresponds to the diagram in Fig. 3.10. If we insert for $\Pi_{12}^{(1)}$ in this diagram, it becomes a double loop, and since the outermost loop is zero, then so is the inner loop. This continues to all orders, since the primitive one-loop diagram is zero, and all higher-order diagrams depend on this one-loop diagram, we conclude that Π_{12} is zero to all orders in λ.

The diagonal self-energy terms are generally nonzero. We recall the O(2) invariant combinations of Kronecker deltas in Eq.(3.86) Only the first of these Kronecker delta terms give rise to diagrams like those of Fig. 3.8b, whereas all terms give rise to a diagram like that of Fig. 3.8a. We write $\Pi_{ii} = M_i^2 - m_i^2$. Eq. (3.36) then yields the following gap equations

$$\begin{aligned} M_1^2 - m_1^2 &= \frac{3\lambda}{2} \oint\!\!\!\!\!\!\int \frac{\omega_n^2 + p^2 + M_2^2}{4\mu^2\omega_n^2 + (\omega_n^2 + p^2 + M_1^2)(\omega_n^2 + p^2 + M_2^2)} \\ &\quad + \frac{\lambda}{2} \oint\!\!\!\!\!\!\int \frac{\omega_n^2 + p^2 + M_1^2}{4\mu^2\omega_n^2 + (\omega_n^2 + p^2 + M_1^2)(\omega_n^2 + p^2 + M_2^2)}, \end{aligned} \tag{3.100}$$

$$\begin{aligned} M_2^2 - m_2^2 &= \frac{3\lambda}{2} \oint\!\!\!\!\!\!\int \frac{\omega_n^2 + p^2 + M_1^2}{4\mu^2\omega_n^2 + (\omega_n^2 + p^2 + M_1^2)(\omega_n^2 + p^2 + M_2^2)} \\ &\quad + \frac{\lambda}{2} \oint\!\!\!\!\!\!\int \frac{\omega_n^2 + p^2 + M_2^2}{4\mu^2\omega_n^2 + (\omega_n^2 + p^2 + M_1^2)(\omega_n^2 + p^2 + M_2^2)}. \end{aligned} \tag{3.101}$$

The gap equations require renormalisation, see Appendix B for details.

Once renormalisation has been carried out, we obtain the renormalised gap equations

$$M_1^2 = m_1^2 + \frac{3\lambda}{2} I_f(M_1^2, M_2^2) + \frac{\lambda}{2} I_f(M_2^2, M_1^2), \tag{3.102}$$

$$M_2^2 = m_2^2 + \frac{\lambda}{2} I_f(M_1^2, M_2^2) + \frac{3\lambda}{2} I_f(M_2^2, M_1^2). \tag{3.103}$$

The integral $I_f(M_i^2, M_j^2)$ is defined in Eq. (B.31). With the renormalisation of the $O(2)$ gap equations and our results from the large-N approximation, we may now renormalise the $O(N)$ Hartree approximation in the chiral limit. We will therefore not study the stationarity conditions of the $O(2)$ model, but rather proceed to the $O(N)$ model.

3.6 The $O(N)$ Hartree approximation

The results from the $O(2)$ model, combined with what we have discovered about the large-N approximation can readily be used to study the $O(N)$-model under the Hartree approximation, provided that either ϕ_0 or ρ_0 is zero. To see this, we begin by studying the inverse propagator,

$$D^{-1} = \begin{pmatrix} \omega_n^2 + p^2 + M_1^2 & \frac{2\lambda}{N}\phi_0\rho_0 + \Pi_{12} & 0 & 0 & \cdots \\ \frac{2\lambda}{N}\phi_0\rho_0 + \Pi_{21} & \omega_n^2 + p^2 + M_2^2 & -2\mu_I\omega_n + \Pi_{23} & 0 & \cdots \\ 0 & 2\mu_I\omega_n + \Pi_{32} & \omega_n^2 + p^2 + M_3^2 & 0 & \cdots \\ 0 & 0 & 0 & \omega_n^2 + p^2 + M_4^2 & \cdots \\ \vdots & \vdots & \vdots & \vdots & \ddots \end{pmatrix}. \tag{3.104}$$

As in the case of the $O(2)$ model, $\Pi_{23} = \Pi_{32} = 0$. Following the same method, we derive the following equation for Π_{12}

$$\Pi_{12} = -\frac{3\lambda}{N} \not\int\!\!\!\!\sum \frac{(\frac{2\lambda}{N}\phi_0\rho_0 + \Pi_{12})(P^2 + M_3^2)}{\mathrm{Det}[D^{-1}(P)]} \tag{3.105}$$

If we assume $\phi_0 = 0$ or $\rho_0 = 0$, we may rewrite this as

$$\Pi_{12}\left[1 + \frac{3\lambda}{N} \not\int\!\!\!\!\sum \frac{P^2 + M_3^2}{\mathrm{Det}[D^{-1}(P)]}\right] = 0. \tag{3.106}$$

Again, the term in the brackets is temperature dependent and generally nonzero, and we therefore conclude that $\Pi_{12} = \Pi_{21} = 0$ if $\phi_0 = 0$ or $\rho_0 = 0$. Under such conditions, $D_{12} = D_{21} = 0$, thus reducing the inverse dressed propagator to diagonal elements and an $O(2)$ block matrix like the one we inverted and renormalised in the previous section. We will therefore study solutions to the gap equations where ϕ_0 or ρ_0 is zero.

We know that at $\mu_I = 0$, we may choose a solution where $\rho_0 = 0$ from symmetry, and thus we may attempt to reproduce the results of Lenaghan and Rischke [51] or Petropoulos [72] at $\mu_I = 0$ as a way of checking the correctness of our numerical results.

The solution $\phi_0 = 0$ matches what is found in the chiral limit of the large-N approximation and at tree-level, along with findings from the NJL model [76]. This stems from the term $-\frac{1}{2}\mu^2\rho^2$ at tree level, which, when unhindered by H serves to make ϕ_2 the direction the global minimum. We will therefore attempt to find a minimum of the effective potential in the chiral limit of the Hartree approximation by assuming that $\phi_0 = 0$. Since all off-diagonal self-energies are zero, we write $\Pi_i \equiv \Pi_{ii}$ to simplify the notation. The stationarity conditions for ϕ_0 and ρ_0 in the chiral limit of the Hartree approximation are

$$\phi_0\left[m^2 + \frac{\lambda}{N}(\phi_0^2 + \rho_0^2) + \Pi_1\right] = 0, \tag{3.107}$$

$$\rho_0\left[m^2 + \frac{\lambda}{N}(\phi_0^2 + \rho_0^2) - \mu_I^2 + \Pi_2\right] = 0. \tag{3.108}$$

At $T = \mu_I = 0$, the bracket in Eq. (3.108) is equal to M_2^2 which is zero in the vacuum in the chiral limit. Thus we are already at the critical chemical potential necessary to have a pion condensate and we conclude that $\mu_c = 0$. As we saw in the large-N approximation, we once more observe that the critical chemical potential is equal to the pion mass in the vacuum. This is as expected, since $H = \mu_I = 0$ yields a rotationally symmetric Lagrangian, and thus a degenerate set of minima of the effective potential. At $\phi_0 = 0$, the first derivative of the effective potential in the direction of ϕ_0 is zero, as can be seen by the stationarity condition. If a minimum of the effective potential is not in the direction of ϕ_2, then we expect that the second derivative of the effective potential should be negative in the direction of ϕ_1. Calulating this second derivative, we see that it is simply equal to M_1^2, as was mentioned in the section on Goldstone's theorem. We therefore see that unless we find a tachyonic sigma particle upon solving the gap equations with $\phi_0 = 0$, it is reasonable to assume that the minimum of the effective potential is in the ϕ_2-direction.

It should be noted – however – that the stationarity conditions also allow for solutions where ϕ_0 and ρ_0 are both nonzero, subtracting the brackets of (3.107) and (3.108) yields

$$\Pi_2 - \Pi_1 = \mu_I^2. \tag{3.109}$$

We note that this is true for $\mu_I = T = 0$, since $m_\pi = 0$ assures that (3.108) is fulfilled. Increasing μ_I breaks the rotational invariance of the effective potential, directly affecting the effective potential along with the charged pion propagators. In particular, the limit of large μ_I is characterised by small ϕ_0 even at the physical point in the large-N approximation [53], the NJL-model [76] and lattice simulations [75]. It is in this limit that we expect the chiral limit to be a good approximation to the physical point, since the scale of $\mu_I \gg m_\pi$ dominates in this region.

A consequence of choosing $\phi_0 = 0$ is that the σ and π^0 are degenerate. Due to the Vafa-Witten theorem [84], a charged pion condensate cannot arise in the vacuum, and hence we must choose $\rho_0 = 0$ and $\phi_0 \neq 0$ at $\mu_I = 0$. The moment the isospin chemical potential is increased from zero, we transition from a chiral condensate to a pion condensate, in agreement with our finding that $\mu_c = 0$. This transition is abrupt in the sense that for $\mu_I \neq 0$ we have $\rho_0 = 0$. Were $H > 0$, this crossover would happen at some finite isospin chemical potential, and the crossover would be somewhat softened. In the chiral limit, however, there is no incentive to retain the chiral condensate once the $O(N)$ symmetry of the effective potential is broken. The chemical potential deepens the effective potential in the ϕ_2-direction, resulting in pion condensation. This discontinuity in the transition is characteristic of the chiral limit. Choosing therefore to use solutions where $\phi_0 = 0$ should be expected to yield a phase diagram akin to what we see in the chiral limit of the large-N approximation. Pion condensation occurs then even at zero chemical potential, with a critical temperature on the order of 150 MeV.

Since the sigma and neutral pion masses are degenerate, we rewrite the inverse tree-level propagator as

$$D_0^{-1} = \begin{pmatrix} \omega_n^2 + p^2 + m_1^2 & -2\mu_I\omega_n & 0 & \cdots \\ 2\mu_I\omega_n & \omega_n^2 + p^2 + m_2^2 & 0 & \cdots \\ 0 & 0 & \omega_n^2 + p^2 + m_3^2 & \cdots \\ \vdots & \vdots & \vdots & \ddots \end{pmatrix}, \tag{3.110}$$

with the tree-level masses

$$m_1^2 = -\mu^2 + m^2 + \frac{3\lambda}{N}\rho_0^2, \tag{3.111}$$

$$m_2^2 = -\mu^2 + m^2 + \frac{\lambda}{N}\rho_0^2, \tag{3.112}$$

$$m_3^2 = m^2 + \frac{\lambda}{N}\rho_0^2. \tag{3.113}$$

As in the case of the $O(2)$ model, $\Phi[D]$ is given by Eq. (3.86)

$$\Phi[D] = \frac{\lambda}{4N}\left(\delta_{ab}\delta_{cd} + \delta_{ac}\delta_{bd} + \delta_{ad}\delta_{bc}\right) D_{ab}D_{cd}. \tag{3.114}$$

From the stationarity condition in Eq. (3.35), we obtain the following gap-equations

$$\begin{aligned} M_1^2 - m_1^2 &= \frac{\lambda}{N}\sum\!\!\!\!\!\!\int \left[3D_{11} + D_{22} + (N-2)D_{33}\right] \\ &= \frac{3\lambda}{N}I(M_1^2) + \frac{\lambda}{N}I(M_2^2) + (N-2)\frac{\lambda}{N}I_N(M_3^2), \end{aligned} \tag{3.115}$$

$$\begin{aligned} M_2^2 - m_2^2 &= \frac{\lambda}{N}\sum\!\!\!\!\!\!\int \left[D_{11} + 3D_{22} + (N-2)D_{33}\right] \\ &= \frac{\lambda}{N}I(M_1^2) + \frac{3\lambda}{N}I(M_2^2) + (N-2)\frac{\lambda}{N}I_N(M_3^2), \end{aligned} \tag{3.116}$$

$$\begin{aligned} M_3^2 - m_3^2 &= \frac{\lambda}{N}\sum\!\!\!\!\!\!\int \left[D_{11} + D_{22} + ND_{33}\right] \\ &= \frac{\lambda}{N}I(M_1^2) + \frac{\lambda}{N}I(M_2^2) + \lambda I_N(M_3^2). \end{aligned} \tag{3.117}$$

$I(M_i^2)$ is the sum-integral defined in Eq. (B.1), and likewise $I_N(M_i^2)$ is defined in Eq. (A.1) Using our results from the preceding chapters, we may split the integrals in the gap equations into finite and divergent parts

$$I(M_i^2) = I_f(M_i^2, M_j^2) + I_d\tilde{M}_i^2, \tag{3.118}$$

$$I_N(M_i^2) = I_{Nf}(M_i^2, M_j^2) + I_d\tilde{M}_i^2. \tag{3.119}$$

Note that the divergent parts of the two integrals are exactly the same. Moreover, $\tilde{m_2^2} = m_3^2$, so in terms of renormalisation, we might expect that since the divergences are independent of μ_I, our results should be the same as those of Fejos *et al.* [50] and Lenaghan and Rischke [51], who studied the linear sigma model at zero isospin chemical potential. Following the same method as we did when renormalising the $O(2)$-model in Appendix B, Eq. (3.115) yields the following three conditions

$$\delta\lambda_A + 2\delta\lambda_B = -\frac{\lambda}{N} I_d \left[(N+2)\delta\lambda_A + 6\delta\lambda_B + (N+8)\lambda\right], \tag{3.120}$$

$$\delta\lambda_A = -\frac{\lambda}{N} I_d \left[(N+2)\delta\lambda_A + 2\delta\lambda_B + (N+4)\lambda\right], \tag{3.121}$$

$$\delta m^2 = -\frac{m^2}{N} I_d \left[N\delta\lambda_A + 2\delta\lambda_B + (N+2)\lambda\right]. \tag{3.122}$$

Solving these equations for $\delta\lambda_A$ and $\delta\lambda_B$ yields

$$\delta\lambda_A = -\lambda^2 I_d \frac{N(N+4) + 2\lambda I_d(N+2)}{(N+2\lambda I_d)(N+\lambda I_d(N+2))}, \tag{3.123}$$

$$\delta\lambda_B = -\frac{2\lambda^2 I_d}{N+2\lambda I_d}. \tag{3.124}$$

As we saw when renormalising the $O(2)$ model, the gap equations of the other particles yield the same counterterms. Note that in the large N limit the counterterms reduce to $\delta\lambda_B \to 0$ and $\delta\lambda_A \to -\frac{\lambda^2 I_d}{1+\lambda I_d}$. This leads to the substitution $\lambda \to \frac{\lambda}{1-\frac{\lambda}{16\pi^2\epsilon}}$, the same substitution we made when renormalising the large-N limit. Similarly, inserting $N = 2$ in the above counterterms we recover the counterterms found in the $O(2)$ model. What remains are the renormalised gap-equations

$$\Pi_1 = M_1^2 - m_1^2 = \frac{3\lambda}{N} I_f(M_1^2, M_2^2) + \frac{\lambda}{N} I_f(M_2^2, M_1^2) + (N-2)\frac{\lambda}{N} I_{Nf}(M_3^2) \tag{3.125}$$

$$\Pi_2 = M_2^2 - m_2^2 = \frac{\lambda}{N} I_f(M_1^2, M_2^2) + \frac{3\lambda}{N} I_f(M_2^2, M_1^2) + (N-2)\frac{\lambda}{N} I_{Nf}(M_3^2) \tag{3.126}$$

$$\Pi_3 = M_3^2 - m_3^2 = \frac{\lambda}{N} I_f(M_1^2, M_2^2) + \frac{\lambda}{N} I_f(M_2^2, M_1^2) + \lambda I_{Nf}(M_3^2) \tag{3.127}$$

Finally, we have the stationarity condition for ρ_0

$$\begin{aligned} 0 = \frac{\delta\Gamma}{\delta\rho_0} &= \rho_0 \left[m^2 - \mu^2 + \frac{\lambda}{N}\rho_0^2 + \frac{\lambda}{N} \not{\sum\!\!\!\!\!\!\int} \left(3D_{11} + D_{22} + (N-2)D_{33}\right) \right] \\ &= \rho_0 \left[m^2 - \mu^2 + \frac{\lambda}{N}\rho_0^2 + \Pi_1 \right] \\ &= \rho_0 \left[M_1^2 - \frac{2\lambda}{N}\rho_0^2 \right] \end{aligned} \tag{3.128}$$

We will solve these equations numerically with respect to the mass modes and ρ_0.

3.7 Numerics and starting parameters

We will use Wolfram Matehematica's [85] built-in numerical equation solver to solve the gap-equations. Unavoidably when performing numerics there will be some limitations to the accuracy of our results due to inaccuracies stemming from the 64-bit representation of floating-point numbers. Our chosen method of renormalisation for the $O(2)$-model involves subtracting some large terms in the integrand of $I(M^2)$, this is particularly vulnerable to numerical noise, since we are subtracting two very large floating point numbers. For this reason, we have introduced a cutoff in the integrals determined by the condition that the integrand divided by the momentum must be larger than 10^{-16}. This is simply to remove the region where we get numerical noise due to large momenta in the integrand, which only happens when the integral and the counterterms are both almost equal in magnitude and very large.

We now tune our parameters to fit the masses of the pions and the sigma particle in the vacuum. At $\mu = T = 0$, $\phi_0 = f_\pi = 93$ MeV by definition of the pion coupling constant f_π, and we use $M_4 = m_\sigma = 600$ MeV,

and $M_1 = M_2 = M_3 = m_\pi = 139$ MeV at the physical point. The insertion of these values into the gap equations and stationarity conditions at $T = \mu_I = 0$ yields conditions which may be used to determine m, λ and H.

3.7.1 Large-N approximation

At $T = 0$, we have

$$I_{Nf}(M^2) = -\frac{M^2}{16\pi^2}\ln\frac{\Lambda^2 e}{M^2}. \tag{3.129}$$

By inserting $M_1 = m_\sigma$ and $M = m_\pi$ in the renormalised gap equation for M (3.58), and the corresponding equation for M_1 we obtain the following conditions for $T = \mu_I = 0$

$$m_\sigma^2 = m^2 + \frac{3\lambda}{N}f_\pi^2 - \frac{\lambda m_\pi^2}{16\pi^2}\ln\frac{\Lambda^2 e}{m_\pi^2}, \tag{3.130}$$

$$m_\pi^2 = m^2 + \frac{\lambda}{N}f_\pi^2 - \frac{\lambda m_\pi^2}{16\pi^2}\ln\frac{\Lambda^2 e}{m_\pi^2}. \tag{3.131}$$

We see from the above that it is convenient to choose $\Lambda = m_\pi e^{-\frac{1}{2}}$, thereby eliminating the above logarithmic terms. This corresponds to choosing there to be no quantum corrections to the tree-level masses at $T = \mu_I = 0$. The stationarity condition for ϕ_0, Eq.(3.61), yields the additional requirement

$$f_\pi m_\pi^2 = H. \tag{3.132}$$

We see that when $H = 0$, we must have $m_\pi = 0$ as one might deduce from Goldstone's theorem. We solve Eqs. (3.130) and (3.131) for λ and m^2 to obtain

$$m^2 = \frac{3m_\pi^2 - m_\sigma^2}{2} \tag{3.133}$$

$$\lambda = \frac{N}{2}\frac{m_\sigma^2 - m_\pi^2}{f_\pi^2}. \tag{3.134}$$

At the physical point we find the parameters $H = 1796853$ MeV^3, $m^2 = -151018.5$ MeV^2 and $\lambda = 78.7788$. In the chiral limit, we find $H = 0$, $m^2 = -180000$ MeV^2 and $\lambda = 83.2466$.

3.7.2 Hartree approximation

Since $I_f = I_{Nf}$ and $M_1 = M_2 = m_\pi$ at $T = \mu = 0$ the renormalised gap equations – Eqs. (3.125), (3.126), and (3.127) – for the pion and sigma mass become

$$m_\sigma^2 = m^2 + \frac{3\lambda}{N}f_\pi^2 - \frac{3\lambda}{N}\frac{m_\sigma^2}{16\pi^2}\ln\frac{\Lambda^2 e}{m_\sigma^2} - (N-1)\frac{\lambda}{N}\frac{m_\pi^2}{16\pi^2}\ln\frac{\Lambda^2 e}{m_\pi^2}, \tag{3.135}$$

$$m_\pi^2 = m^2 + \frac{3\lambda}{N}f_\pi^2 - \frac{\lambda}{N}\frac{m_\sigma^2}{16\pi^2}\ln\frac{\Lambda^2 e}{m_\sigma^2} - (N+1)\frac{\lambda}{N}\frac{m_\pi^2}{16\pi^2}\ln\frac{\Lambda^2 e}{m_\pi^2}. \tag{3.136}$$

The stationarity condition for the sigma particle can be written as

$$f_\pi\left[m^2 + \frac{\lambda}{N}f_\pi^2 - \frac{3\lambda}{N}\frac{m_\sigma^2}{16\pi^2}\ln\frac{\Lambda^2 e}{m_\sigma^2} - (N-1)\frac{\lambda}{N}\frac{m_\pi^2}{16\pi^2}\ln\frac{\Lambda^2 e}{m_\pi^2}\right] = H. \tag{3.137}$$

We anticipate that $m_\pi = 0$ in the chiral limit of the Hartree approximation, and so we choose $\Lambda = m_\pi e^{-\frac{1}{2}}$ in order to once more remove all quantum corrections at $T = \mu_I = 0$. In the chiral limit, $H = 0$, and we insert Eq. (3.136) into the brackets of the stationarity condition to obtain

$$f_\pi m_\pi^2\left[1 + \frac{2\lambda}{N}\frac{1}{16\pi^2}\ln\frac{m_\pi^2}{m_\sigma^2}\right] = 0. \tag{3.138}$$

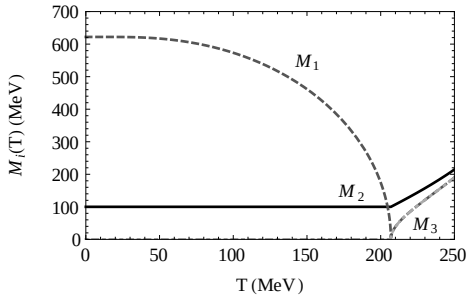

(a) The mass modes.

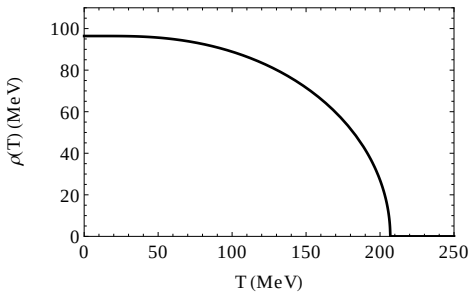

(b) The pion condensate density ρ.

Figure 3.11: Quasiparticle masses and pion condensate density as a function of temperature in the chiral limit of the large-N approximation at $\mu_I = 100$ MeV.

We see that taking the limit $m_\pi \to 0$ satisfies this condition and conclude that $m_\pi = 0$ in the chiral limit of the Hartree approximation. Note that this was dependent upon our choice of renormalisation scale, and that for other renormalisation scales, $m_\pi = 0$ is not a valid solution. This is in agreement with Lenaghan and Rischke [51], who found that there is only one consistent renormalisation scale for the Hartree approximation in the chiral limit. Eqs. (3.135) and (3.136) are now

$$m_\sigma^2 = m^2 + \frac{3\lambda}{N} f_\pi^2, \tag{3.139}$$

$$0 = m^2 + \frac{\lambda}{N} f_\pi^2. \tag{3.140}$$

Our choice of Λ has eliminated the quantum corrections from Eqs. (3.135) and (3.136). They now coincide with the corresponding equations in the chiral limit of the large-N approximation. We therefore obtain the same parameters, namely $m^2 = -180000$ MeV^2 and $\lambda = 83.2466$.

At the physical point, the choice of renormalisation scale becomes less obvious. In order to verify our results against those of Lenaghan and Rischke [51], we have used their renormalisation scale, namely

$$\Lambda = \exp\left[\frac{m_\sigma^2(\ln m_\sigma^2 - 1) - m_\pi^2(\ln m_\pi^2 - 1)}{2(m_\sigma^2 - m_\pi^2)}\right] \tag{3.141}$$

This renormalisation scale preserves the value of λ found at the physical point in the large-N approximation. By solving Eqs. (3.135), (3.136), and (3.137) numerically, we obtain the parameters $H = 1.79685{\cdot}10^6$ MeV^3, $m^2 = -106331$ MeV^2 and $\lambda = 78.7788$.

3.8 Results and discussion

Fig. 3.11 shows the quasiparticle masses and pion condensate density as a function of temperature in the chiral limit of the large-N approximation. As predicted, the transition to a pion condensate is second order for all temperatures and chemical potentials. We find the critical exponent ν – defined by $\rho \approx C\,|T - T_c|^\nu$ for T close to T_c and some constant C – to be 0.49902 with 300 samples and a variance of 10^{-4}, this is consistent with the expected 0.5 characteristic of mean-field theory. The slight deviation is due to our inability to sample $\ln|T - T_c|$ too close to T_c with sufficient precision. The quasiparticle masses and condensate densities at the physical point and zero temperature is plotted as a function of chemical potential in Fig. 3.12, and as a function of temperature at $\mu_I = 100$ MeV in Fig. 3.13. In addition, we plot the pion condensate density ρ_0 as a function of T and μ_I in Fig. 3.14 As predicted, ρ_0 remains zero up to the critical chemical potential $\mu_c = m_\pi$, after which pion condensation occurs. This phase transition is second order in the pion condensate, whereas the chiral condensate decreases abruptly following the onset of pion condensation in the manner of a crossover. These results reproduce those found by Andersen [53].

The masses in Fig. 3.13 behave peculiarly in the area around T_c. Near the critical temperature, the mass of the π^- rises abruptly, while M_σ declines. The reason for this is the transition to $\rho_0 = 0$, which implies $M_{\pi^-} = M_{\pi^0} + \mu_I = M_{\pi^+} + 2\mu_I$. At the same time, M_σ must approach M_{π^0} when $T \to \infty$, since we expect $\phi_0 \to 0$ in this limit. Thus M_σ and M_{π^-} must cross near $T = T_c$.

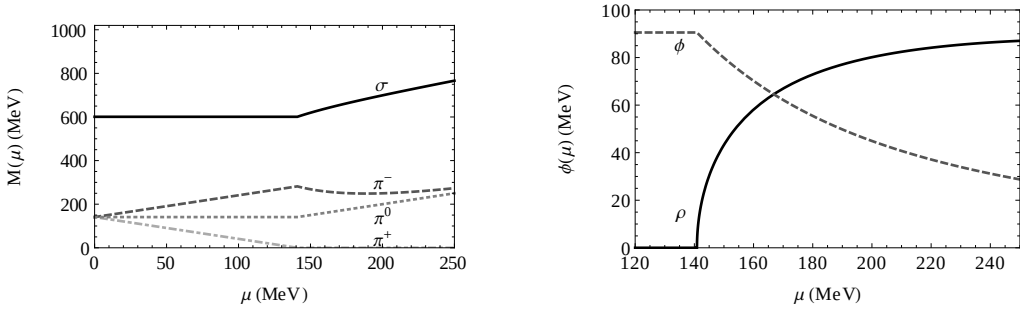

(a) The quasiparticle masses. (b) The condensate densities.

Figure 3.12: Quasiparticle masses and condensate densities at the physical point of the large-N approximation as a function of μ_I at $T = 0$

.

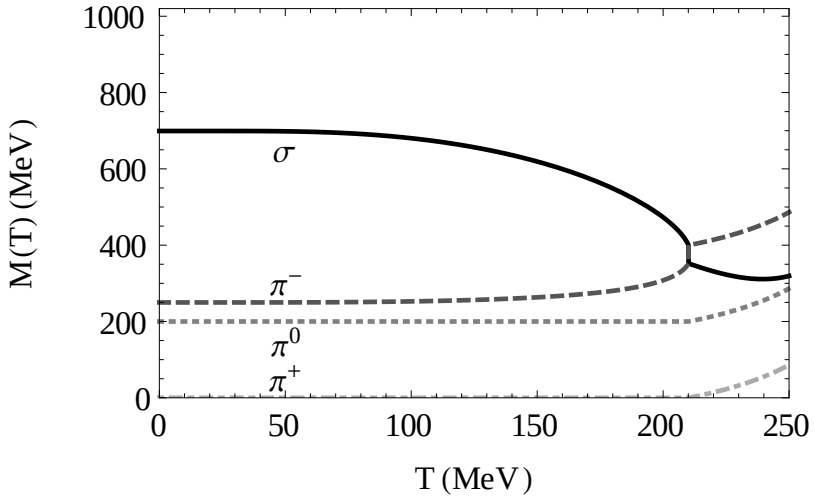

Figure 3.13: The quasiparticle masses as a function of temperature at the physical point of the large-N approximation as a function of T with $\mu_I = 200$.

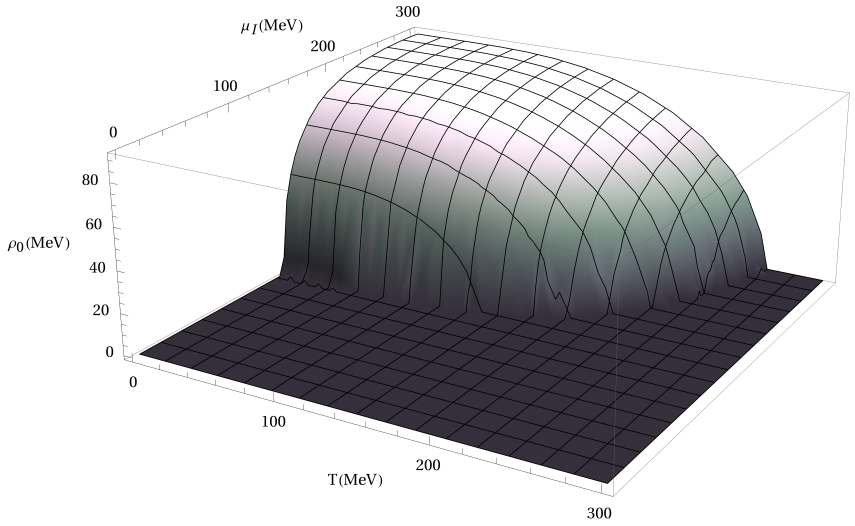

Figure 3.14: The pion condensate ρ_0 as a function of T and μ_I in the large-N approximation at the physical point.

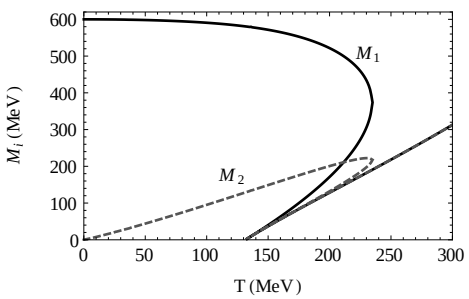

(a) The quasiparticle masses, M_2 and M_3 are degenerate.

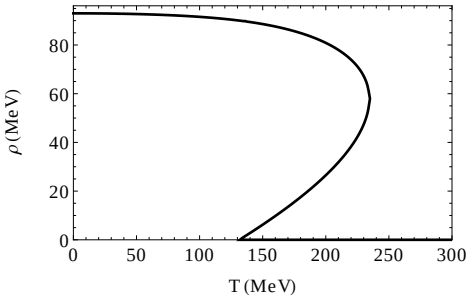

(b) The pion condensate density ρ.

Figure 3.15: Quasiarticle masses and condensate density in the chiral limit of the Hartree approximation as a function of temperature at $\mu_I = 0$.

Fig. 3.15 shows the masses and condensate density as a function of temperature at zero chemical potential in the Hartree approximation. It matches exactly the results of Lenaghan and Rischke [51]. In this plot, since $\mu_I = 0$ we have

$$M_1 = M_{\pi^-}, \tag{3.142}$$

$$M_2 = M_3 = M_{\pi^0} = M_{\pi^+}. \tag{3.143}$$

It is apparent that Goldstone's theorem is not obeyed in the Hartree approximation. Were it obeyed, we would expect $M_2 = 0$, however M_2 manages to reach a mass $M_2(235) \approx 200$ MeV $> m_\pi$. The reason for this violation is the incompleteness of the approximation, which fails to take into account the setting-sun diagram [58, 72, 83]. As mentioned before, the $\frac{1}{N}$ expansion obeys Goldstone's theorem order by order [54].

Increasing the potential to $\mu_I = 100$, the mass modes and particle masses are plotted as a function of temperature in Fig. 3.16. The slight kink in M_2 is likely due to this mode becoming tachyonic at low temperatures, at which point the numerics become unstable. It is important to note that $M_2 \neq M_\sigma$, thus this is not an indication that $\phi \neq 0$ as discussed in the previous section. A possible explanation for this low-temperature behaviour is that it is due to to the exponential $e^{\epsilon_\pm(p)/T}$ in the distribution function, which in the low-T limit is highly dependent upon the behaviour of $\epsilon_\pm$. For $M_2 < \mu_I$, ϵ_- becomes imaginary, producing poles which break the stability of our numerical methods. Thus the numerics become unstable at low temperatures, but should be correct for $T \geq \mu_I$. Another possible explanation for this behaviour is that the Hartree approximation at finite isospin density breaks the residual $O(2)$ symmetry. As discussed for the sigma particle, a negative M_2^2 indicates that the second derivative of the effective potential is negative in the direction of ϕ_2, and would thus suggest that the true minimum of the effective potential lies in the plane spanned by ϕ_1 and ϕ_2, in spite of the fact that the Lagrangian is $O(2)$-symmetric with respect to these fields. Clearly this is not possible, and we are forced to conclude that if so, the violation of the $O(2)$ symmetry in the Hartree approximation leads to large inconsistencies. By not including the setting sun diagram for ϕ_2, we have already observed a violation of Goldstone's theorem, implying the absence of the residual $O(2)$ symmetry even at $\mu_I = 0$. Further increasing μ_I, and hence also ρ_0 might serve to exacerbate the matter. However, Nemoto *et. al.* have shown that M_2^2 does not entirely coincide with the second derivative of the effective potential [58]. If so, this means that the effective potential might still retain its symmetry in spite of the somewhat unusual quasiparticle masses, and its second derivatices might yield more sensible physical masses as a result.

In both of the above plots, the density (and hence M_1) curve back on themselves, so that from some temperature $T \approx 130$ MeV and upwards there exists three solutions to the gap equations. The reason for this becomes apparent in Fig. 3.17, where we plot the effective potential as a function of ρ_0 for selected values of T. At $T = 220$ MeV the global minimum of the effective potential is for $\rho_0 \approx 77$ MeV. In addition there is a local maximum at $\rho_0 \approx 35$ MeV and a local minimum at $\rho = 0$, yielding a total of three solutions to the stationarity condition for ρ_0. At $T = 230$ MeV, while there is still a local minimum present at $\rho_0 \neq 0$, the global minimum is now at $\rho_0 = 0$. Thus the order parameter ρ_0 jumps discontinuously from $\rho_0 \geq 60$ MeV to $\rho_0 = 0$, indicating a first order phase transition, as opposed to the second order phase transition found in the large-N approximation.

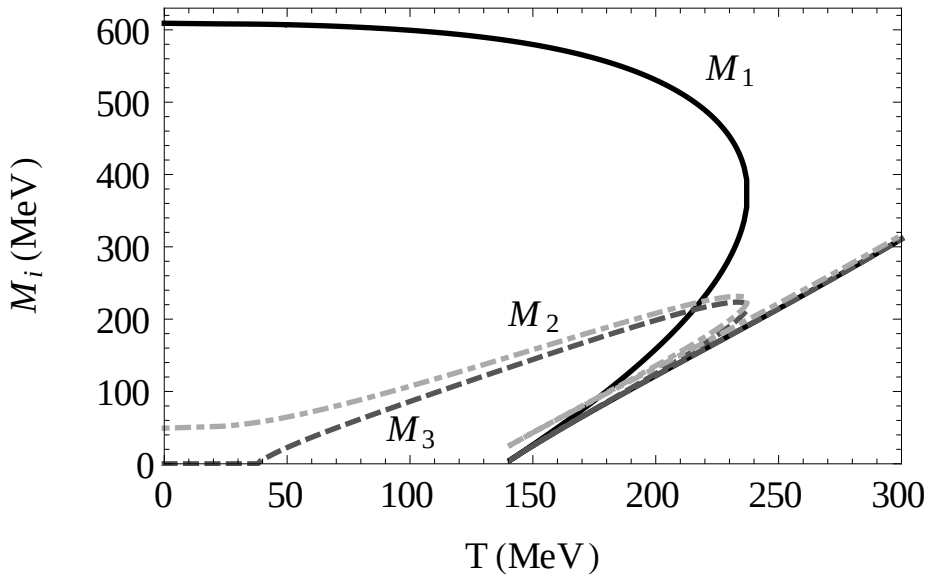

(a) The mass modes.

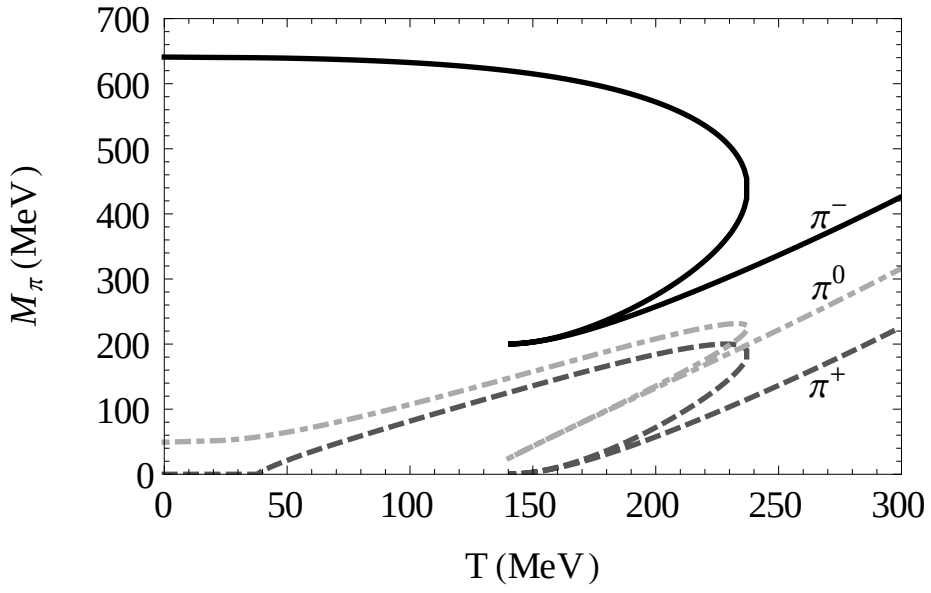

(b) The pion masses.

Figure 3.16: Mass modes and quasiparticle masses as a function of temperature at $\mu_I = 100$ in the chiral limit of the Hartree approximation.

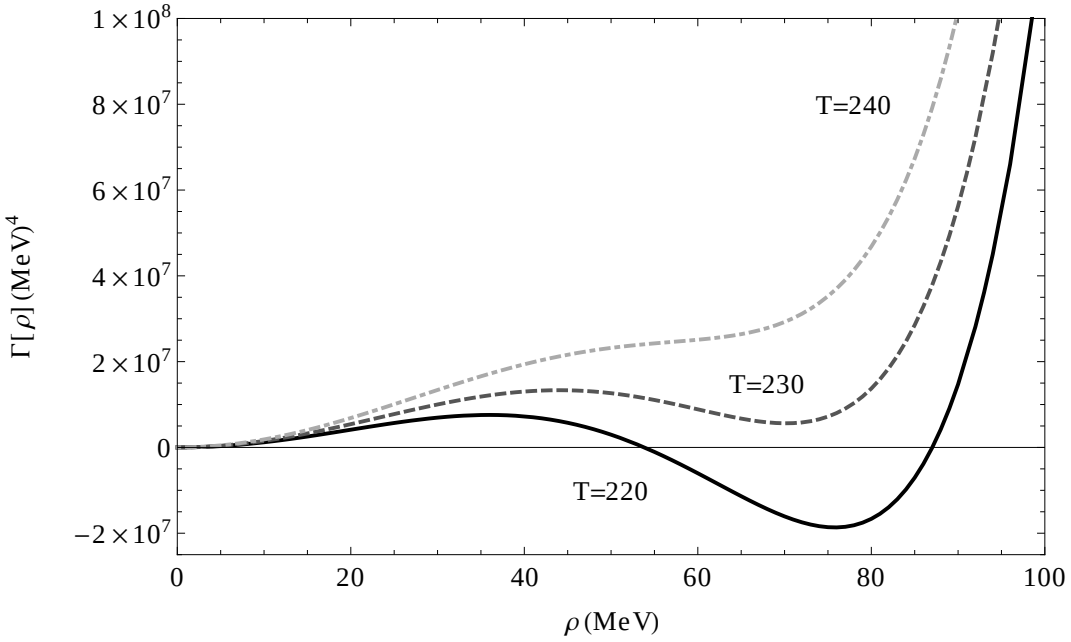

Figure 3.17: The effective potential as a function of condensate density at $\mu_I = 100$ and different temperatures.

T_c must thus be found for a given μ_I by finding the point at which the two minima of the effective potential are equal. The phase diagram in the Hartree approximation is plotted alongside the results found for the large-N approximation in Fig. 3.18. In the Hartree approximation, $T_c(\mu_I = 0) = 224.1$ MeV, larger than that of the large-N approximation. This is a drastic change, however for $N = 4$ we should expect a correction to the large-N approximation on the order of $\frac{1}{N} = 0.25$. The ratio between $T_c(\mu_I = 0)$ in the Hartree and large-N approximation is roughly 1.4, this is a bit larger than the expected 1.25, but seems within reason. It is also consistent with the results found at next-to-leading order in the 1PI large-N approximation by Andersen and Brauner [68].

However, T_c ascends much slower than in the large-N case due to the corrections imposed by the loop integrals containing $\pi^\pm$. As the large-N approximation only takes into account the mass of the neutral pion, which is largely unaffected by the chemical potential, we can only expect this approximation to be valid for small μ_I. The low rate of ascent is similar to that found by Andersen and Kyllingstad in the Nambu-Jona-Lasinio model [76]. Based on this, we may speculate that T_c in the Hartree approximation at the physical point will grow more quickly than the large-N approximation around $\mu_I = m_\pi$, but will since flatten, asymptotically approaching the results found in the chiral limit for $\mu_I \gg m_\pi$.

The results of Kogut and Sinclair for lattice simulations [75], along with the chiral perturbation studies performed by Splittorff *et. al.* [86] predict that μ_I close to $\mu_c = m_\pi$ is characterised by a second order transition in the pion condensate, which for increasing μ_I becomes a first order transition from a condensate phase to the symmetry restored phase. Kogut and Sinclair predict that this critical point is at $\mu_I \approx \frac{4}{3} m_\pi = 185$ MeV. At higher μ_I, T_c is predicted to increase much slower than below the critical point. The first order nature of the Hartree approximation, along with its slow growth matches this prediction well for high μ_I, the domain in which the chiral limit is expected to be close to the results for the physical point. However, the introduction of a nonzero H is known to soften the phase transition from a chiral condensate at $\mu_I = 0$ [87], as can be seen in the results of Lenaghan and Rischke [51]. It is unknown whether this will also affect the transition from the pion condensate, seeing as H couples to the chiral condensate. However, it is possible that a nonzero H will produce a crossover between the chiral condensate and the pion condensate, and that the Hartree approximation might then have a tricritical point. Results from the NJL model [76, 88], along with results from chiral perturbation theory [6, 7] have found only second-order transitions. As mentioned by Andersen and Kyllingstad, the second-order behaviour might be due to the nature of mean-field approximations, if so it is curious that the Hartree approximation might yield a first-order phase transition.

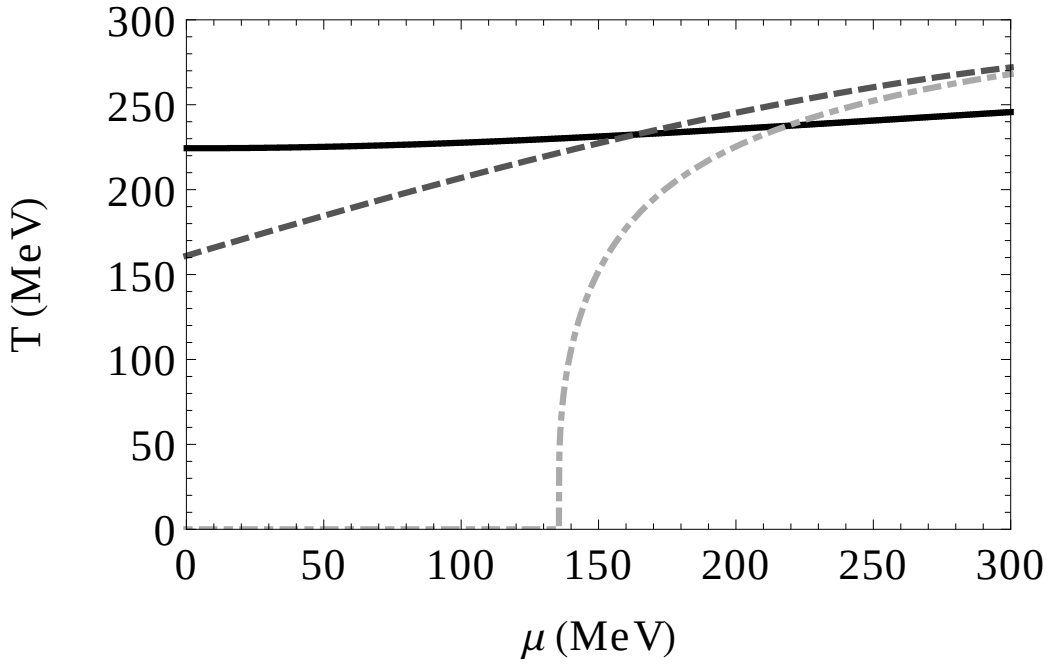

Figure 3.18: The phase diagram in the Hartree and large-N approximations. The solid line shows the critical temperature T_c as a function of μ_I in the Hartree approximation chiral limit. The dashed line shows the results from the large-N approximation in the chiral limit, and the dash-dotted line shows the results of the large-N approximation at the physical point.

Without further study of the physical point – and in particular without allowing for a crossover phase where both ϕ_0 and ρ_0 are nonzero – we will not be able to study the nature of the phase transition in the region where it is expected to be of first order. It is possible that the off-diagonal terms $\frac{\lambda}{N}\phi_0\rho_0$ in the tree-level propagator along with a nonzero value of H is sufficient to ensure a first-order phase transition between a chiral and a pion condensate.

For completeness, we have also reproduced the results of Lenaghan and Rischke at the physical point, these are plotted in Fig. 3.19. It is clear that a nonzero H has softened the deconfinement transition, turning it into a gradual crossover transition for increasing temperatures.

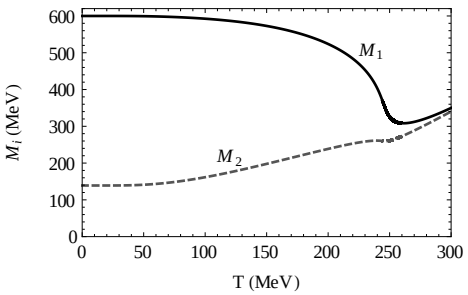

(a) Quasiparticle masses.

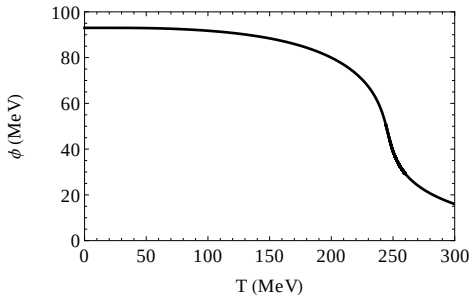

(b) Chiral condensate density ϕ_0.

Figure 3.19: Quasiparticle masses and chiral condensate density at the physical point in the Hartree approximation for $\mu_I = 0$.

Chapter 4

Conclusions and outlook

In this thesis we have studied pion condensation at finite temperature and isospin chemical potential in the context of the linear sigma model. While being a simple model, the sigma model allows for many of the features of low-energy QCD. In particular, we have seen how the explicit symmetry breaking at the physical point turns the melting of the chiral condensate into a crossover transition. Similarly, we have seen examples of the phase transition to a pion condensate being both first and second order. The Hartree and Large-N approximations have been studied and were found to yield very different results. The Large-N approximation yields results typical for mean-field approaches, including a second order transition from a pion condensate beginning at $\mu_c = m_\pi$ and a critical exponent $\nu = 0.5$. In comparison with results from other models and particularly lattice QCD, however, the Large-N approximation displays an unbounded increase in the critical temperature of pion condensation for increasing isospin chemical potentials, limiting its validity to low μ_I. We have only been able to fully describe the Hartree approximation when either the pion or chiral condensate is zero. In particular we have been able to study the phase diagram of the Hartree approximation in the chiral limit of $m_\pi = 0$, and have observed a much slower growth rate in T_c than in the large-N approximation. In the chiral limit, the transition from a pion condensate is first order, in agreement with the lattice QCD results of Kogut and Sinclair at high μ_I. It is therefore possible that the Hartree approximation at the physical point allows for a tricritical point, with a crossover transition to the quark-gluon plasma at low isospin chemical potentials, a second order transition to pion condensation at high isospin chemical potential, and a first order phase transition at high temperatures and chemical potential. The validity of the Hartree approximation is compromised, however, by its lack of adherence to symmetries. We have seen a large violation of Goldstone's theorem, and tachyonic behaviour which may or may not be due to this lack of symmetry in the model.

A natural next step would be to apply the condition of charge neutrality to the linear sigma model, complementing the work done in the NJL model by Ebert and Klimenko [65], Abuki *et al.* [88] and Andersen and Kyllingstad [76]. The condition of charge neutrality provides that nuclear matter should be electrically neutral. The reason behind this is the large energetic cost of a net electrical charge, due to Coulomb forces [89].

Since a pion condensate has a net electrical charge, there must be a background field of charged particles to compensate for the excess electrical charge in the pion condensate. A simple way to accomplish this is by introducing a non-interacting electron field to the Lagrangian. The electron and quark fields are connected through the weak process of β decay, we therefore require the system to be in β-equilibrium. β decay stems from the process

$$d \leftrightarrow \nu + e + u, \tag{4.1}$$

and we assume that this is as likely to happen in both directions. Neutrinos only participate in weak interactions, and will therefore escape the interior of a quark star after being produced, contributing to cooling of the neutron star. We will therefore make no assumption about conservation of neutrino numbers, but will include an ideal electron gas in the Lagrangian by adding the term

$$\mathcal{L}_e = \bar{\psi}_e \left[i\gamma^\mu \partial_\mu - \gamma^0 \mu_Q - m_e \right] \psi_e \tag{4.2}$$

We have introduced the electric chemical potential $\mu_Q = -\mu_e$ – where μ_e is the chemical potential coupling to preservation of electron numbers, $j^\mu = \bar{\psi}_e \gamma^\mu \psi_e$ – by adding a static gauge field coupling to the electron

field ψ_e. To a first approximation, we let the electrons be massless, $m_e = 0$. The isospin chemical potential contributes to μ_Q through the chemical potentials μ_u and μ_d

$$\mu_I = \mu_u - \mu_d. \tag{4.3}$$

β-equilibrium implies

$$\mu_d = -\mu_Q + \mu_u. \tag{4.4}$$

Which leads to the relation

$$\mu_I = \mu_Q, \tag{4.5}$$
$$\tag{4.6}$$

We could have deduced this directly from the quark charges $Q_u = \frac{2}{3}e$ and $Q_d = -\frac{1}{3}e$, the result is a consequence of charge-conservation in β decay. In order to introduce charge neutrality, we use the relation [36]

$$Q = -\frac{\partial \mathcal{F}}{\partial \mu_Q}. \tag{4.7}$$

The electron field contributes to the free energy through the term

$$\Omega_e = \mathrm{Tr} \ln D_e^{-1} = \sum\!\!\!\!\!\!\int \ln(\gamma^\mu p_\mu - \mu_Q). \tag{4.8}$$

We have calculated and renormalised the corresponding term Ω_p for the charged pions in Appendix B, they are given by (B.60)

$$\begin{aligned}\Omega_p = \frac{1}{2}\mathrm{Tr} \ln D^{-1} = \frac{\tilde{M_1}^4}{32\pi^2}\left(\ln\frac{\Lambda^2}{M_1^2} + \frac{3}{2}\right) + \frac{\tilde{M_2}^4}{32\pi^2}\left(\ln\frac{\Lambda^2}{M_2^2} + \frac{3}{2}\right) \\ + \frac{T}{\pi^2}\int dp p^2 \left(\ln(1 - e^{\frac{\epsilon_+}{T}}) + \ln(1 - e^{\frac{\epsilon_-}{T}})\right).\end{aligned} \tag{4.9}$$

Following the same procedure for Ω_e, we calculate the Matsubara sum in Eq. (4.8)

$$\Omega_e = -2\int \frac{d^d p}{(2\pi)^d}\left[|p| + T\ln\left(1 + e^{-\beta(|p|-\mu_Q)}\right) + T\ln\left(1 + e^{-\beta(|p|+\mu_Q)}\right)\right]. \tag{4.10}$$

The first term in the square brackets is a power divergence and vanishes in dimensional regularisation. We find

$$\Omega_e = -\frac{\mu_Q^4}{12\pi^2} - \frac{\mu_Q^2 T^2}{6} - \frac{7\pi^2}{180}T^4. \tag{4.11}$$

Charge neutrality is imposed by requiring

$$\frac{\partial \Omega}{\partial \mu_Q} = \frac{\partial \Omega_p}{\partial \mu_Q} + \frac{\partial \Omega_e}{\partial \mu_Q} = 0. \tag{4.12}$$

The above requirement puts an additional constraint on the phase diagram, reducing it to a point. For every temperature there is only one chemical potential which results in charge-neutrality, and it is this dependence which determines whether pion condensation may or may not occur. Abuki studied the charge-neutral pion condensate in the NJL model as a function of the physical pion mass and found that pion condensation can only occur for low pion masses, far from the physical point [88].

Another avenue of interest would be the study of the Hartree approximation with the possibility of both ϕ_0 and ρ_0 being nonzero. This will make renormalisation even more complex, as the determinant of the inverse propagator becomes sixth order in ω_n, but will allow one to study the nature of the transition from a chiral to a pion condensate, possibly confirming the existence of a tricritical point. It would also be of interest to study the mass modes stemming from the second derivatives of the effective potential, proposed by Nemoto *et. al.* [58]. An even more promising vein would be to study the next-to-leading order $\frac{1}{N}$ expansion, which would include all the diagrams of the Hartree approximation and adhere to symmetries. However, this will include the setting sun diagrams, turning the gap equations into momentum-dependent integral equations and further increasing the complexity of the calculations.

Appendices

Appendix A

Renormalising the Large-N approximation

We recall the gap equation, Eq. (3.55)

$$M_4^2 = m_4^2 + \lambda \sum\!\!\!\!\!\!\int_Q \frac{1}{Q^2 + M_4^2}.$$

The sum-integral will require renormalisation, we define

$$I_N(M_4^2) \equiv \sum\!\!\!\!\!\!\int_Q \frac{1}{Q^2 + M_4^2} \tag{A.1}$$

We have already calculated the Matsubara sum and regularised this integral in chapters 2.5 and 2.8, but we will outline the process here once more for continuity. Renormalisation has been carried out iteratively by Andersen [53], here we will utilise a method outlined by Fejos *et al.* [50] which is equivalent to the iterative method. We introduce counterterms by making the substitutions

$$m^2 \to m^2 + \delta m^2, \tag{A.2}$$

$$\lambda \to \lambda + \delta\lambda. \tag{A.3}$$

Inserting this into the gap equation, we obtain two counterterms

$$M_4^2 - m_4^2 = (\lambda + \delta\lambda) I_N(M_4^2) + \delta m^2 + \frac{\delta\lambda}{N}(\phi_0^2 + \rho_0^2). \tag{A.4}$$

The sum in I_N can be carried out as a contour integral in the complex plane. By inserting the poles $\omega = \pm\sqrt{p^2 + M_4^2}$ into our general formula for Matsubara sums, Eq. (2.57) we obtain

$$I_N(M_4^2) = \left(\frac{e^\gamma \Lambda^2}{4\pi}\right)^\epsilon \int \frac{d^d p}{(2\pi)^d} \frac{1}{\sqrt{p^2 + M_4^2}} \left[\frac{1}{2} + \frac{1}{e^{\sqrt{p^2+M_4^2}/T} - 1}\right]. \tag{A.5}$$

The first term is UV-divergent, calculating it using dimensional regularisation yields

$$I_N(M_4^2) = -\frac{M_4^2}{16\pi^2}\left(\frac{\Lambda^2}{M_4^2}\right)^\epsilon \left[\frac{1}{\epsilon} + 1\right] + \int \frac{d^d q}{(2\pi)^d} \frac{1}{\sqrt{q^2 + M_4^2}} \frac{1}{e^{\sqrt{q^2+M_4^2}/T} - 1}. \tag{A.6}$$

We Taylor expand $\left(\frac{\Lambda^2}{M_4^2}\right)^\epsilon$ around $\epsilon = 0$ in the above equation to obtain a logarithmic term in the limit of $\epsilon \to 0$

$$I_N(M_4^2) = -\frac{M_4^2}{16\pi^2}\left[\frac{1}{\epsilon} + \ln\left(\frac{\Lambda^2}{M_4^2}\right)\right] + \int \frac{d^3 q}{(2\pi)^3} \frac{1}{\sqrt{q^2 + M_4^2}} \frac{1}{e^{\sqrt{q^2+M_4^2}/T} - 1}. \tag{A.7}$$

We may now isolate the divergent and convergent parts of the integral by making the following definitions

$$I_N(M_4^2) = I_d M_4^2 + I_{Nf}(M_4^2), \tag{A.8}$$

$$I_d = -\frac{1}{16\pi^2\epsilon}, \tag{A.9}$$

$$I_{Nf} = -\frac{M_4^2}{16\pi^2}\ln\left(\frac{\Lambda^2}{M_4^2}\right) + \int \frac{d^dq}{(2\pi)^d}\frac{1}{\sqrt{q^2+M_4^2}}\frac{1}{e^{\sqrt{q^2+M_4^2}/T}-1}. \tag{A.10}$$

We may now require the cancellation of all divergences in the gap equation, this yields the requirement

$$0 = \lambda I_d M_4^2 + \delta\lambda\left(I_{Nf}(M_4^2) + I_d M_4^2\right) + \delta m^2 + \frac{\delta\lambda}{N}(\phi_0^2+\rho_0^2). \tag{A.11}$$

The renormalised gap equation is

$$M_4^2 = m_4^2 + I_{Nf}(M_4^2). \tag{A.12}$$

A key step in this renormalisation process, is to insert the renormalised gap equation into (A.11) in order to obtain two conditions for the cancellation of divergences and subdivergences.

$$0 = I_{Nf}(M_4^2)\left(\delta\lambda + \lambda^2 I_d + \lambda\delta\lambda I_d\right) + \lambda I_d m_4^2 + \delta\lambda I_d m_4^2 + \delta m^2 + \frac{\delta\lambda}{N}(\phi_0^2+\rho_0^2). \tag{A.13}$$

The cancellation of subdivergences is achieved by requiring the term proportional to $I_{Nf}(M_4^2)$ to be zero. We therefore obtain two equations

$$0 = \left(\delta\lambda + \lambda^2 I_d + \lambda\delta\lambda I_d\right), \tag{A.14}$$

$$0 = \delta m^2 + I_d m^2(\lambda+\delta\lambda) + \delta m^2 + \frac{\phi_0^2+\rho_0^2}{N}\left[\delta\lambda + \lambda I_d(\lambda+\delta\lambda)\right]. \tag{A.15}$$

Solving these for $\delta\lambda$ and δm^2 yields

$$\delta\lambda = -\lambda\frac{\lambda I_d}{1+\lambda I_d}, \tag{A.16}$$

$$\delta m^2 = -m^2\frac{\lambda I_d}{1+\lambda I_d}. \tag{A.17}$$

Thus, in the gap equations we end up making the substitutions

$$\lambda \to \frac{\lambda}{1-\frac{\lambda}{16\pi^2\epsilon}}, \tag{A.18}$$

$$m^2 \to \frac{m^2}{1-\frac{\lambda}{16\pi^2\epsilon}}. \tag{A.19}$$

Interestingly, we see that $\frac{\lambda}{m^2}$ is unaltered by these substitutions. These results agree with those found by Andersen [53].

Appendix B

Renormalising the $O(2)$ model

We wish to calculate and renormalise the gap equations, Eqs. (3.100) and (3.101). Once more, we will do this by following the method of Fejos *et al.* [50] utilising $O(2)$-invariants to renormalise simultaneously to all orders in λ. We define

$$I(M_i^2, M_j^2) \equiv \oint_Q \frac{Q^2 + M_j^2}{4\mu_I^2 Q_0^2 + (Q^2 + M_1^2)(Q^2 + M_2^2)}, \tag{B.1}$$

where $j \neq i$ The gap equations can then be rewritten as

$$M_1^2 - m_1^2 = \frac{3\lambda}{2} I(M_1^2, M_2^2) + \frac{\lambda}{2} I(M_2^2, M_1^2), \tag{B.2}$$

$$M_2^2 - m_2^2 = \frac{\lambda}{2} I(M_1^2, M_2^2) + \frac{3\lambda}{2} I(M_2^2, M_1^2). \tag{B.3}$$

We need to introduce counterterms for each $O(2)$ invariant. The Kronecker delta-terms of Eq. (3.86) each represent such an invariant, and we should thus in general introduce a counterterm for each of them. In the case of the Hartree approximation, however, the last two terms in the brackets of Eq. (3.86) give rise to the same Feynman diagrams, and it thus suffices to introduce one counterterm for these two invariants. We therefore introduce the counterterms δm^2, $\delta\lambda_A$ and $\delta\lambda_B$ in the following manner

$$m^2 \to m^2 + \delta m^2, \tag{B.4}$$

$$\lambda\delta_{ab}\delta_{cd} \to (\lambda + \delta\lambda_A)\delta_{ab}\delta_{cd}, \tag{B.5}$$

$$\lambda(\delta_{ac}\delta_{bd} + \delta_{ad}\delta_{bc}) \to (\lambda + \delta\lambda_B)(\delta_{ac}\delta_{bd} + \delta_{ad}\delta_{bc}). \tag{B.6}$$

By making these substitutions in Eqs. (B.2) and (B.3), we find

$$M_1^2 - m_1^2 = \frac{3\lambda + \delta\lambda_A + 2\delta\lambda_B}{2} I(M_1^2) + \frac{\lambda + \delta\lambda_A}{2} I(M_2^2) + \delta m^2 + \frac{\delta\lambda_A + 2\delta\lambda_B}{2}\phi_0^2, \tag{B.7}$$

$$M_2^2 - m_2^2 = \frac{\lambda + \delta\lambda_A}{2} I(M_1^2) + \frac{3\lambda + \delta\lambda_A + 2\delta\lambda_B}{2} I(M_2^2) + \delta m^2 + \frac{\delta\lambda_A}{2}\phi_0^2. \tag{B.8}$$

We now need to calculate the divergent terms of $I(M_i^2, M_j^2)$. The result should be symmetric with respect to interchanging i and j, so let $i = 2$ and $j = 1$. The Matsubara sum can be carried out as a contour integral in the complex energy plane. We find the poles of the summand by solving the following equation for ω

$$0 = -4\mu_I^2\omega^2 + (-\omega^2 + p^2 + M_1^2)(-\omega^2 + p^2 + M_2^2). \tag{B.9}$$

This is a quadratic equation in ω^2, and we obtain the poles

$$\omega^2 = \epsilon_\pm^2 = a \pm b, \tag{B.10}$$

$$a \equiv \frac{M_1^2 + M_2^2}{2} + p^2 + 2\mu_I^2, \tag{B.11}$$

$$b \equiv \sqrt{\left(\frac{M_1^2 - M_2^2}{2}\right)^2 + 4\mu_I^2\left(\frac{M_1^2 + M_2^2}{2} + \mu_I^2 + p^2\right)}. \tag{B.12}$$

Inserting these poles into the general formula for Matsubara sums, Eq. (2.57) yields

$$I(M_2^2, M_1^2) = K_+ + K_-, \tag{B.13}$$

where

$$K_\pm \equiv \frac{1}{2}\left(\frac{e^\gamma \Lambda^2}{4\pi}\right)^\epsilon \int \frac{d^d p}{(2\pi)^d} \mp \frac{M_1^2 + p^2 - (a \pm b)}{2b\sqrt{a \pm b}} \left(1 + \frac{2}{e^{\sqrt{a\pm b}/Ti} - 1}\right). \tag{B.14}$$

It will be convenient to describe this integral in terms of μ_I-independent constants, to make explicit any dependence on the chemical potential. We recall that both M_1^2 and M_2^2 contains the summand $-\mu_I^2$, bearing that in mind we now introduce the new constants

$$k_1^2 \equiv \frac{M_1^2 + M_2^2}{2} + \mu_I^2, \tag{B.15}$$

$$k_2^2 \equiv \frac{M_1^2 - M_2^2}{2}. \tag{B.16}$$

The distribution function in the brackets of Eq. (B.14) is exponentially suppressed and does not give rise to divergences, while the first term is UV-divergent and corresponds to a vacuum term. For convenience, we omit the convergent last term in further calculations. We will recover it before we derive the counterterms. There are several divergent terms in $K_\pm$, so we will split it by defining

$$K_\pm = d_\pm + e_\pm, \tag{B.17}$$

$$d_\pm \equiv \frac{1}{4}\left(\frac{e^\gamma \Lambda^2}{4\pi}\right)^\epsilon \int \frac{d^d p}{(2\pi)^d} \mp \frac{k_2^2 - 2\mu_I^2}{\sqrt{k_2^4 + 4\mu_I^2(k_1^2 + p^2)}\sqrt{p^2 + k_1^2 + \mu_I^2 \pm \sqrt{k_2^4 + 4\mu_I^2(k_1^2 + p^2)}}}, \tag{B.18}$$

$$e_\pm \equiv \frac{1}{4}\left(\frac{e^\gamma \Lambda^2}{4\pi}\right)^\epsilon \int \frac{d^d p}{(2\pi)^d} \frac{1}{\sqrt{p^2 + k_1^2 + \mu_I^2 \pm \sqrt{k_2^4 + 4\mu_I^2(k_1^2 + p^2)}}}. \tag{B.19}$$

In $d_\pm$, we extract a factor $p^2 + k_1^2 + \mu_I^2$ from the quotient

$$d_\pm = \frac{1}{4}\left(\frac{e^\gamma \Lambda^2}{4\pi}\right)^\epsilon \int \frac{d^d p}{(2\pi)^d} \mp \frac{k_2^2 - 2\mu_I^2}{2\mu_I(p^2 + k_1^2 + \mu_I^2)} \frac{1}{(1+x)^{\frac{1}{2}}}, \tag{B.20}$$

$$x \equiv \frac{k_2^4 - 4\mu_I^4}{(p^2 + k_1^2 + \mu_I^2)} \pm \frac{(4\mu_I^2(p^2 + k_1^2) + k_2^4)^{\frac{3}{2}}}{4\mu_I^2(p^2 + k_1^2 + \mu_I^2)^2}. \tag{B.21}$$

In the limit of large momenta, we have $x \ll 1$ and hence we Taylor expand the square root around x to isolate the UV-divergent terms

$$d_\pm = \frac{1}{4}\left(\frac{e^\gamma \Lambda^2}{4\pi}\right)^\epsilon \int \frac{d^d p}{(2\pi)^d} \mp \frac{k_2^2 - 2\mu_I^2}{2\mu_I(p^2 + k_1^2 + \mu_I^2)} \left(1 - x + O(x^2)\right). \tag{B.22}$$

When we sum over d_+ and d_-, only those terms which do not change signs will remain, and hence, the remaining divergent term stems from the second term in x. Upon summing d_+ and d_- we therefore obtain the logarithmically divergent term d_d:

$$\begin{aligned} d_d \equiv & \frac{k_2^2 - 2\mu_I^2}{4}\left(\frac{e^\gamma \Lambda^2}{4\pi}\right)^\epsilon \int \frac{d^d p}{(2\pi)^d} \frac{|p|^3}{(p^2 + k_1^2 + \mu_I^2)^3} \\ = & \frac{k_2^2 - 2\mu_I^2}{(4\pi)^2}\left(\frac{\Lambda^2}{k_1^2 + \mu_I^2}\right)^\epsilon \left[\frac{1}{\epsilon} + \frac{1}{2} - 2\log 2 + O(\epsilon)\right]. \end{aligned} \tag{B.23}$$

Similarly, we expand $e_\pm$ around $p^2+k_1^2+\mu_I^2$ to obtain

$$\begin{aligned}
e_\pm =&\frac{1}{4}\left(\frac{e^\gamma\Lambda^2}{4\pi}\right)^\epsilon\int\frac{d^dp}{(2\pi)^d}\frac{1}{\sqrt{p^2+k_1^2+\mu_I^2}}\left(1\pm\frac{2\mu_I(p^2+k_1^2+\frac{k_2^4}{4\mu_I^2})^{\frac{1}{2}}}{p^2+k_1^2+\mu_I^2}\right)^{-\frac{1}{2}}\\
=&\frac{1}{4}\left(\frac{e^\gamma\Lambda^2}{4\pi}\right)^\epsilon\int\frac{d^dp}{(2\pi)^d}\frac{1}{\sqrt{p^2+k_1^2+\mu_I^2}}\\
&\times\left(1\mp\frac{\mu_I(p^2+k_1^2+\frac{k_2^4}{4\mu_I^2})^{\frac{1}{2}}}{p^2+k_1^2+\mu_I^2}+\frac{3}{2}\frac{\mu_I^2(p^2+k_1^2+\frac{k_2^4}{4\mu_I^2})}{(p^2+k_1^2+\mu_I^2)^2}\mp\cdots\right).
\end{aligned}\tag{B.24}$$

The second term in the bracket cancels when summing over e_+ and e_-. From summing these we obtain the two divergent terms e_{d1} and e_{d2}

$$\begin{aligned}
e_{d1}=&\frac{1}{2}\left(\frac{e^\gamma\Lambda^2}{4\pi}\right)^\epsilon\int\frac{d^dp}{(2\pi)^d}\frac{1}{\sqrt{p^2+k_1^2+\mu_I^2}}\\
=&-\frac{1}{(4\pi^2)}(k_1^2+\mu_I^2)\left(\frac{\Lambda^2}{k_1^2+\mu_I^2}\right)^\epsilon\left[\frac{1}{\epsilon}+1+O(\epsilon)\right],
\end{aligned}\tag{B.25}$$

$$\begin{aligned}
e_{d2}=&\frac{3\mu_I^2}{4}\left(\frac{e^\gamma\Lambda^2}{4\pi}\right)^\epsilon\int\frac{d^dp}{(2\pi)^d}\frac{p^2}{(p^2+k_1^2+\mu_I^2)^{\frac{5}{2}}}\\
=&\frac{\mu_I^2}{(4\pi)^2}\left(\frac{\Lambda^2}{k_1^2+\mu_I^2}\right)^\epsilon\left[\frac{3}{\epsilon}-2+O(\epsilon)\right].
\end{aligned}\tag{B.26}$$

We now combine all the divergences, and separate the renormalisation scale from the divergence by series expansion. We find

$$\begin{aligned}
d_d+e_{d1}+e_{d2}=&-\frac{1}{(4\pi)^2}(M_2^2+\mu_I^2)\frac{1}{\epsilon}\\
&+\frac{1}{(4\pi)^2}\left[\left(\frac{1}{2}-2\ln 2\right)\left(k_2^2-2\mu_I^2\right)-k_1^2-3\mu_I^2-\left(M_2^2+\mu_I^2\right)\ln\left(\frac{\Lambda^2}{k_1^2+\mu_I^2}\right)\right].
\end{aligned}\tag{B.27}$$

Similarly, the divergent part of $I(M_1^2,M_2^2)$ can be found by substituting M_1^2 for M_2^2 in the above equation. We now split $I(M_i^2,M_j^2)$ into a finite part and a divergent part

$$I(M_i^2,M_j^2)=I_d\tilde{M_i^2}+I_f(M_i^2,M_j^2),\tag{B.28}$$

where

$$I_d\equiv-\frac{1}{(4\pi)^2\epsilon},\tag{B.29}$$

$$\tilde{M_i^2}\equiv M_i^2+\mu_I^2,\tag{B.30}$$

$$\begin{aligned}
I_f(M_i^2,M_j^2)=&\sum\!\!\!\!\!\!\int\frac{\omega_n^2+p^2+M_j^2}{\epsilon(\omega_n,p)}-\frac{M_j^2-M_i^2-4\mu_I^2}{16\pi^2}\int_0^\infty dp\frac{p^5}{(p^2+\frac{M_i^2+M_j^2}{2}+2\mu_I^2)^3}\\
&-\frac{1}{4\pi^2}\int_0^\infty dp\frac{p^2}{\sqrt{p^2+\frac{M_i^2+M_j^2}{2}+2\mu_I^2}}-\frac{3\mu_I^2}{8\pi^2}\int_0^\infty dp\frac{p^4}{(p^2+\frac{M_i^2+M_j^2}{2}+2\mu_I^2)^{\frac{5}{2}}}\\
&+\frac{1}{(4\pi)^2}\left[\left(\frac{1}{2}-2\ln 2\right)\left(\frac{M_i^2+M_j^2}{2}-\mu_I^2\right)-\frac{M_i^2+M_j^2}{2}-4\mu_I^2-\left(M_i^2+\mu_I^2\right)\ln\left(\frac{\Lambda^2}{\frac{M_i^2+M_j^2}{2}+2\mu_I^2}\right)\right].
\end{aligned}\tag{B.31}$$

Since M_i^2 contains the summand $-\mu_I^2$, the constant $\tilde{M_i^2}$ is independent of the chemical potential μ_I. Hence the divergence of I is the same as the one we found in the simpler, μ_I-independent sum-integral

from the large-N approximation. Recalling the gap equations of Eqs. (B.7) and (B.8), we insert the finite parts to obtain the renormalised gap equations

$$M_1^2 - m_1^2 = \frac{3\lambda}{2} I_f(M_1^2, M_2^2) + \frac{\lambda}{2} I_f(M_2^2, M_1^2), \tag{B.32}$$

$$M_2^2 - m_2^2 = \frac{\lambda}{2} I_f(M_1^2, M_2^2) + \frac{3\lambda}{2} I_f(M_2^2, M_1^2). \tag{B.33}$$

We now require the cancellation of all the counterterms, this leads to the conditions

$$\begin{aligned} 0 = {} & \frac{3\lambda}{2} I_d \tilde{M}_1^2 + \frac{\delta\lambda_A + 2\delta\lambda_B}{2} \left(I_f(M_1^2, M_2^2) + I_d \tilde{M}_1^2 \right) \\ & + \frac{\lambda}{2} I_d \tilde{M}_2^2 + \frac{\delta\lambda_A}{2} \left(I_f(M_2^2, M_1^2) + I_d \tilde{M}_2^2 \right) \\ & + \delta m^2 + \frac{\delta\lambda_A + 2\delta\lambda_B}{2} \phi_0^2, \end{aligned} \tag{B.34}$$

$$\begin{aligned} 0 = {} & \frac{\lambda}{2} I_d \tilde{M}_1^2 + \frac{\delta\lambda_A}{2} \left(I_f(M_1^2, M_2^2) + I_d \tilde{M}_1^2 \right) \\ & + \frac{3\lambda}{2} I_d \tilde{M}_2^2 + \frac{\delta\lambda_A + 2\delta\lambda_B}{2} \left(I_f(M_2^2, M_1^2) + I_d \tilde{M}_2^2 \right) \\ & + \delta m^2 + \frac{\delta\lambda_A}{2} \phi_0^2. \end{aligned} \tag{B.35}$$

Once more we substitute the renormalised equations for $\tilde{M}_i^2$ into the terms proportional to I_d, thus producing equations for the cancellation of the main divergence as well as subdivergences caused by renormalisation

$$\begin{aligned} 0 = {} & \delta m^2 + \frac{\delta\lambda_A + 2\delta\lambda_B}{2} \phi_0^2 + I_d \left[\frac{3\lambda + \delta\lambda_A + 2\delta\lambda_B}{2} \tilde{m_1^2} + \frac{\lambda + \delta\lambda_A}{2} \tilde{m_2^2} \right] \\ & + I_f(M_1^2, M_2^2) \left[\frac{\delta\lambda_A + 2\delta\lambda_B}{2} + \frac{\lambda}{2} I_d \left(\frac{\delta\lambda_A}{2} + 3\frac{\delta\lambda_A + 2\delta\lambda_B}{2} + 5\lambda \right) \right] \\ & + I_f(M_2^2, M_1^2) \left[\frac{\delta\lambda_A}{2} + \frac{\lambda}{2} I_d \left(\frac{3\delta\lambda_A}{2} + \frac{\delta\lambda_A + 2\delta\lambda_B}{2} + 3\lambda \right) \right], \end{aligned} \tag{B.36}$$

$$\begin{aligned} 0 = {} & \delta m^2 + \frac{\delta\lambda_A}{2} \phi_0^2 + I_d \left[\frac{\lambda + \delta\lambda_A}{2} \tilde{m_1^2} + \frac{3\lambda + \delta\lambda_A + 2\delta\lambda_B}{2} \tilde{m_2^2} \right] \\ & + I_f(M_1^2, M_2^2) \left[\frac{\delta\lambda_A}{2} + \frac{\lambda}{2} I_d \left(\frac{3\delta\lambda_A}{2} + \frac{\delta\lambda_A + 2\delta\lambda_B}{2} + 3\lambda \right) \right] \\ & + I_f(M_2^2, M_1^2) \left[\frac{\delta\lambda_A + 2\delta\lambda_B}{2} + \frac{\lambda}{2} I_d \left(\frac{\delta\lambda_A}{2} + 3\frac{\delta\lambda_A + 2\delta\lambda_B}{2} + 5\lambda \right) \right]. \end{aligned} \tag{B.37}$$

The conditions for the vanishing of subdivergences are that the terms proportional to $I_f(M_i^2, M_j^2)$ are zero. These conditions are the same in both Eqs. (B.36) and (B.37) and what remains are the two conditions

$$\delta\lambda_A + 2\delta\lambda_B = -\lambda I_d \left(2\delta\lambda_A + 3\delta\lambda_B + 5\lambda \right), \tag{B.38}$$

$$\delta\lambda_A = -\lambda I_d \left(2\delta\lambda_A + \delta\lambda_B + 3\lambda \right). \tag{B.39}$$

We can use Eq. (B.39) to eliminate $\delta\lambda_A$ from Eq. (B.38), this yields

$$\delta\lambda_A = -\lambda^2 I_d \frac{3 + 2\lambda I_d}{(1 + \lambda I_d)(1 + 2\lambda I_d)}, \tag{B.40}$$

$$\delta\lambda_B = -\lambda \frac{\lambda I_d}{1 + \lambda I_d}. \tag{B.41}$$

We are now ready to calculate δm^2. Requiring once more that Eqs. (B.36) and (B.37) are fulfilled, we write $\tilde{m_i^2}$ in terms of ϕ_0^2 and m^2 to obtain

$$\begin{aligned} 0 &= \delta m^2 + I_d m^2(\delta\lambda_A + \delta\lambda_B + 2\lambda) \\ &\quad + \frac{\phi_0^2}{2}\left[\delta\lambda_A + 2\delta\lambda_B + \lambda I_d(2\delta\lambda_A + 3\delta\lambda_B + 5\lambda)\right], \end{aligned} \tag{B.42}$$

$$\begin{aligned} 0 &= \delta m^2 + I_d m^2(\delta\lambda_A + \delta\lambda_B + 2\lambda) \\ &\quad + \frac{\phi_0^2}{2}\left[\delta\lambda_A + \lambda I_d(2\delta\lambda_A + \delta\lambda_B + 3\lambda)\right]. \end{aligned} \tag{B.43}$$

The brackets next to ϕ_0^2 are zero due to Eqs. (B.38) and (B.39). What remains is

$$\delta m^2 = -I_d m^2(\delta\lambda_A + \delta\lambda_B + 2\lambda). \tag{B.44}$$

This demonstrates that it is possible to choose the counterterms in a consistent manner such that all divergences are removed from the gap equations.

Next, we should study the terms in the 2PI effective potential, to make sure they are also sufficiently renormalised. For reference, the 2PI effective potential is

$$\Gamma[\rho_0, D] = \frac{1}{2}(m^2 - \mu_I^2)\rho_0^2 + \frac{\lambda}{8N}\rho_0^4 + \frac{1}{2}\mathrm{Tr}\ln D^{-1} + \frac{1}{2}\mathrm{Tr}D_0^{-1}D + \Phi[D].$$

We follow the steps in Ref. [52], taking the terms in reverse order we have

$$\begin{aligned} \Phi[D] &= \frac{\lambda}{4N}\left(\sum\!\!\!\!\!\!\int D_{11} + \sum\!\!\!\!\!\!\int D_{22}\right)^2 \\ &\quad + \frac{\lambda}{2N}\left(\left(\sum\!\!\!\!\!\!\int D_{11}\right)^2 + \left(\sum\!\!\!\!\!\!\int D_{22}\right)^2\right). \end{aligned} \tag{B.45}$$

The above sum-integrals are the same as the ones we just renormalised in the gap equations, namely $\sum\!\!\!\!\!\!\int D_{11} = I(M_1^2)$ and $\sum\!\!\!\!\!\!\int D_{22} = I(M_2^2)$. Upon applying the same counterterms, we find

$$\begin{aligned} \Phi[D] &= \frac{\lambda}{4N}\left[I_f(M_1^2, M_2^2) + I_f(M_2^2, M_1^2)\right]^2 \\ &\quad + \frac{\lambda}{2N}\left[I_f(M_1^2, M_2^2)^2 + I_f(M_2^2, M_1^2)^2\right]. \end{aligned} \tag{B.46}$$

The term $\mathrm{Tr}D_0^{-1}D$ can be rewritten as

$$\mathrm{Tr}D_0^{-1}D = \mathrm{Tr}[\mathbb{1} - \Pi D] \tag{B.47}$$

The first term – the trace of the identity matrix – is a constant term which is zero in dimensional regularisation. Recalling that $\Pi_{ii} = M_i^2 - m_i^2$, we write

$$\mathrm{Tr}D_0^{-1}D = -(M_i^2 - m_i^2)\sum\!\!\!\!\!\!\int D_{ii}. \tag{B.48}$$

Again we see the same sum-integral as we saw in the gap-equations. Inserting the same counterterms, we find

$$\mathrm{Tr}D_0^{-1}D = -(M_i^2 - m_i^2)I_f(M_i^2, M_j^2). \tag{B.49}$$

In the above formula we are summing over i, and j is always the opposite of i. Finally, we come to the term $\frac{1}{2}\mathrm{Tr}[\ln D^{-1}]$. Using the identity $\mathrm{Tr}\ln M = \ln \mathrm{Det} M$, this term becomes

$$\mathrm{Tr}\ln D^{-1} = \sum\!\!\!\!\!\!\int \ln[(\omega_n^2 + \epsilon_+^2)(\omega_n^2 + \epsilon_-^2)] = \sum\!\!\!\!\!\!\int \ln(\omega_n^2 + \epsilon_+^2) + \sum\!\!\!\!\!\!\int \ln(\omega_n^2 + \epsilon_-^2). \tag{B.50}$$

We now differentiate with respect to $\epsilon_\pm^2$ in order to get the sum-integrals on a more familiar form.

$$\sum\!\!\!\!\!\!\int \ln(\omega_n^2 + \epsilon_\pm^2) = \int d\epsilon_\pm^2 \sum\!\!\!\!\!\!\int \frac{1}{\omega_n^2 + \epsilon_\pm^2} \tag{B.51}$$

The sum-integral has poles at $\omega = \pm\epsilon_\pm$. Inserting this into (2.57) yields

$$\begin{aligned}\sum\!\!\!\!\!\!\int \ln(\omega_n^2+\epsilon_\pm^2) &= \int \frac{d^dp}{(2\pi)^d}\int d\epsilon_\pm^2 \frac{1}{\epsilon_\pm}\left(\frac{1}{2}+\frac{1}{1-e^{\frac{\epsilon_\pm}{T}}}\right)\\ &= \int \frac{d^dp}{(2\pi)^d}\int d\epsilon_\pm\left(1+\frac{2}{1-e^{\frac{\epsilon_\pm}{T}}}\right) = \int \frac{d^dp}{(2\pi)^d}\left(\epsilon_\pm + 2T\ln(1-e^{-\frac{\epsilon_\pm}{T}})\right).\end{aligned} \tag{B.52}$$

The logarithmic term is clearly convergent. The term proportional to ϵ, however, is not. Let us examine this term in some detail. From dimensional analysis, we expect to find divergences behaving like $\frac{M_1^4}{\epsilon}$. That is, we expect divergent terms like $\sqrt{p^2+\tilde{M}_1^2}$. Let us therefore study the term $\frac{\epsilon_+ + \epsilon_-}{2}$ in some detail.

$$\frac{\epsilon_+ + \epsilon_-}{2} = \frac{1}{2}\left(\sqrt{p^2+\tilde{M}_1^2-\frac{\tilde{M}_1^2-\tilde{M}_2^2}{2}+\mu_I^2+b}+\sqrt{p^2+\tilde{M}_1^2-\frac{\tilde{M}_1^2-\tilde{M}_2^2}{2}+\mu_I^2-b}\right) \tag{B.53}$$

b is the same term as we found when calculating the Matsubara sums in the gap equations, and is hence defined in Eq. (B.12). We extract a term $E_1 \equiv \sqrt{p^2+\tilde{M}_1^2}$ from each of the square roots and series expand to obtain

$$\frac{\epsilon_+ + \epsilon_-}{2} = E_1\left(1+\frac{\frac{1}{2}(\tilde{M}_2^2-\tilde{M}_1^2)+\mu_I^2}{2E_1^2}-\frac{1}{8}\frac{\left(\frac{1}{2}(\tilde{M}_2^2-\tilde{M}_1^2)+\mu_I^2\right)^2+b^2}{E_1^4}+O\left(E_1^{-5}\right)\right) \tag{B.54}$$

Lower orders in E_1 are convergent, with the exception of one term which we will discuss later. We now do the same for $E_2 \equiv \sqrt{p^2+\tilde{M}_2^2}$ and write

$$\begin{aligned}\epsilon_+ + \epsilon_- = E_1 + E_2 &- \frac{1}{4}(\tilde{M}_1^2-\tilde{M}_2^2)\left(\frac{1}{E_1}-\frac{1}{E_2}\right)+\frac{\mu_I^2}{2}\left(\frac{1}{E_1}+\frac{1}{E_2}\right)\\ &-\frac{1}{8}\left[\frac{1}{4}(\tilde{M}_1^2-\tilde{M}_2^2)^2\left(\frac{1}{E_1^3}+\frac{1}{E_2^3}\right)-(\tilde{M}_1^2-\tilde{M}_2^2)\mu_I^2\left(\frac{1}{E_1^3}-\frac{1}{E_2^3}\right)\right.\\ &\left.+\mu_I^4\left(\frac{1}{E_1^3}+\frac{1}{E_2^3}\right)+b^2\left(\frac{1}{E_1^3}+\frac{1}{E_2^3}\right)\right].\end{aligned} \tag{B.55}$$

The first two terms are the expected divergent terms, the rest we expect to cancel. By utilising that $E_2^2 = E_1^2 - (\tilde{M}_1^2-\tilde{M}_2^2)$ to series expand E_2, we see that $\frac{1}{E_1^3} = \frac{1}{E_2^3} + O(E_1^{-5})$. Inserting this into the terms we expect to cancel, we obtain.

$$\frac{1}{E_1^3}\left[\frac{1}{16}\frac{(\tilde{M}_1^2-\tilde{M}_2^2)^2}{E_1^3}+\mu_I^2\left(p^2+\frac{1}{2}(\tilde{M}_1^2+\tilde{M}_2^2)\right)+\frac{1}{4}\mu_I^2\left(\tilde{M}_1^2-\tilde{M}_2^2\right)-\frac{1}{4}\mu_I^4-\frac{1}{4}b^2\right] = -\frac{1}{4}\frac{\mu_I^4}{E_1^3}. \tag{B.56}$$

What remains is a μ_I-dependent term. This term is to counter the p-dependent term in b. To order E_1^{-5}, there is a term in (B.54) behaving like

$$\frac{3}{8}\frac{\mu_I^2 b^2}{E_1^5} = \frac{3}{2}\frac{\mu_I^4}{E_1^3}+O(E_1^{-7}). \tag{B.57}$$

To the next order, there will be yet another term

$$-\frac{5}{64}\frac{b^4}{E_1^7} = -\frac{5}{4}\frac{\mu_I^4}{E_1^3}+O(E_1^{-7}). \tag{B.58}$$

Altogether, these terms cancel. What remains are the original divergences, which are readily calculated in dimensional regularization.

$$\int \frac{d^dp}{(2\pi)^d}\sqrt{p^2+\tilde{M}_1^2} = \frac{\tilde{M}_1^4}{32\pi^2}\left(\frac{\Lambda^2}{\tilde{M}_1^2}\right)^\epsilon\left(\frac{1}{\epsilon}+\frac{3}{2}\right). \tag{B.59}$$

The divergence is also here removed by the original counterterms, what remains is

$$\frac{1}{2}\mathrm{Tr}\ln D^{-1} = \frac{T}{\pi^2}\int dpp^2\left(\ln(1-e^{\frac{\epsilon_+}{T}})+\ln(1-e^{\frac{\epsilon_-}{T}})\right) + \frac{\tilde{M_1^4}}{32\pi^2}\left(\ln\frac{\Lambda^2}{M_1^2}+\frac{3}{2}\right)+\frac{\tilde{M_2^4}}{32\pi^2}\left(\ln\frac{\Lambda^2}{M_2^2}+\frac{3}{2}\right). \tag{B.60}$$

The effective potential is now fully renormalised.

Appendix C

Mathematica numerics

The following pages contain the Mathematica [85] notebook "on_numerics.nb", which performs all the numerics used to obtain the graphs and results herein.

```
(* Some parameters *)
```

```
M = 4.
```

```
4.
```

```
m = 424.26406871192853 i
```

```
0. + 424.264 i
```

```
Λ = 600 / Exp[0.5]
```

```
363.918
```

```
λ = 83.24661810613944`
```

```
83.2466
```

```
H = 0
```

```
0
```

```
fpi = 93.
```

```
93.
```

```
msigma = 600.
```

```
600.
```

```
mpi = 139.
```

```
139.
```

```
(* Dispersion relations *)
```

```
Disp1[p_, M1_, M2_, M3_, T_, μ_] := Sqrt[(1 / 2) * (M1^2 + M2^2) + p^2 +
   μ^2 + Sqrt[(1 / 4) * (M1^2 - M2^2)^2 + 4 * μ^2 * ((1 / 2) * (M1^2 + M2^2) + p^2)]]
```

```
Disp2[p_, M1_, M2_, M3_, T_, μ_] := Sqrt[(1 / 2) * (M1^2 + M2^2) + p^2 +
   μ^2 - Sqrt[(1 / 4) * (M1^2 - M2^2)^2 + 4 * μ^2 * ((1 / 2) * (M1^2 + M2^2) + p^2)]]
```

```
Disp3[p_, M1_, M2_, M3_, T_, μ_] := Sqrt[p^2 + M3^2]
```

```
(* Integrands for the propagator *)
```

```
f1c[p_, M1_, M2_, M3_, T_, μ_] :=
```

$$\left(\frac{1}{2\pi^2}\,p^2\left(-\frac{p^3\left(\frac{1}{2}\left(-M1^2+M2^2\right)-2\mu^2\right)}{4\left(\frac{1}{2}\left(M1^2+M2^2\right)+p^2+\mu^2\right)^3}-\frac{3p^2\mu^2}{4\left(\frac{1}{2}\left(M1^2+M2^2\right)+p^2+\mu^2\right)^{5/2}}-\frac{1}{2\sqrt{\frac{1}{2}\left(M1^2+M2^2\right)+p^2+\mu^2}}+\right.\right.$$

```
(1 / 4) * ((1 / Disp1[p, M1, M2, M3, T, μ]) + (1 / Disp2[p, M1, M2, M3, T, μ])) +
(1 / 4) * ((1 / Disp1[p, M1, M2, M3, T, μ]) - (1 / Disp2[p, M1, M2, M3, T, μ])) *
 ((1 / 2) * (M1^2 - M2^2) + 2 μ^2) /

  Sqrt[(1 / 4) * (M1^2 - M2^2)^2 + 4 * μ^2 * ((1 / 2) * (M1^2 + M2^2) + p^2)]
```

$$\left.\left.\right)\right)$$

```
f1t[p_, M1_, M2_, M3_, T_, μ_] :=
```

$$\left(\frac{1}{2\pi^2}\,p^2\left(\left(\left(2\Big/\left(-1+e^{\frac{\sqrt{\frac{1}{2}\left(M1^2+M2^2\right)+p^2+\mu^2-\sqrt{\frac{1}{4}\left(M1^2-M2^2\right)^2+4\left(\frac{1}{2}\left(M1^2+M2^2\right)+p^2\right)\mu^2}}}{T}}\right)\right)\left(M2^2+\frac{1}{2}\left(-M1^2-M2^2\right)-\right.\right.\right.$$

$$\left.\left.\left.2\mu^2+\sqrt{\frac{1}{4}\left(M1^2-M2^2\right)^2+4\left(\frac{1}{2}\left(M1^2+M2^2\right)+p^2\right)\mu^2}\right)\right)\Big/$$

$$\left(4\sqrt{\frac{1}{4}\left(M1^2-M2^2\right)^2+4\left(\frac{1}{2}\left(M1^2+M2^2\right)+p^2\right)\mu^2}\right.$$

$$\left.\sqrt{\left(\frac{1}{2}\left(M1^2+M2^2\right)+p^2+\mu^2-\sqrt{\frac{1}{4}\left(M1^2-M2^2\right)^2+4\left(\frac{1}{2}\left(M1^2+M2^2\right)+p^2\right)\mu^2}\right)}\right)-$$

$$\left(\left(\left(2\Big/\left(-1+e^{\frac{\sqrt{\frac{1}{2}\left(M1^2+M2^2\right)+p^2+\mu^2+\sqrt{\frac{1}{4}\left(M1^2-M2^2\right)^2+4\left(\frac{1}{2}\left(M1^2+M2^2\right)+p^2\right)\mu^2}}}{T}}\right)\right)\right.\right.$$

$$\left.\left.\left(M2^2+\frac{1}{2}\left(-M1^2-M2^2\right)-2\mu^2-\sqrt{\frac{1}{4}\left(M1^2-M2^2\right)^2+4\left(\frac{1}{2}\left(M1^2+M2^2\right)+p^2\right)\mu^2}\right)\right)\Big/$$

$$\left(4\sqrt{\frac{1}{4}\left(M1^2-M2^2\right)^2+4\left(\frac{1}{2}\left(M1^2+M2^2\right)+p^2\right)\mu^2}\right.$$

$$\left.\left.\left.\sqrt{\left(\frac{1}{2}\left(M1^2+M2^2\right)+p^2+\mu^2+\sqrt{\frac{1}{4}\left(M1^2-M2^2\right)^2+4\left(\frac{1}{2}\left(M1^2+M2^2\right)+p^2\right)\mu^2}\right)}\right)\right)\right)$$

```
(* The special case M1 = M2 *)
```

```
f1dc[p_, M1_, M2_, M3_, T_, μ_] :=
```

$$\frac{1}{8\pi^2}\,p^2\left(\frac{2\,p^3\,\mu^2}{\left(M1^2+p^2+\mu^2\right)^3}-\frac{3\,p^2\,\mu^2}{\left(M1^2+p^2+\mu^2\right)^{5/2}}-\frac{2}{\sqrt{M1^2+p^2+\mu^2}}+\frac{1}{\sqrt{M1^2+p^2+\mu^2-2\sqrt{\left(M1^2+p^2\right)\mu^2}}}+\right.$$

$$\frac{1}{\sqrt{M1^2+p^2+\mu^2+2\sqrt{\left(M1^2+p^2\right)\mu^2}}}+$$

$$\left(\mu^2\left(-\frac{1}{\sqrt{M1^2+p^2+\mu^2-2\sqrt{\left(M1^2+p^2\right)\mu^2}}}+\frac{1}{\sqrt{M1^2+p^2+\mu^2+2\sqrt{\left(M1^2+p^2\right)\mu^2}}}\right)\right)\Big/$$

$$\left.\left(\sqrt{\left(M1^2+p^2\right)\mu^2}\right)\right)$$

```
f1dt[p_, M1_, M2_, M3_, T_, μ_] :=
```

$$\left(p^2\left(\left(-\mu^2+\sqrt{\left(M1^2+p^2\right)\mu^2}\right)\Big/\left(\left(-1+e^{\frac{\sqrt{M1^2+p^2+\mu^2-2\sqrt{\left(M1^2+p^2\right)\mu^2}}}{T}}\right)\sqrt{M1^2+p^2+\mu^2-2\sqrt{\left(M1^2+p^2\right)\mu^2}}\right)+\right.\right.$$

$$\left(\mu^2+\sqrt{\left(M1^2+p^2\right)\mu^2}\right)\Big/$$

$$\left.\left.\left(\left(-1+e^{\frac{\sqrt{M1^2+p^2+\mu^2+2\sqrt{\left(M1^2+p^2\right)\mu^2}}}{T}}\right)\sqrt{M1^2+p^2+\mu^2+2\sqrt{\left(M1^2+p^2\right)\mu^2}}\right)\right)\right)\Big/\left(4\pi^2\sqrt{\left(M1^2+p^2\right)\mu^2}\right)$$

```
(* Counterterms *)

c1c[M1_, M2_, M3_, T_, μ_] :=
```

$$\frac{1}{16\pi^2}\left(\frac{1}{2}\left(-M1^2-M2^2\right)-3\,\mu^2+\left(\frac{1}{2}\left(-M1^2+M2^2\right)-2\,\mu^2\right)\left(\frac{1}{2}-2\,\text{Log}[2]\right)-M1^2\,\text{Log}\left[\frac{\Lambda^2}{\frac{1}{2}\left(M1^2+M2^2\right)+\mu^2}\right]\right)$$

```
c1dc[M1_, M2_, M3_, T_, μ_] :=
```

$$-\frac{M1^2-\mu^2\,(-4+\text{Log}[16])+M1^2\,\text{Log}\left[\frac{\Lambda^2}{M1^2+\mu^2}\right]}{16\,\pi^2}$$

```
c2c[M1_, M2_, M3_, T_, μ_] := c1c[M2, M1, M3, T, μ]

f2c[p_, M1_, M2_, M3_, T_, μ_] := f1c[p, M2, M1, M3, T, μ]
```

```
f2t[p_, M1_, M2_, M3_, T_, μ_] := f1t[p, M2, M1, M3, T, μ]

(* Similar definitions for the μ-indepentend part *)

f3t[p_, M1_, M2_, M3_, T_, μ_] :=
 (1 / (2 * π^2)) * (p^2 / Sqrt[p^2 + M3^2]) * (1 / (Exp[Sqrt[p^2 + M3^2] / T] - 1))

c3c[M1_, M2_, M3_, T_, μ_] := -(M3^2 / (16 * π^2)) * (-Log[M3^2 / Λ^2] + 1)

c3c[M1_, M2_, 0., T_, μ_] := 0.

(* The thermal integrals *)

i1t[M1_, M2_, M3_, T_, μ_] :=
 NIntegrate[f1t[p, M1, M2, M3, T, μ], {p, 0, Infinity}, AccuracyGoal → 8]

i1t[M1_, M2_, M3_, 0., μ_] := 0.

i1dt[M1_, M2_, M3_, T_, μ_] :=
 NIntegrate[f1dt[p, M1, M2, M3, T, μ], {p, 0, Infinity}, AccuracyGoal → 8]

i1dt[M1_, M2_, M3_, 0., μ_] := 0.

i2t[M1_, M2_, M3_, T_, μ_] :=
 NIntegrate[f2t[p, M1, M2, M3, T, μ], {p, 0, Infinity}, AccuracyGoal → 8]

i2t[M1_, M2_, M3_, 0., μ_] := 0.

i3t[M1_, M2_, M3_, T_, μ_] :=
 NIntegrate[f3t[p, M1, M2, M3, T, μ], {p, 0, Infinity}, AccuracyGoal → 8]

i3t[M1_, M2_, M3_, 0., μ_] := 0.

(* Some functions which calculate when to do a cutoff.
   This is to avoid numerical noise in the counterterm-part
   of the integral *)

cutoff1[M1_, M2_, M3_, T_, μ_, steplength_] := (
      q = 0;
      quot = 1;
      While[quot > 10^(-16),
           q = q + steplength;
           k = f1c[q, M1, M2, M3, T, μ];
           quot = Abs[k / q]
       ];
      Return[q])


cutoff2[M1_, M2_, M3_, T_, μ_, steplength_] := cutoff1[M2, M1, M3, T, μ, steplength]

(* Same for M1=M2 *)
```

```
cutoff1d[M1_, M2_, M3_, T_, μ_, steplength_] := (
  q = 0;
  quot = 1;
  While[quot > 10^(-16),
        q = q + steplength;
        k = f1dc[q, M1, M2, M3, T, μ];
        quot = Abs[k / q]
  ];
  Return[q]
 )

(* T-independent integrals *)

i1c[M1_, M2_, M3_, T_, μ_] := (
  NIntegrate[f1c[p, M1, M2, M3, T, μ],
    {p, 0, cutoff1[M1, M2, M3, T, μ, 100 000]}, AccuracyGoal → 8] + c1c[M1, M2, M3, T, μ]
 )

i2c[M1_, M2_, M3_, T_, μ_] := (
  NIntegrate[f2c[p, M1, M2, M3, T, μ],
    {p, 0, cutoff2[M1, M2, M3, T, μ, 100 000]}, AccuracyGoal → 8] + c2c[M1, M2, M3, T, μ]
 )

i1dc[M1_, M2_, M3_, T_, μ_] := (
  NIntegrate[f1dc[p, M1, M2, M3, T, μ],
    {p, 0, cutoff1d[M1, M2, M3, T, μ, 100 000]}, AccuracyGoal → 8] + c1dc[M1, M2, M3, T, μ]
 )

(* Tr Log D^-1 in the effective potential *)

lfc[p_, M1_, M2_, M3_, T_, μ_] := ((1 / (2 * π^2)) * p^2 *
   (Disp1[p, M1, M2, M3, T, μ] + Disp2[p, M1, M2, M3, T, μ] + (M - 2) * Disp3[p, M1, M2, M3, T, μ] -
     Sqrt[p^2 + M1^2] - Sqrt[p^2 + M2^2] - (M - 2) * Sqrt[p^2 + M3^2]))

cutoff3[M1_, M2_, M3_, T_, μ_, steplength_] := (
  q = 0;
  quot = 1;
  While[quot > 10^(-8),
        q = q + steplength;
        k = lfc[q, M1, M2, M3, T, μ];
        quot = Abs[k / q]
  ];
  Return[q])

lcc[M1_, M2_, M3_, T_, μ_] := -(M1^4 / (32 * π^2)) * (Log[Λ^2 / M1^2] + (3 / 2)) -
  (M2^4 / (32 * π^2)) * (Log[Λ^2 / M2^2] + (3 / 2)) -
  (M - 2) * (M3^4 / (32 * π^2)) * (Log[Λ^2 / M3^2] + (3 / 2))

liic[M1_, M2_, M3_, T_, μ_] :=
 NIntegrate[lfc[p, M1, M2, M3, T, μ], {p, 0, cutoff3[M1, M2, M3, T, μ, 100]}] +
  lcc[M1, M2, M3, T, μ]
```

```
liit[M1_, M2_, M3_, T_, μ_] :=
 ((T / π^2) * NIntegrate[p^2 * (Log[1 - Exp[-Disp1[p, M1, M2, M3, T, μ] / T]] +
       Log[1 - Exp[-Disp2[p, M1, M2, M3, T, μ] / T]] +
       (M - 2) * Log[1 - Exp[-Disp3[p, M1, M2, M3, T, μ] / T]]), {p, 0, Infinity}])

liit[M1_, M2_, M3_, 0., μ_] := 0.

ldii[M1_?NumericQ, M2_?NumericQ, M3_?NumericQ, T_?NumericQ, μ_?NumericQ] :=
 (liic[M1, M2, M3, T, μ] + liit[M1, M2, M3, T, μ])

(* Propagator *)

d11[M1_?NumericQ, M2_?NumericQ, M3_?NumericQ, T_?NumericQ, μ_?NumericQ] :=
 (i1t[M1, M2, M3, T, μ] + i1c[M1, M2, M3, T, μ])

d22[M1_?NumericQ, M2_?NumericQ, M3_?NumericQ, T_?NumericQ, μ_?NumericQ] :=
 (i2t[M1, M2, M3, T, μ] + i2c[M1, M2, M3, T, μ])

d33[M1_?NumericQ, M2_?NumericQ, M3_?NumericQ, T_?NumericQ, μ_?NumericQ] :=
 (i3t[M1, M2, M3, T, μ] + c3c[M1, M2, M3, T, μ])

(* M1=M2-Degenerate propagator *)

dd11[M1_?NumericQ, M2_?NumericQ, M3_?NumericQ, T_?NumericQ, μ_?NumericQ] :=
 (i1dt[M1, M2, M3, T, μ] + i1dc[M1, M2, M3, T, μ])

(* ρ^2 and masses calculated from the stationarity condition *)

dens[M1_, μ_] := (M / (2 * λ)) * (M1^2 - μ^2)

m1[M1_, pot_] := Re[m^2] + 1.5 * (M1^2 - pot^2)

m2[M1_, pot_] := Re[m^2] + 0.5 * (M1^2 - pot^2)

m3[M1_, pot_] := m2[M1, pot]

(* the masses calculated from ρ *)

m1[density_] := Re[m^2] + (3 * λ / M) * density^2

m2[density_] := Re[m^2] + (λ / M) * density^2

m3[density_] := m2[density]

(* Perturbation theory, Iterate[x]==x implies a solution to
   the gap equations. vec is a vector of the form {M1,M2,M3}
   The stationarity condition is implied here. weight says
   how slowly to step in the new direction. This is necessary
   as our theory is highly non-perturbative *)
```

```
Iterate[vec_, temp_, pot_, weight_] := (
  l1 = d11[vec[[1]], vec[[2]], vec[[3]], temp, pot];
  l2 = d22[vec[[1]], vec[[2]], vec[[3]], temp, pot];
  l3 = d33[vec[[1]], vec[[2]], vec[[3]], temp, pot];
  new = {Re[Sqrt[m1[vec[[1]], pot] + (3 * λ / M) * (l1) + (λ / M) * (l2) + (λ / M) * (M - 2) * l3]],
    Re[Sqrt[m2[vec[[1]], pot] + (λ / M) * l1 + (3 * λ / M) * l2 + (λ / M) (M - 2) * l3]],
    Re[Sqrt[m3[vec[[1]], pot] + (λ / M) * l1 + (λ / M) * l2 + λ * l3]]};
  Return[(1 / weight) * ((weight - 1) * vec + new)]
 )

(* A similar function, but here given some ρ, this is
   useful for drawing a graph of the effective potential *)

RhoIterate[vec_, temp_, pot_, density_, weight_] := (
  l1 = Round[d11[vec[[1]], vec[[2]], vec[[3]], temp, pot], 10^-3];
  l2 = Round[d22[vec[[1]], vec[[2]], vec[[3]], temp, pot], 10^-3];
  l3 = Round[d33[vec[[1]], vec[[2]], vec[[3]], temp, pot], 10^-3];
  new = {Re[Sqrt[m1[density] + (3 * λ / M) * (l1) + (λ / M) (l2) + (λ / M) * (M - 2) * l3]],
    Re[Sqrt[m2[density] + (λ / M) * l1 + (3 * λ / M) * l2 + (λ / M) (M - 2) * l3]],
    Re[Sqrt[m3[density] + (λ / M) * l1 + (λ / M) * l2 + λ * l3]]
   };
  Return[(1 / weight) * ((weight - 1) * vec + new)]
 )

PhiIterate[vec_, temp_, pot_, density_?NumericQ, weight_] := (
  l1 = d33[vec[[1]], vec[[2]], vec[[1]], temp, pot];
  l2 = dd11[vec[[2]], vec[[2]], vec[[3]], temp, pot];
  l3 = d33[vec[[1]], vec[[2]], vec[[3]], temp, pot];
  new = {Re[Sqrt[m1[density] + (3 * λ / M) * (l1) + (2 * λ / M) (l2) + (λ / M) * (M - 3) * l3]],
    Re[Sqrt[m2[density] + (λ / M) * (l1) + (4 * λ / M) (l2) + (λ / M) * (M - 3) * l3]],
    Re[Sqrt[m2[density] + (λ / M) * (l1) + (2 * λ / M) (l2) + (λ / M) * (M - 1) * l3]]
   };
  Return[(1 / weight) * ((weight - 1) * vec + new)]
 )

(* A function which solves the gap equations for a range of
   densities, produces a table with masses for each density *)

TrackRho[startvec_, temp_, pot_, rho0_, rho1_, rhostep_] := (
  curr = startvec;
  tmp = {};
  r = rho0;
  While[r ≤ rho1,
   curr = {p1, p2, p3} /. FindRoot[RhoIterate[{p1, p2, p3}, temp, pot, r, 10] == {p1, p2, p3},
      {{p1, curr[[1]]}, {p2, curr[[2]]}, {p3, curr[[3]]}}];
   Print[{r, curr}];
   tmp = Append[tmp, {r, curr}];
   r += rhostep
  ];
  Return[tmp]
 )
```

```
(* Solves the gap equations using Iterate[vec]==vec as its condition,
   p1max is used to set the maximum value which M1 is allowed to take.
   This is to find the highly unstable second solution to the gap
   equations in the second-order phase transition *)

FinalRun[start_, temp_, pot_, OptionsPattern[]] :=
 Return[{p1, p2, p3} /. FindRoot[Iterate[{p1, p2, p3}, temp, pot, 10] == {p1, p2, p3},
    {{p1, start[[1]], 0, OptionValue[p1max]}, {p2, start[[2]], 0, Infinity},
     {p3, start[[3]], 0, Infinity}}, AccuracyGoal → 4, PrecisionGoal → 4]]

FinalPhi[start_, temp_?NumericQ, pot_?NumericQ] :=
 Return[{p1, p2, p3, r} /. FindRoot[{PhiIterate[{p1, p2, p3}, temp, pot, r, 10] == {p1, p2, p3},
     r * (p1^2 - (2 * λ / M) * r^2) == H},
    {{p1, start[[1]], 0, Infinity}, {p2, start[[2]], 0, Infinity}, {p3, start[[3]], 0,
      Infinity}, {r, start[[4]], 0, Infinity}}, AccuracyGoal → 4, PrecisionGoal → 4
   ]]

Options[FinalRun] = {p1max → Infinity}
```

```
{p1max → ∞}
```

```
(* Solves the gap-equations for a range of different temperatures,
   producing a table with the results. *)

TempSweep[vec_, t1_, t2_, step_, pot_, OptionsPattern[]] := (
  tmp = {};
  curr = vec;
  etemp = t1;
  While[etemp <= t2, (
    curr = FinalRun[curr, etemp, pot, p1max -> OptionValue[p1max]];
    Print[etemp, " ", curr];
    tmp = Append[tmp, {etemp, curr}];
    etemp += step;
   )];
  Return[tmp]
 )

Options[TempSweep] = {p1max → Infinity}
```

```
{p1max → ∞}
```

```
(* Same as above, but in reverse. *)
```

```
RevTempSweep[vec_, t1_, t2_, step_, pot_, OptionsPattern[]] := (
  tmp = {};
  curr = vec;
  etemp = t1;
  While[etemp >= t2, (
    curr = FinalRun[curr, etemp, pot, p1max → OptionValue[p1max]];
    Print[etemp, " ", curr];
    tmp = Append[tmp, {etemp, curr}];
    etemp -= step;
   )];
  Return[tmp]
 )

Options[RevTempSweep] = {p1max → Infinity}
```

$\{\text{p1max} \to \infty\}$

```
PotSweep[vec_, temp_, pot1_, pot2_, step_] := (
  tmp = {};
  curr = vec;
  epot = pot1;
  While[epot ≤ pot2, (
    curr = FinalRun[curr, temp, epot];
    Print[epot, " ", curr];
    tmp = Append[tmp, {epot, curr}];
    epot += step;
   )];
  Return[tmp]
 )

(* Calculates the effective potential *)

EffPot[vec_, temp_, pot_, density_] := (
  l1 = d11[vec[[1]], vec[[2]], vec[[3]], temp, pot];
  l2 = d22[vec[[1]], vec[[2]], vec[[3]], temp, pot];
  l3 = d33[vec[[1]], vec[[2]], vec[[3]], temp, pot];
  condensate = ((1 / 2) * (Re[m^2] - pot^2) * density^2 + (λ / (4 * M)) * density^4);
  hartreeloops =
   (λ / (4 * M)) * (l1 + l2 + (M - 2) * l3)^2 + 2 * (λ / (4 * M)) * (l1^2 + l2^2 + (M - 2) * l3^2);
  setrace = -(1 / 2) * ((vec[[1]]^2 - Re[m^2] - (3 * λ / M) * density^2) * l1 +
      (vec[[2]]^2 - Re[m^2] - (λ / M) * density^2) * l2 +
      (M - 2) * (vec[[3]]^2 - Re[m^2] - (λ / M) * density^2) * l3);
  logdressed = 0.5 * ldii[vec[[1]], vec[[2]], vec[[3]], temp, pot];
  Return[condensate + hartreeloops + setrace + logdressed]
 )

(* Does the same as final run, but for M1=M2 (ρ=0) *)
```

```
DegenFinalRun[M1_, M3_, temp_, pot_] := (
  {p1, p3} /. FindRoot[{(p1^2 == Re[m^2] + (4 * λ / M) * dd11[p1, p1, p3, temp, pot] +
        (λ / M) * (M - 2) * d33[p1, p1, p3, temp, pot]),
     (p3^2 == Re[m^2] + (2 * λ / M) * dd11[p1, p1, p3, temp, pot] +
        λ * d33[p1, p1, p3, temp, pot])}, {{p1, M1, 0., Infinity}, {p3, M3, 0., Infinity}}]
 )

DegenTempSweep[M1_, M3_, t1_, t2_, tstep_, pot_] := (
  tmp = {};
  etemp = t1;
  curr = {M1, M3};
  While[etemp ≤ t2,
   curr = DegenFinalRun[curr[[1]], curr[[2]], etemp, pot];
   Print[etemp, " ", curr];
   tmp = Append[tmp, {etemp, {curr[[1]], curr[[1]], curr[[2]]}}];
   etemp += tstep
  ];
  Return[tmp]
 )

DegenEffPot[M1_, M3_, temp_, pot_] := (
  l1 = dd11[M1, M1, M3, temp, pot];
  l2 = l1;
  l3 = d33[M1, M1, M3, temp, pot];
  density = 0;
  hartreeloops =
   (λ / (4 * M)) * (l1 + l2 + (M - 2) * l3)^2 + 2 * (λ / (4 * M)) * (l1^2 + l2^2 + (M - 2) * l3^2);
  setrace = -(1 / 2) * (2 * (M1^2 - Re[m^2]) * l1 + (M - 2) * (M3^2 - Re[m^2]) * l3);
  logdressed = 0.5 * ldii[M1, M1, M3, temp, pot];
  Return[hartreeloops + setrace + logdressed]
 )

(* Degenerate and μ=0 *)

DegenZeroFinalRun[M1_, temp_, pot_] := (
  p1 /. FindRoot[
    p1^2 == Re[m^2] + ((M + 2) / M) * λ * d33[p1, p1, p1, temp, pot], {p1, M1, 0, Infinity}]
 )
```

```
DegenZeroTempSweep[M1_, t1_, t2_, tstep_] := (
  tmp = {};
  curr = M1;
  etemp = t1;
  While[etemp <= t2,
   (
    curr = DegenZeroFinalRun[curr, etemp, 0.];
    Print[etemp, " ", curr];
    tmp = Append[tmp, {etemp, {curr, curr, curr}}];
    etemp += tstep
   )
  ];
  Return[tmp]
 )

DegenZeroEffPot[M1_, temp_, pot_] := (
  l3 = d33[M1, M1, M1, temp, pot];
  l1 = l3;
  l2 = l3;
  density = 0;
  condensate = 0;
  hartreeloops =
   (λ / (4 * M)) * (l1 + l2 + (M - 2) * l3)^2 + 2 * (λ / (4 * M)) * (l1^2 + l2^2 + (M - 2) * l3^2);
  setrace = -(1 / 2) * ((M1^2 - Re[m^2] - (3 * λ / M) * density) * l1 +
      (M1^2 - Re[m^2] - (λ / M) * density) * l2 +
      (M - 2) * (M1^2 - Re[m^2] - (λ / M) * density) * l3);
  logdressed = 0.5 * ldii[M1, M1, M1, temp, pot];
  Return[condensate + hartreeloops + setrace + logdressed]
 )

(* Maps out the phase diagram and returns a table with the results.
   It assumes that the critical temperature is an increasing function
   of potential *)
```

```
MapEffPot[normvec_, degenvec_, temp_, tstep_, pot1_, pot2_, potstep_] := (
  tmp = {};
  epot = pot1;
  etemp = temp;
  norm = normvec;
  dege = degenvec;
  While[epot <= pot2,
   norm = FinalRun[norm, etemp, epot];
   dege = DegenFinalRun[dege[[1]], dege[[2]], etemp, epot];
   While[EffPot[norm, etemp, epot, Sqrt[dens[norm[[1]], epot]]] ≤
     DegenEffPot[dege[[1]], dege[[2]], etemp, epot],
    etemp += tstep;
    norm = FinalRun[norm, etemp, epot];
    dege = DegenFinalRun[dege[[1]], dege[[2]], etemp, epot];
   ];
   tmp = Append[tmp, {epot, etemp}];
   Print[epot, " ", etemp];
   (*Print[norm," ",dege];*)
   epot += potstep;
   dege[[1]] += potstep;
  ];
  Print[norm, dege];
  Return[tmp]
 )

(* A filter removing bad solutions returned by FindRoot. *)

FilterSweep[sweep_, pot_, accuracy_] := (
  tmp = {};
  For[i = 1, i <= Length[sweep], i++,
   If[Max[Abs[sweep[[i]][[2]] - Iterate[sweep[[i]][[2]], sweep[[i]][[1]], pot, 1]]] <
     accuracy,
    tmp = Append[tmp, sweep[[i]]]]];
  Return[tmp]
 )

FilterRSweep[sweep_, temp_, pot_, accuracy_] := (
  tmp = {};
  For[i = 1, i <= Length[sweep], i++,
   If[
    Max[Abs[sweep[[i]][[2]] - RhoIterate[sweep[[i]][[2]], temp, pot, sweep[[i]][[1]], 1]]] <
     accuracy,
    tmp = Append[tmp, sweep[[i]]]]];
  Return[tmp]
 )

(* Generates a plot of quasiparticle masses as a function of temperature at μ=0 *)

(* We start by following the solution up past the turning point*)

ts0 = Quiet[TempSweep[{600., 0., 0.}, 0., 240., 1., 0.]];
```

```
(* We filter the results so that invalid solutions at large T disappear *)

cleants0 = FilterSweep[ts0, 0., 2.];

(* We now fill in the second half of the
  curve by sweepiing backwards and requiring that M1 < 375 *)

revts0 = RevTempSweep[{352.42460588925564`, 211.71435917141304`, 211.71436284001194`},
   234., 130., 0.01, 0., p1max → 375];

(* We filter these results as well to remove bad solutions. We
 have to use a coarse filter as these solutions are unstable. *)

cleanrevts0 = FilterSweep[revts0, 0., 5.];

(* now we map out the solutions where ρ=0 *)

lowts0 = DegenZeroTempSweep[1., 132., 300., 1.];

(* Join them together *)

fullsweep0 = Join[cleants0, cleanrevts0, lowts0];

(* and plot the results. *)

Show[ListPlot[
  {Table[{fullsweep0[[i]][[1]], fullsweep0[[i]][[2]][[1]]}, {i, Length[fullsweep0]}],
   Table[{fullsweep0[[i]][[1]], fullsweep0[[i]][[2]][[2]]}, {i, Length[fullsweep0]}]},
  Joined → True, PlotRange → {{0, 300}, {0, 620.}}, Frame → True,
  PlotStyle → {{Black, Thick}, {Darker[Gray], Thick, Dashed}},
  FrameLabel → {"T (MeV)", Graphics[Text["M_i (MeV)", {0, 0}, {0, 0}, {0, 1}],
     BaseStyle → {FontSize → 14}, ImageSize → 40]},
  BaseStyle → {FontSize → 14}, RotateLabel → False],
 Graphics[Text["M_1", {231, 510}, {0, 0}, {1, 0}],
  BaseStyle → {FontSize → 14}, ImageSize → 70],
 Graphics[Text["M_2", {120, 180}, {0, 0}, {1, 0}],
  BaseStyle → {FontSize → 14}, ImageSize → 70]
]

(* To join plot the condensate we calculate it
 from the stationarity condition in the two first cases.
  It is zero in the results found by DegenZeroTempSweep *)

stat = Join[cleants0, cleanrevts0];

ListPlot[
 Join[Table[{stat[[i]][[1]], Sqrt[dens[stat[[i]][[2]][[1]], 0.]]}, {i, Length[stat]}],
  {{132., 0.}, {300., 0.}}], Joined → True, PlotRange → {{0, 300}, {0, 96.1}},
 Frame → True, PlotStyle → {Black, Thick}, FrameLabel → {"T (MeV)", Graphics[
    Text["ρ (MeV)", {0, 0}, {0, 0}, {0, 1}], BaseStyle → {FontSize → 14}, ImageSize → 40]},
 BaseStyle → {FontSize → 14}, RotateLabel → False]

(* Due to the tachyonic behaviour at low T,
we find low-temperature solutions by sweeping backwards from T=50 *)

lowrevts100 = Quiet[RevTempSweep[{620., 110., 60.}, 50., 0., 1., 100.]];
```

```
cleanlowrevts100 =
 Quiet[FilterSweep[Table[lowrevts100[[-i]], {i, Length[lowrevts100]}], 100., 0.001]]

(* And forwards from T=50 *)

ts100 = Quiet[TempSweep[
    {615.2804159630317`, 102.49303151708844`, 64.5825666077857`}, 50., 240., 1., 100.]];

cleants100 = FilterSweep[ts100, 100., 0.001]

(* backwards again *)

hlowrevts100 =
  Quiet[RevTempSweep[{368.64928767698467`, 235.47439469801859`, 221.1442956389476`},
    237., 140., 1., 100., p1max → 400.]];

cleanhlowrevts100 = Quiet[cleanhlowrevts100 = FilterSweep[hlowrevts100, 100., 0.001]]

(* And forwards with ρ=0 *)

degents100 =
  Quiet[DegenTempSweep[100.1602584636055`, 26.144608461478125`, 140., 300., 1., 100.]];

fullts100 = Join[cleanlowrevts100, cleants100, cleanhlowrevts100, degents100];

(* Plot the mass modes *)

Show[ListPlot[{Table[{fullts100[[i]][[1]], Re[Sqrt[fullts100[[i]][[2]][[1]]^2 - 10 000]]},
    {i, Length[fullts100]}], Table[{fullts100[[i]][[1]],
     Re[Sqrt[fullts100[[i]][[2]][[2]]^2 - 10 000.]]}, {i, Length[fullts100]}],
   Table[{fullts100[[i]][[1]], Re[Sqrt[fullts100[[i]][[2]][[3]]^2]]},
    {i, Length[fullts100]}]}, Joined → True, PlotStyle →
   {{Black, Thick}, {Darker[Gray], Thick, Dashed}, {Lighter[Gray], Thick, DotDashed}},
  PlotRange → {{0, 300}, {0, 630}}, Frame → True,
  BaseStyle → {FontSize → 14}, RotateLabel → False,
  FrameLabel → {"T (MeV)", Graphics[Text["M_i (MeV)", {0, 0}, {0, 0}, {0, 1}],
     BaseStyle → {FontSize → 14}, ImageSize → 40]}],
 Graphics[Text["M_1", {230, 550}, {0, 0}, {1, 0}], BaseStyle → {FontSize → 14},
  ImageSize → 70],
 Graphics[Text["M_2", {150, 210}, {0, 0}, {1, 0}],
  BaseStyle → {FontSize → 14}, ImageSize → 70],
 Graphics[Text["M_3", {100, 50}, {0, 0}, {1, 0}], BaseStyle → {FontSize → 14}, ImageSize → 70]]

(* plot the quasiparticle masses *)
```

```
Show[ListPlot[{Table[{fullts100[[i]][[1]],
     Re[Disp1[0., fullts100[[i]][[2]][[1]], fullts100[[i]][[2]][[2]], 0., 0., 100.]]},
    {i, Length[fullts100]}], Table[{fullts100[[i]][[1]],
     Re[Disp2[0., fullts100[[i]][[2]][[1]], fullts100[[i]][[2]][[2]], 0., 0., 100.]]}, {i,
     Length[fullts100]}],
   Table[{fullts100[[i]][[1]], fullts100[[i]][[2]][[3]]}, {i, Length[fullts100]}]},
  Joined → True, PlotStyle → {{Black, Thick}, {Darker[Gray], Thick, Dashed},
    {Lighter[Gray], Thick, DotDashed}}, PlotRange → {{0, 300}, {0, 700}},
  Frame → True, BaseStyle → {FontSize → 14}, RotateLabel → False,
  FrameLabel → {"T (MeV)", Graphics[Text["M$_\pi$ (MeV)", {0, 0}, {0, 0}, {0, 1}],
     BaseStyle → {FontSize → 14}, ImageSize → 40]}],
 Graphics[Text["π⁻", {270, 400}, {0, 0}, {1, 0}], BaseStyle → {FontSize → 14},
  ImageSize → 70],
 Graphics[Text["π⁰", {270, 290}, {0, 0}, {1, 0}],
  BaseStyle → {FontSize → 14}, ImageSize → 70],
 Graphics[Text["π⁺", {270, 140}, {0, 0}, {1, 0}],
  BaseStyle → {FontSize → 14}, ImageSize → 70]
]

(* Plot the phase diagram *)

fd = Quiet[MapEffPot[{477.2494878304713`, 217.58648328062264`, 217.58673492040526`},
    {164.0583723748556`, 164.0583723748556`}, 220., 0.1, 0.1, 300., 0.1]];

fdh = ListPlot[fd, Joined → True, PlotRange → {{0, 300}, {0, 300}},
  Frame → True, PlotStyle → {Black, Thick}, FrameLabel →
   {"μ (MeV)", Graphics[Text["T (MeV)", {0, 0}, {0, 0}, {0, 1}], BaseStyle → {FontSize → 14},
     ImageSize → 40]}, BaseStyle → {FontSize → 14}, RotateLabel → False]

(* The effective potential *)

(* Solve the gap equations for fixed  ρ *)

m220 = Table[Print[r];
  {r, {p1, p2, p3} /. FindRoot[RhoIterate[{p1, p2, p3}, 220., 100., r, 10] == {p1, p2, p3},
     {{p1, 200 + 5 * r}, {p2, 200.1 + r}, {p3, 100.1 + r}}]}, {r, 0., 120., 1.}]

m230 = Table[Print[r];
  {r, {p1, p2, p3} /. FindRoot[RhoIterate[{p1, p2, p3}, 230., 100., r, 10] == {p1, p2, p3},
     {{p1, 200 + 5 * r}, {p2, 200.1 + r}, {p3, 100.1 + r}}]}, {r, 0., 120., 1.}]

m240 = Table[Print[r];
  {r, {p1, p2, p3} /. FindRoot[RhoIterate[{p1, p2, p3}, 240., 100., r, 10] == {p1, p2, p3},
     {{p1, 200 + 5 * r}, {p2, 200.1 + r}, {p3, 100.1 + r}}]}, {r, 0., 120., 1.}]

(* Filter *)

mc220 = Quiet[FilterRSweep[m220, 220., 100., 0.0003]];

mc230 = Quiet[FilterRSweep[m230, 230., 100., 0.0003]];

mc240 = FilterRSweep[m240, 240., 100., 0.0003];

(* calculate the effective potential from these solutions *)
```

```
ep0220 = Quiet[EffPot[mc220[[1]][[2]], 220., 100., mc220[[1]][[1]]]];

ep0230 = Quiet[EffPot[mc230[[1]][[2]], 230., 100., mc230[[1]][[1]]]];

ep0240 = Quiet[EffPot[mc240[[1]][[2]], 240., 100., mc240[[1]][[1]]]];

(* Plot *)

Show[Quiet[ListPlot[
   {Table[{mc220[[i]][[1]], EffPot[mc220[[i]][[2]], 220., 100., mc220[[i]][[1]]] - ep0220},
     {i, Length[mc220]}], Table[{mc230[[i]][[1]],
      EffPot[mc230[[i]][[2]], 230., 100., mc230[[i]][[1]]] - ep0230}, {i, Length[mc230]}],
    Table[{mc240[[i]][[1]], EffPot[mc240[[i]][[2]], 240., 100., mc240[[i]][[1]]] - ep0240},
     {i, Length[mc240]}]}, Joined → True, PlotStyle →
    {{Black, Thick}, {Darker[Gray], Thick, Dashed}, {Lighter[Gray], Thick, DotDashed}},
   PlotRange → {{0, 100}, {-2.5 * 10^7, 10^8}}, Frame → True,
   BaseStyle → {FontSize → 14}, RotateLabel → False,
   FrameLabel → {"ρ (MeV)", Graphics[Text["Γ[ρ] (MeV)^4", {0, 0}, {0, 0}, {0, 1}],
      BaseStyle → {FontSize → 14}, ImageSize → 40]}]],
 Graphics[Text["T=220", {50, -10^7}, {0, 0}, {1, 0}],
  BaseStyle → {FontSize → 14}, ImageSize → 70],
 Graphics[Text["T=230", {68, 1.5 * 10^7}, {0, 0}, {1, 0}],
  BaseStyle → {FontSize → 14}, ImageSize → 70],
 Graphics[Text["T=240", {78, 8 * 10^7}, {0, 0}, {1, 0}],
  BaseStyle → {FontSize → 14}, ImageSize → 70]
]

(* Large-N *)

(* Chiral Limit Parameters *)

Λ = 139 * Exp[-0.5]

84.3078

(* Calculate the density *)

RhoC[temp_, pot_] := Re[Sqrt[(M / λ) * (pot^2 - Re[m^2] - λ * d33[pot, pot, pot, temp, pot])]]

(* Masses *)

MassC[temp_, pot_] := (
  r = RhoC[temp, pot];
  If[r == 0., Return[
    Re[p1 /. FindRoot[p1^2 - m^2 == λ * d33[p1, p1, p1, temp, pot], {p1, 150, 0, Infinity}]]],
   Return[Abs[pot]]]
 )

Mass1C[temp_, pot_] := (
  r = RhoC[temp, pot];
  If[r == 0., p1 = MassC[temp, pot];
   Return[Re[Sqrt[m^2 + λ * d33[p1, p1, p1, temp, pot]]]], Return[pot]]
 )
```

```
Mass2C[temp_, pot_] := (
  r = RhoC[temp, pot];
  If[r == 0., p1 = MassC[temp, pot];
   Return[Re[Sqrt[m^2 - pot^2 + λ * d33[p1, p1, p1, temp, pot]]]],
   Re[Sqrt[m^2 - pot^2 + (3 * λ / M) * r^2 + λ * d33[pot, pot, pot, temp, pot]]]]
 )

Mass3C[temp_, pot_] := (
  Sqrt[MassC[temp, pot]^2 - pot^2]
 )

(* Plot the masses *)

Show[Quiet[Plot[{MassC[t, 100.], Mass2C[t, 100.], Mass3C[t, 100.]}, {t, 0, 250},
    PlotRange → {{0, 250}, {0, 700}}, PlotStyle →
     {{Black, Thick}, {Darker[Gray], Thick, Dashed}, {Lighter[Gray], Thick, DotDashed}},
    Frame → True, BaseStyle → {FontSize → 14}, RotateLabel → False,
    FrameLabel → {"T (MeV)", Graphics[Text["M_i(T) (MeV)", {0, 0}, {0, 0}, {0, 1}],
       BaseStyle → {FontSize → 14}, ImageSize → 40]}]],
 Graphics[Text["M_1", {150, 550}, {0, 0}, {1, 0}], BaseStyle → {FontSize → 14},
  ImageSize → 70],
 Graphics[Text["M_2", {180, 150}, {0, 0}, {1, 0}],
  BaseStyle → {FontSize → 14}, ImageSize → 70],
 Graphics[Text["M_3", {230, 50}, {0, 0}, {1, 0}], BaseStyle → {FontSize → 14}, ImageSize → 70]
]

Plot[RhoC[t, 100.], {t, 0, 250}, PlotRange → {{0, 250}, {0, 110}}, PlotStyle →
  {{Black, Thick}, {Darker[Gray], Thick, Dashed}, {Lighter[Gray], Thick, DotDashed}},
 Frame → True, BaseStyle → {FontSize → 14}, RotateLabel → False,
 FrameLabel → {"T (MeV)", Graphics[
    Text["ρ(T) (MeV)", {0, 0}, {0, 0}, {0, 1}], BaseStyle → {FontSize → 14}, ImageSize → 40]}]

(* Finds the critical temperature *)

RhoCritC[pot_] := T /. FindRoot[pot^2 - Re[m^2] - λ * d33[pot, pot, pot, T, pot], {T, 155}]

(* Plot the phase diagram *)

fdnc = Plot[RhoCritC[x], {x, 0, 300}, PlotRange → {{0, 300}, {0, 300}},
  Frame → True, PlotStyle → {Darker[Gray], Thick, Dashed}, FrameLabel →
   {"μ (MeV)", Graphics[Text["T (MeV)", {0, 0}, {0, 0}, {0, 1}], BaseStyle → {FontSize → 14},
     ImageSize → 40]}, BaseStyle → {FontSize → 14}, RotateLabel → False]

(* Calculate the critical exponent by linear fit to a log-log table *)

CritExp[pot_] := (
  rhc = RhoCritC[pot];
  Return[CoefficientList[Fit[Table[{Log[Abs[t - rhc]], Log[RhoC[t, pot]]},
       {t, 0.99 * rhc, 0.9999 * rhc, 0.0001 * rhc}], {1, x}, x], x][[2]]]
 )

ce = Quiet[Table[CritExp[s], {s, 1., 300., 1.}]];

(* some statistics *)
```

```
Mean[ce]
```

```
0.49902
```

```
StandardDeviation[ce]
```

```
0.000139096
```

```
(* Physical Point *)
```

```
mh = Sqrt[-0.5 * (600^2 - 3 * 139^2)]
```

```
0. + 388.611 i
```

```
λh = M * (600^2 - 139^2) / 93^2
```

```
157.558
```

```
H = 93 * 139^2
```

```
1796853
```

```
RhoP[temp_, pot_] := (M / λ) * (pot^2 - Re[mh^2]) - H^2 / pot^4 - M * d33[pot, pot, pot, temp, pot]
```

```
RhoCritP[pot_] :=
 If[RhoP[0., pot] > 0, T /. FindRoot[RhoP[T, pot], {T, 50., 0., Infinity}], 0.]
```

```
MassP[temp_, pot_] := (
  r = Re[Sqrt[RhoP[temp, pot]]];
  If[r == 0., Return[
    Re[p1 /. FindRoot[p1^2 == mh^2 + (λ / M) * (H^2 / p1^4) + λ * d33[p1, p1, p1, temp, pot],
       {p1, 150., 0., Infinity}]]], Return[pot]]
 )
```

```
Mass1P[temp_, pot_] := (
  r = Re[Sqrt[RhoP[temp, pot]]];
  If[r == 0., p1 = MassP[temp, pot];
   Return[Re[Sqrt[mh^2 + (3 * λ / M) * (H^2 / p1^4) + λ * d33[p1, p1, p1, temp, pot]]]],
   tw = Re[mh^2 + λ * d33[pot, pot, pot, temp, pot]]; Return[
    Sqrt[3.5 * pot^2 - tw + 0.5 * Sqrt[(5 * pot^2 - 2 * tw)^2 - 24 * (λ / M) * (H^2 / pot^2)]]]]
 )
```

```
MassPi1[temp_, pot_] := (
  r = Re[Sqrt[RhoP[temp, pot]]];
  If[r == 0., Return[MassP[temp, pot] + pot],
   tw = Re[mh^2 + λ * d33[pot, pot, pot, temp, pot]]; Return[
    Sqrt[3.5 * pot^2 - tw - 0.5 * Sqrt[(5 * pot^2 - 2 * tw)^2 - 24 * (λ / M) * (H^2 / pot^2)]]]]
 )
```

```
MassPi2[temp_, pot_] := (
  r = Re[Sqrt[RhoP[temp, pot]]];
  If[r == 0., Return[MassP[temp, pot] - pot], Return[0.]]
 )
```

```
(* Masses as a function of μ *)
```

```
Show[Plot[{Mass1P[0., t], MassPi1[0., t], MassPi2[0., t], MassP[0., t]},
  {t, 0, 250}, PlotRange → {{0, 250}, {0, 1020}},
  PlotStyle → {{Black, Thick}, {Darker[Gray], Thick, Dashed},
    {Lighter[Gray], Thick, DotDashed}, {Gray, Thick, Dotted}},
  Frame → True, BaseStyle → {FontSize → 14}, RotateLabel → False,
  FrameLabel → {"μ (MeV)", Graphics[Text["M(μ) (MeV)", {0, 0}, {0, 0}, {0, 1}],
     BaseStyle → {FontSize → 14}, ImageSize → 40]}],
 Graphics[Text["σ", {200, 750}, {0, 0}, {1, 0}], BaseStyle → {FontSize → 14},
  ImageSize → 70],
 Graphics[Text["π⁻", {200, 300}, {0, 0}, {1, 0}],
  BaseStyle → {FontSize → 14}, ImageSize → 70],
 Graphics[Text["π⁰", {200, 140}, {0, 0}, {1, 0}],
  BaseStyle → {FontSize → 14}, ImageSize → 70],
 Graphics[Text["π⁺", {200, 40}, {0, 0}, {1, 0}], BaseStyle → {FontSize → 14}, ImageSize → 70]
]

(* Mass modes at μ=200 as a function of temperature *)

Show[Plot[{Mass1P[t, 200.], MassPi1[t, 200.], MassPi2[t, 200.], MassP[t, 200.]},
  {t, 0, 250}, PlotRange → {{0, 250}, {0, 1020}},
  PlotStyle → {{Black, Thick}, {Darker[Gray], Thick, Dashed},
    {Lighter[Gray], Thick, DotDashed}, {Gray, Thick, Dotted}},
  Frame → True, BaseStyle → {FontSize → 14}, RotateLabel → False,
  FrameLabel → {"T (MeV)", Graphics[Text["M(T) (MeV)", {0, 0}, {0, 0}, {0, 1}],
     BaseStyle → {FontSize → 14}, ImageSize → 40]}],
 Graphics[Text["σ", {50, 650}, {0, 0}, {1, 0}], BaseStyle → {FontSize → 14},
  ImageSize → 70],
 Graphics[Text["π⁻", {50, 300}, {0, 0}, {1, 0}],
  BaseStyle → {FontSize → 14}, ImageSize → 70],
 Graphics[Text["π⁰", {50, 140}, {0, 0}, {1, 0}],
  BaseStyle → {FontSize → 14}, ImageSize → 70],
 Graphics[Text["π⁺", {50, 50}, {0, 0}, {1, 0}], BaseStyle → {FontSize → 14}, ImageSize → 70]
]

(* The cross-over of the condensates *)
```

```
Show[Plot[{Re[Sqrt[RhoP[0., t]]], H / (MassP[0., t]^2)}, {t, 120., 250},
  PlotRange → {{120, 250}, {0, 100}}, PlotStyle →
   {{Black, Thick}, {Darker[Gray], Thick, Dashed}, {Lighter[Gray], Thick, DotDashed}},
  Frame → True, BaseStyle → {FontSize → 14}, RotateLabel → False,
  FrameLabel → {"μ (MeV)", Graphics[Text["ϕ(μ) (MeV)", {0, 0}, {0, 0}, {0, 1}],
     BaseStyle → {FontSize → 14}, ImageSize → 40]}],
 Graphics[Text["ρ", {135, 15}, {0, 0}, {1, 0}], BaseStyle → {FontSize → 14}, ImageSize → 70],
 Graphics[Text["ϕ", {135, 85}, {0, 0}, {1, 0}], BaseStyle → {FontSize → 14}, ImageSize → 70]
]
```

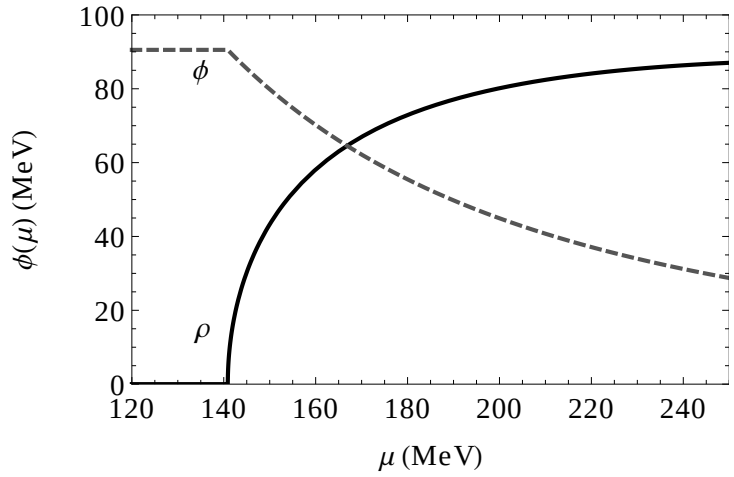


```
(* Phase diagram *)

fdnp = Quiet[Plot[RhoCritP[x], {x, 0, 300}, PlotRange → {{0, 300}, {0, 300}},
    Frame → True, PlotStyle → {Lighter[Gray], Thick, DotDashed},
    FrameLabel → {"μ (MeV)", Graphics[Text["T (MeV)", {0, 0}, {0, 0}, {0, 1}], BaseStyle →
        {FontSize → 14}, ImageSize → 40]}, BaseStyle → {FontSize → 14}, RotateLabel → False]]

(* combined phase diagram *)

Show[fdh, fdnc, fdnp]

(* 3d plot of the condensate *)

Plot3D[Re[Sqrt[RhoP[t, p]]], {t, 0, 300}, {p, 0, 300}, ColorFunction → "PigeonTones",
 AxesLabel → {"T(MeV)", "μI(MeV)", "ρ0(MeV)"}]

(* Hartree approximation at the physical point. *)

Λ = Exp[0.5 * ((msigma^2 * (Log[msigma^2] - 1) - mpi^2 * (Log[mpi^2] - 1)) / (msigma^2 - mpi^2))]
```

```
395.389
```

```
{H, m, λ} = {Re[Hp], mp, Re[λp]} /. FindRoot[{Hp == fpi * (msigma^2 - (2 * λp / M) * fpi^2),
    msigma^2 == mp^2 + (3 * λp / M) * fpi^2 +
      (3 * λp / M) * d33[0., 0., msigma, 0., 0.] + (M - 1) * (λp / M) * d33[0., 0., mpi, 0., 0.],
    mpi^2 == mp^2 + (λp / M) * (fpi^2) + (λp / M) * d33[0., 0., msigma, 0., 0.] +
      (M + 1) * (λp / M) * d33[0., 0., mpi, 0., 0.]}, {{Hp, 1000000}, {mp, i * 400}, {λp, 80.}}]
```

```
{1.79685 × 10^6, 0. + 326.085 i, 78.7788}
```

```
(* Starting condition *)

buff = {600., 139., 139., 93.}
```

```
{600., 139., 139., 93.}
```

```
(* Table with varying step lengths to make sure we don't lose the solution *)

PhysM0 =
  Table[If[Mod[t, 5.] == 0, Print[t]]; buff = FinalPhi[buff, t, 1.]; {t, buff}, {t, 0., 200.}];

PM0Det = Table[If[Mod[t, 5] == 0, Print[t]];
   buff = FinalPhi[buff, t, 1.]; {t, buff}, {t, 200.1, 230., 0.1}];

PM0hp = Table[If[Mod[t, 1] == 0, Print[t]];
   buff = FinalPhi[buff, t, 1.]; {t, buff}, {t, 230.02, 244., 0.02}];

PM0hp = Join[PM0hp,
   Table[Print[t]; buff = FinalPhi[buff, t, 1.]; {t, buff}, {t, 244.001, 260., 0.001}]];

PM0end = Table[If[Mod[t, 1] == 0, Print[t]];
   buff = FinalPhi[buff, t, 1.]; {t, buff}, {t, 260.01, 265., 0.01}];

PM0end = Join[PM0end, Table[If[Mod[t, 1] == 0, Print[t]];
    buff = FinalPhi[buff, t, 1.]; {t, buff}, {t, 265.1, 300., 0.1}]];

pm0 = Join[PhysM0, PM0Det, PM0hp, PM0end];

(* Masses as a function of temperature *)

Show[ListPlot[{Table[{pm0[[i]][[1]], pm0[[i]][[2]][[1]]}, {i, Length[pm0]}],
   Table[{pm0[[i]][[1]], pm0[[i]][[2]][[2]]}, {i, Length[pm0]}]},
  Joined → True, PlotRange → {{0, 300.}, {0., 620.}},
  Frame → True, PlotStyle → {{Black, Thick}, {Darker[Gray], Thick, Dashed}},
  FrameLabel → {"T (MeV)", Graphics[Text["M_i (MeV)", {0, 0}, {0, 0}, {0, 1}],
     BaseStyle → {FontSize → 14}, ImageSize → 40]},
  BaseStyle → {FontSize → 14}, RotateLabel → False],
 Graphics[Text["M_1", {235, 510}, {0, 0}, {1, 0}],
  BaseStyle → {FontSize → 14}, ImageSize → 70],
 Graphics[Text["M_2", {120, 220}, {0, 0}, {1, 0}],
  BaseStyle → {FontSize → 14}, ImageSize → 70]]

(* ϕ as a function of temperature *)

ListPlot[Table[{pm0[[i]][[1]], pm0[[i]][[2]][[4]]}, {i, Length[pm0]}],
 Joined → True, PlotRange → {{0., 300.}, {0., 100.}},
 Frame → True, PlotStyle → {Black, Thick}, FrameLabel →
  {"T (MeV)", Graphics[Text["ϕ (MeV)", {0, 0}, {0, 0}, {0, 1}], BaseStyle → {FontSize → 14},
    ImageSize → 40]}, BaseStyle → {FontSize → 14}, RotateLabel → False]
```

Bibliography

[1] F. Wilczek, (2002), hep-ph/0201222.

[2] R. Gupta, Introduction to Lattice QCD, Lectures given at the LXVIII Les Houches Summer School "Probing the Standard Model of Particle Interactions", 1998, hep-lat/9807028.

[3] D. B. Kaplan, Effective Field Theories, Lectures given at the Seventh Summer School in Nuclear Physics: "Symmetries", 1995, nucl-th/9506035.

[4] A. Pich, Effective Field Theory, Lectures at the 1997 Les Houches Summer School "Probing the Standard Model of Particle Interactions", 1998, hep-ph/9806303.

[5] J. Polchinski, (1992), hep-th/9210046.

[6] D. Son and M. A. Stephanov, Physical Review Letters **86**, 592 (2001).

[7] K. Splittorff, D. Son, and M. A. Stephanov, Physical Review D **64** (2001).

[8] E. Noether, Transport Theory and Statistical Physics **1**, 186 (1971), physics/0503066.

[9] A. Zee, *Quantum Field Theory in a Nutshell* (Princeton University Press, 2003).

[10] M. E. Peskin and D. V. Schroeder, *An Introduction to Quantum Field Theory* (Westview Press, 1995).

[11] J. Goldstone, Il Nuovo Cimento **19**, 154 (1961).

[12] J. Goldstone, A. Salam, and S. Weinberg, Physical Review **127**, 965 (1962).

[13] H. Nielsen and S. Chadha, Nuclear Physics B **105**, 445 (1976).

[14] D. Griffiths, An Introduction to Elementary Particles, 1987.

[15] V. Barnes *et al.*, Physical Review Letters **12**, 204 (1964).

[16] G. Zweig, CERN-TH-412 (1964).

[17] M. Gell-Mann, Physics Letters **8**, 214 (1964).

[18] O. Greenberg, Physical Review Letters **13**, 598 (1964).

[19] M.-Y. Han and Y. Nambu, Physical Review **139**, B1006 (1965).

[20] Y. Nambu, Physics Letters B **80**, 372 (1979).

[21] E. Eichten, K. Gottfried, T. Kinoshita, K. Lane, and T. Yan, Physical Review D **17**, 3090 (1978).

[22] G. Bali and K. Schilling, Physical Review D **46**, 2636 (1992).

[23] K. Schilling, Nuclear Physics B - Proceedings Supplements **83-84**, 140 (2000).

[24] T. Takahashi, H. Matsufuru, Y. Nemoto, and H. Suganuma, Physical Review Letters **86**, 18 (2001).

[25] T. Takahashi, H. Suganuma, Y. Nemoto, and H. Matsufuru, Physical Review D **65**, 1 (2002).

[26] F. Wilczek, (2000), hep-ph/0003183.

[27] J. S. Bell and R. Jackiw, Il Nuovo Cimento A **60**, 47 (1969).

[28] S. Adler, Physical Review **177**, 2426 (1969).

[29] C. Callan, R. Dashen, and D. Gross, Physical Review D **17**, 2717 (1978).

[30] E. V. Shuryak, Nuclear Physics B **302**, 559 (1988).

[31] M. C. Chu, S. Huang, and J. W. Negele, Physical Review D **48**, 3340 (1993).

[32] D. H. Rischke, Progress in Particle and Nuclear Physics **52**, 197 (2004).

[33] K. Rajagopal and F. Wilczek, *The Condensed Matter Physics of QCD, from Festschrift in honor of B. L. Ioffe, "At the Frontier of Particle Physics / Handbook of QCD"* (World Scientific Pub Co Inc, 2000), chap. 35, hep-ph/0011333.

[34] H. Yukawa, On the interaction of elementary particles, in *Proc. Phys. Math. Soc. Jap* Vol. 17, p. 3, 1935.

[35] C. M. G. Lattes, H. Muirhead, G. P. S. Occhialini, and C. F. Powell, Nature **159**, 694 (1947).

[36] J. O. Andersen, *Introduction to Statistical Mechanics*, 2 ed. (NTNU-trykk, 2008).

[37] T. Schäfer, (2003), hep-ph/0304281.

[38] M. Alford, A. Schmitt, K. Rajagopal, and T. Schäfer, Reviews of Modern Physics **80**, 1455 (2008), arXiv:0709.4635v2 [hep-ph].

[39] E. V. Shuryak, Nuclear Physics A **750**, 64 (2005).

[40] A. Schmitt, p. 10 (2010), 1001.3294.

[41] D. Page, M. Prakash, J. Lattimer, and A. Steiner, Physical Review Letters **106**, 1 (2011).

[42] J. Kogut and D. Toublan, Physical Review D **64** (2001).

[43] H. Mao, N. Petropoulos, S. Shu, and W.-Q. Zhao, Journal of Physics G: Nuclear and Particle Physics **32**, 2187 (2006).

[44] J. B. Hartle, R. F. Sawyer, and D. J. Scalapino, The Astrophysical Journal **199**, 471 (1975).

[45] S. Hands, (2001), hep-lat/0109034.

[46] R. P. Feynman, Reviews of Modern Physics **20**, 367 (1948).

[47] J. I. Kapusta and C. Gale, *Finite-Temperature Field Theory: Principles and Applications* (Cambridge University Press, 2006).

[48] M. Le Bellac, *Thermal field theory* (Cambridge University Press, 2000).

[49] J. Cornwall, R. Jackiw, and E. Tomboulis, Physical Review D **10**, 2428 (1974).

[50] G. Fejos, A. Patkos, and Z. Szep, Nuclear Physics A **803**, 21 (2007), 0711.2933.

[51] J. Lenaghan and D. H. Rischke, Journal of Physics G: Nuclear and Particle Physics **26**, 431 (2000).

[52] J. O. Andersen and L. E. Leganger, Nuclear Physics A **828**, 360 (2009), 0810.5510.

[53] J. O. Andersen, Physical Review D **75**, 1 (2007).

[54] G. Aarts, D. Ahrensmeier, R. Baier, J. Berges, and J. Serreau, Physical Review D **66**, 045008 (2002), hep-ph/0201308.

[55] P. Stevenson, B. Allès, and R. Tarrach, Physical Review D **35**, 2407 (1987).

[56] Y. Ivanov, F. Riek, and J. Knoll, Physical Review D **71**, 13 (2005), hep-ph/0502146.

[57] Y. Ivanov, F. Riek, H. van Hees, and J. Knoll, Physical Review D **72**, 11 (2005), hep-ph/0506157.

[58] Y. Nemoto, K. Naito, and M. Oka, The European Physical Journal A **9**, 245 (2000).

[59] H.-S. Roh and T. Matsui, The European Physical Journal A - Hadrons and Nuclei **1**, 205 (1998).

[60] B. Delamotte, American Journal of Physics **72**, 170 (2004).

[61] H. Bethe, Physical Review **72**, 339 (1947).

[62] P. Kraus and D. Griffiths, American Journal of Physics **60**, 1013 (1992).

[63] G. t' Hooft and M. Veltman, Nuclear Physics B **44**, 189 (1972).

[64] A. Barducci, R. Casalbuoni, G. Pettini, and L. Ravagli, Physical Review D **71** (2005).

[65] D. Ebert and K. Klimenko, The European Physical Journal C **46**, 771 (2006).

[66] L. He, M. Jin, and P. Zhuang, Physical Review D **71** (2005), hep-ph/0503272.

[67] M. Loewe and C. Villavicencio, Physical Review D **67** (2003).

[68] J. O. Andersen and T. Brauner, Physical Review D **78**, 12 (2008), arXiv:0804.4604v2[hep-ph].

[69] J. Baacke and S. Michalski, Physical Review D **67** (2003).

[70] T. Brauner, Physical Review D **74**, 13 (2006), hep-ph/0607102.

[71] M. L. El-Sheikh and M. Loewe, p. 12 (2007), hep-ph/0701100.

[72] N. Petropoulos, Journal of Physics G: Nuclear and Particle Physics **25**, 2225 (1999).

[73] M. Gell-Mann and M. Lévy, Il Nuovo Cimento **16**, 705 (1960).

[74] M. G. Alford, M. Braby, and A. Schmitt, Journal of Physics G: Nuclear and Particle Physics **35**, 115007 (2008).

[75] J. Kogut and D. Sinclair, Physical Review D **66**, 23 (2002), hep-lat/0202028.

[76] J. O. Andersen and L. T. Kyllingstad, Journal of Physics G: Nuclear and Particle Physics **37**, 015003 (2010), hep-ph/0701033.

[77] K. Rajagopal and F. Wilczek, Nuclear Physics B **399**, 395 (1993).

[78] W. Lin and B. D. Serot, Nuclear Physics A **512**, 637 (1990).

[79] S. Weinberg, Physical Review D **9**, 3357 (1974).

[80] S. Chiku and T. Hatsuda, Physics , 20 (1998), hep-ph/9803226.

[81] F. Karsch, A. Patkos, and P. Petreczky, Physics Letters B **401**, 69 (1997), hep-ph/9702376.

[82] J.-P. Blaizot, E. Iancu, and U. Reinosa, Nuclear Physics A **736**, 149 (2004).

[83] G. Amelino-Camelia, Physics Letters B **407**, 268 (1997).

[84] C. Vafa and E. Witten, Physical Review Letters **53**, 535 (1984).

[85] W. R. Inc., Mathematica Edition: Version 8.0, 2010.

[86] K. Splittorff, D. Toublan, and J. J. M. Verbaarschot, Nuclear Physics B **639**, 524 (2002), hep-ph/0204076.

[87] H. Meyer-Ortmanns, H.-J. Pirner, and A. Patkós, Physics Letters B **295**, 255 (1992).

[88] H. Abuki, R. Anglani, R. Gatto, M. Pellicoro, and M. Ruggieri, Physical Review D **79**, 6 (2009), 0809.2658.

[89] M. Alford and K. Rajagopal, Journal of High Energy Physics **2002**, 031 (2002).